



Politecnico di Milano

SCHOOL OF CIVIL, ENVIRONMENTAL AND LAND MANAGEMENT ENGINEERING

Master of Science – Environmental and Land Planning Engineering

**Design and building of a laboratory-scale
physical model to investigate erosion in
embankments**

Supervisor

Prof. Donatella Valeria STERPI

Co-Supervisor

Dr. Marco CARUSO

Candidate

Gabriele BIANCHI – 945163

Academic Year 2020 – 2021

Abstract

L'erosione interna è un fenomeno che può indurre il collasso di rilevati in terra e si manifesta con differenti modalità. Consiste nel distacco e dilavamento delle particelle più fini del terreno ad opera di un flusso d'acqua sotterraneo, che può avvenire in modo diffuso (*suffusion*) o localizzato (*piping*). Sono stati sviluppati nel corso degli anni numerosi modelli sperimentali fisici a piccola e media scala per valutare l'influenza dei diversi fattori sui fenomeni di erosione interna, ma caratterizzati da alcune limitazioni. L'obiettivo della tesi è stato quello di realizzare un nuovo dispositivo più versatile, denominato Erosion-Piping Box (EPBox) che superasse alcune di queste limitazioni. L'EPBox permette di analizzare i fenomeni di erosione interna su modelli di varie dimensioni, effettuando test in pressione per raggiungere alti gradienti e ricostruendo il modello per strati che hanno una inclinazione prescelta rispetto alla direzione del flusso. Lo schema generale di funzionamento dell'EPBox può essere descritto con un serbatoio di monte e uno di valle tramite i quali una differenza di carico idraulico, e quindi un gradiente, viene applicata al campione, o al modello di rilevato, posizionato tra essi. Il dispositivo è dotato di un circuito idraulico che consente di mantenere costanti i livelli dei serbatoi, di un sistema di misurazione delle pressioni neutre, e di un sistema di raccolta del materiale che viene eroso. Per le prove di validazione si è utilizzato un materiale con gradazione suscettibile all'erosione interna, ovvero sferette di vetro di diametro compreso tra 0.07 mm e 2 mm, di cui sono state stimate la conducibilità idraulica tramite un permeametro e le proprietà di compattazione. Il permeametro è stato opportunamente modificato per misurare anche la quantità di materiale eroso nel tempo, quando si applicano gradienti idraulici sempre più elevati. Dopo aver realizzato alcune prove per collaudare l'EPBox, si è proceduto con una serie di test con gradienti differenti, per verificarne l'effetto sulla quantità di materiale eroso nel tempo e sulla conducibilità idraulica, valutando anche come le diverse particelle vengono dislocate all'interno del campione. Dalle prove svolte si è potuto osservare l'effetto del gradiente sulla stima di k e sul quantitativo di materiale eroso, che risultano crescere con i sia nelle prove verticali che orizzontali. I test sull'EPBox hanno mostrato una diminuzione del materiale eroso nel corso delle

prove anche a causa della formazione di pipes che permettono all'acqua di passare facilmente all'interno del campione. Inoltre, il processo di erosione interna agisce sulle particelle medie e fini trascinandole verso il serbatoio di valle.

Internal erosion is a phenomenon that can lead to the collapse of earth works and occurs in different ways. It consists of the detachment and washout of the finest soil particles by a flow of underground water, which may occur in a diffuse (*suffusion*) or localised (*piping*) manner. Several small- and medium-scale physical experimental models have been developed over the years to assess the influence of different factors on internal erosion phenomena, but they are characterised by some limitations. The aim of this thesis was to develop a new, more versatile device called the Erosion-Piping Box (EPBox) that overcomes some of these limitations. The EPBox allows to analyse internal erosion phenomena on models of various dimensions, performing pressurised tests to reach high gradients and reconstructing the model for layers that have a chosen inclination with respect to the flow direction. The general operating scheme of the EPBox can be described with an upstream and a downstream reservoir through which a hydraulic head difference, and hence a gradient, is applied to the sample, or embankment model, placed between them. The device is equipped with a hydraulic circuit to maintain constant levels in the reservoirs, a system for measuring pore pressures, and a system for collecting material that is eroded. For the validation tests, a material with a gradation susceptible to internal erosion was used, consisting of glass spheres with diameters between 0.07 mm and 2 mm, whose hydraulic conductivity was estimated using a permeameter and whose compaction properties were estimated. The permeameter was suitably modified to also measure the amount of eroded material over time when progressively higher hydraulic gradients were applied. After a few tests to validate the EPBox, a series of tests were carried out with different gradients to see the effect on the amount of material eroded over time and the hydraulic conductivity, including how the different particles are displaced within the sample. From the tests it was possible to observe the effect of the gradient on the estimation of k and on the amount of eroded material, which increased with i in both vertical and horizontal tests. The EPBox tests showed a decrease in the amount of eroded material during the tests also due to the formation of pipes that allow water to pass easily through the sample. In addition, the internal erosion process acts on the medium and fine particles, dragging them towards the downstream reservoir.

Contents

Abstract	iii
Contents	vii
List of Figures	xiii
List of Tables	xv
Introduction	1
1 Erosion in soils	5
1.1 The piping phenomenon	7
1.1.1 Description of the process	7
1.1.2 Hystorical analytical approaches	11
1.1.3 Backward erosion	13
1.2 Suffosion and suffusion	20
1.3 Other erosion mechanisms	22
1.3.1 Internal erosion	22
1.3.2 Tunnelling or jugging	22
1.3.3 Heave	23
2 Literature review of experimental tests	25
2.1 Purposely designed laboratory test	25
2.1.1 A tiltable model for internal erosion investigation	25
2.1.2 True-triaxial piping test apparatus	31
2.1.3 Suffusion experimental investigation	37
2.2 Assessment of erodibility properties	39
2.2.1 Hole Erosion Test	40
2.2.2 Slot Erosion Test	42
2.2.3 Results	44
2.3 A real scale test	45
2.4 Summary and remarks	50

3	The EPBox	53
3.1	Functioning of the system	54
3.2	The box	55
3.3	The cover and the removable cap	57
3.4	The filters	59
3.5	The holes and screws	64
3.6	The PVC base and the steel support	69
3.7	The hydraulic connections and the measuring instruments	70
3.8	The trap box	72
4	Materials	75
4.1	Selection of the material	75
4.2	Material characterisation	77
4.2.1	Grain specific weight	77
4.2.2	Grain size distribution curve	78
4.2.3	Velocity of deposition	80
4.3	Preparation of material for the tests	82
4.3.1	Grain size distribution	82
4.3.2	Void ratio	83
5	Vertical seepage	87
5.1	Purpose of tests with permeameters	87
5.2	Tests in permeameter	89
5.2.1	The device employed	89
5.2.2	The material	90
5.2.3	The setup of the test	91
5.3	Test results	92
5.3.1	First set	92
5.3.2	Second set	96
6	Horizontal seepage in EPBox	101
6.1	Comparing horizontal and vertical seepage tests	102
6.2	The EPBox tests	104
6.2.1	Setup and testing of the device	104
6.2.2	First test	106
6.2.3	Second test	107
6.2.4	Third test	110
6.2.5	Fourth test	113

6.2.6 Comparison between the tests	115
Conclusions	119
Bibliography	124

List of Figures

Figure 1.1	Geomorphic and climatic distribution of pipes: (a) frequency of <i>piping</i> in different landsurface units; (b) frequency and mean size of pipes in different climatic zones (Canocher and Dalrymple 1977, NULM classification)	7
Figure 1.2	Pipe development in laboratory tests (Van Beek, Knoeff, et al. 2011)	8
Figure 1.3	<i>Piping</i> in the interface between a dyke and the soil (Van Beek, Van Essen, et al. 2015)	10
Figure 1.4	Large "sand boil" at the base of the landside of the levee on Coutts Island Road, New Zealand (Green and Cubrinovski 2010) . . .	11
Figure 1.5	Vertical and horizontal distances at ground-structure contact (Richards and Reddy 2007)	12
Figure 1.6	Embankment on a sandy layer (Van Beek, Knoeff, et al. 2011)	15
Figure 1.7	Embankment on a cohesive layer but with the presence of an artificial channel crossing it (Van Beek, Knoeff, et al. 2011)	16
Figure 1.8	Local fracture in the cohesive layer (Van Beek, Knoeff, et al. 2011)	16
Figure 1.9	Formation of the "sand volcanoes" (Van Beek, Knoeff, et al. 2011)	17
Figure 1.10	Development of a pipe (Van Beek, Knoeff, et al. 2011)	17
Figure 1.11	Motion initiation as a result of the drag force (Van Beek, Knoeff, et al. 2011)	18
Figure 1.12	Forces acting on the particle according to the White theory (Van Beek, Knoeff, et al. 2011)	19
Figure 1.13	Collapse of the levee (Van Beek, Knoeff, et al. 2011)	20
Figure 1.14	Sinking of the levee (Van Beek, Knoeff, et al. 2011)	20
Figure 1.15	<i>Piping</i> and <i>suffusion</i> phenomena (Xiao and Shwiyhat 2012) .	21
Figure 1.16	Heave zones lifted by pore water pressure in cohesionless soils where upper layer is less permeable than lower layer (Koltuk et al. 2019)	23
Figure 2.1	Direction of flow in different areas of an earth embankment (Pachideh and Hosseini 2019)	26

Figure 2.2	Overview of the tiltable apparatus developed for internal erosion studies (Pachideh and Hosseini 2019)	26
Figure 2.3	Schematic representation of the apparatus (Pachideh and Hosseini 2019)	27
Figure 2.4	Sample container components and loading frame (Pachideh and Hosseini 2019)	28
Figure 2.5	Different modes of testing (Pachideh and Hosseini 2019) . . .	30
Figure 2.6	An example of the shape of the pipes in the tests (Pachideh and Hosseini 2019)	31
Figure 2.7	Components of the TTPTA (Richards and Reddy 2012)	32
Figure 2.8	Detail of sample box of the TTPTA, with a third air bladder in the plane of the page (Richards and Reddy 2012)	32
Figure 2.9	Flownet through isotropic soil samples (Richards and Reddy 2012)	33
Figure 2.10	Grain-size distribution of (a) field soils and (b) mixed soils prepared by mixing commercial uniform sand (QS) with kaolin (K), montmorillonite (M), or gravel (G) (Richards and Reddy 2012)	34
Figure 2.11	(a) General stress states (A, B, C, D, E) for initial tests; (b) general stress states (A, B, C) for subsequent tests (Richards and Reddy 2012)	35
Figure 2.12	<i>Suffusion</i> experimental triaxial cell (Xiao and Shwiyhat 2012)	37
Figure 2.13	Modified base of the triaxial cell (Xiao and Shwiyhat 2012) . .	38
Figure 2.14	Schematic drawing of the HET apparatus (Wan and Fell 2004)	40
Figure 2.15	Estimation of erosion rate per unit area as a function of shear stress (Wan and Fell 2004)	42
Figure 2.16	Schematic drawing of the SET apparatus (Wan and Fell 2004)	43
Figure 2.17	Initial shear stress versus erosion rate index (Wan and Fell 2004)	44
Figure 2.18	Filling of the basin with sand and construction of the levee (Van Beek, Knoeff, et al. 2011)	45
Figure 2.19	Cross-section of the experiment (Van Beek, Knoeff, et al. 2011)	46
Figure 2.20	Crater of sand increasing (Van Beek, Knoeff, et al. 2011) . . .	47
Figure 2.21	Local decrease of water pressure (pale blue line) caused by formation of pipes compared to initial water level (blue line) (Van Beek, Knoeff, et al. 2011)	48
Figure 2.22	Cumulative amount of transported sand in test 3 (Van Beek, Knoeff, et al. 2011)	48

Figure 2.23 Change of water pressure in the sand as a result of channel enlargement (red line) compared to initial one (blue line) (Van Beek, Knoeff, et al. 2011)	49
Figure 2.24 Widening of the channel with a consequent increase in the eroded material (Van Beek, Knoeff, et al. 2011)	49
Figure 2.25 Collapse of the levee (Van Beek, Knoeff, et al. 2011)	50
Figure 3.1 General look of EPBox	55
Figure 3.2 The EPBox on its support	56
Figure 3.3 Technical drawing of the EPBox, lateral view	56
Figure 3.4 Corner of the box and highlight on the interlocking system where the two slabs are glued	58
Figure 3.5 Box with cover positioned on the top	58
Figure 3.6 Technical drawing of the removable cap (mm)	60
Figure 3.7 Detail of the removable cap with its O-Ring put in place	60
Figure 3.8 Details of the filter employed by Celada and Magno 2013 (mm)	61
Figure 3.9 Filter realised by superposition of the two slotted slabs	62
Figure 3.10 Technical drawing of the filter used (mm)	63
Figure 3.11 Filters positioned into the box with their supports	63
Figure 3.12 L-shaped angle profiles used as rails to fix the filters	64
Figure 3.13 Technical drawing of passing holes	65
Figure 3.14 Hole with cavity for the positioning of the squared screw head	65
Figure 3.15 Grey screw bolted with a white nut and with the addition of a circular silicon protection gasket	66
Figure 3.16 Gaskets for screws M20 and M4	67
Figure 3.17 Cavity on the screw and its O-Ring	67
Figure 3.18 Drawings and dimensions of screws	68
Figure 3.19 Technical drawing of PVC base (mm)	70
Figure 3.20 Detail of the hydraulic connection in the upstream reservoir	71
Figure 3.21 System of inlet and disposal of water, to balance the equilibrium of upstream and downstream reservoirs	71
Figure 3.22 The continuous overflow system	72
Figure 3.23 Trap box employed for collecting the eroded material	73
Figure 3.24 Schematic connection between the downstream reservoir and the trap box	73
Figure 4.1 Picture of the material employed	75
Figure 4.2 Grain size distribution curve class A	78

Figure 4.3	Grain size distribution curve class B	79
Figure 4.4	Grain size distribution curve class C	79
Figure 4.5	Graduated cylinder employed for the test	82
Figure 4.6	Grain size distribution of the sample employed for the tests . .	83
Figure 4.7	Effect of grain separation of the fine and medium particles from the coarser ones for highly compacted samples	85
Figure 4.8	No separation observed on the compacted sample in wet condition	86
Figure 5.1	Schematic diagram representing a constant hydraulic head test (Germaine 2009)	88
Figure 5.2	The permeameter employed for the tests	90
Figure 5.3	Hydraulic conductivity tests with i from 0.15 to 0.63	94
Figure 5.4	Mean values of the last three measurements of k for each test .	95
Figure 5.5	Eroded mass measured in the first set of tests as percent over the total	95
Figure 5.6	Particle size distribution along depth in the first set of tests .	96
Figure 5.7	Hydraulic conductivity tests with i from 0.05 to 1.89	97
Figure 5.8	Comparison of the mean values of the last three measurements of k both set of tests	98
Figure 5.9	Eroded mass measured in the second set of tests	99
Figure 5.10	Particle size distribution along depth in the second set of tests	100
Figure 6.1	Schematic representation of a fully horizontal seepage test . .	101
Figure 6.2	Schematic representation of a seepage test on a partially satu- rated sample	101
Figure 6.3	Seepage direction in different areas of an embankment dam (Xiong et al. 2021)	104
Figure 6.4	Effectiveness of confinement of the upstream reservoir by means of a bag filled with water	105
Figure 6.5	Hydraulic conductivity test in EPBox with $i = 0.84$	106
Figure 6.6	Hydraulic conductivity test in EPBox with $i = 0.16$	108
Figure 6.7	Grain size distribution of the superficial part of the sample . .	109
Figure 6.8	Grain size distribution of the deep part of the sample	109
Figure 6.9	Picture showing the pipe formed during the test	110
Figure 6.10	Cumulated eroded mass in percentage of class B and C ($i = 0.64$)	111
Figure 6.11	Hydraulic conductivity test in EPBox with $i = 0.64$	112
Figure 6.12	Joint representation of cumulated eroded mass and k	112
Figure 6.13	Hydraulic conductivity test in EPBox with $i = 0.18$	114

Figure 6.14	Cumulated eroded mass in percentage of class B and C ($i = 0.18$)	114
Figure 6.15	Joint representation of cumulated eroded mass and k	115
Figure 6.16	Graphical representation of the three horizontal seepage tests performed on new samples in the EPBox	116
Figure 6.17	Comparison of vertical and horizontal seepage test results	117
Figure 6.18	Schematic layout of direction of flow in relation with the disposition of fine material	117

List of Tables

Table 1.1	Typical values of hydraulic conductivity of saturated soils . . .	9
Table 1.2	Bligh’s line of creep recommended values for <i>pip</i> ing stability (Richards and Reddy 2007)	12
Table 1.3	Lane’s weighted creep recommended values for <i>pip</i> ing stability (Richards and Reddy 2007)	14
Table 2.1	Summary of test series (Richards and Reddy 2012)	36
Table 2.2	Testing program (Van Beek, Knoeff, et al. 2011)	46
Table 2.3	Relative density and hydraulic conductivity obtained by the first three tests (Van Beek, Knoeff, et al. 2011)	47
Table 3.1	Dimension and quantity of holes	69
Table 3.2	Type of screws	69
Table 4.1	Classification of particle size for common natural materials . .	76
Table 4.2	Diameter of glass beads chosen	76
Table 4.3	Values of G_s for different classes of material	77
Table 4.4	Classes of uniformity of soil	80
Table 4.5	Values of C_u obtained in the tests	81
Table 4.6	Time of deposition of the sample	81
Table 4.7	Results of void ratio on dry material	85
Table 4.8	Results of void ratio on wet material	86
Table 5.1	List of gradients for the tests	91
Table 5.2	F_s for the first set of tests	93
Table 6.1	Summary of tests carried out in the EPBox	102
Table 6.2	Total eroded mass and percentage over the initial mass of each class in first test	107

Introduction

Earth works are used either as structures to prevent the overflow of watercourses or as gravity barriers to delimit a reservoir. In the first case they are termed levees, while if they have the function of permanent confinement of water basins they are referred to as embankments.

Internal erosion is one of the most critical phenomena that may induce a collapse or failure in embankments. Statistical investigations have highlighted that approximately 0.5% of embankment dams worldwide have experienced failure due to internal erosion (Fell and Fry 2007). Localised internal erosion phenomena such as *piping* can lead to the collapse of the structure, through the formation of cavities due to the continuous transport of material, with failures causing overtopping of the embankment crest and allowing the uncontrolled passage of water downstream of the structure. The triggering of the pipe is marked on the valley side of the earth dam by the presence of "sand volcanoes" consisting of the eroded material from which the filtering water emerges. Equally dangerous are distributed erosion processes such as *suffusion*, a phenomenon that occurs when the dragging action of the water is exerted on the finer particles and the solid skeleton consisting of the coarser component of the grains is left intact. If there is collapse in the soil, the phenomenon becomes more dangerous and is termed *suffosion*.

The effects of the action of water on earth works have been studied since their first construction, almost 5000 years ago, such as the structures built in the area around the Nile by the first colonies that inhabited its delta to protect themselves from flooding or in the Tigris and Euphrates river valleys. The design approach was mostly empirical but with good results, considering that some of these structures - which could be built with stone blocks used as bricks or with earth materials - have lasted for many centuries with few damages. For example, the Proserpina dam, one of the first hydraulic constructions, was built by the Romans, has a lifetime of 2000 years and still today is in function, though with some modifications and adjustments

in the last centuries (Jansen 1983). The phenomenon of *piping* became an engineering concern only in 1898, after the collapse of the Narora Dam on the Ganges River in India. In this incident, internal erosion was recognised as the trigger and therefore the beginning of the first investigations into this issue (Jones 1981).

The importance of the study of internal erosion phenomena such as *piping* and *suffusion* in a laboratory scale is given by the lack of standardized procedures, especially in soils constituted by non-cohesive materials. Various experimental physical models at small and medium scales have been developed over the years to assess the influence of different factors on the initiation and development of internal erosion processes in soils, often with many limitations due to sample size, applicable gradients and the possibility of analysing only a single internal erosion phenomenon. Models made at full scale are rarer, but extremely useful for reproducing the phenomenon in its totality up to the collapse of the structure, and thus evaluating the correspondence of the results obtained from tests made at a smaller scale. Usually it is common to perform simulations with finite element analysis to evaluate risks related to internal erosion, but the role of laboratory tests is irreplaceable (Richards and Reddy 2007).

The objective of this thesis is to build a new device and verify its feasibility and reliability in performing laboratory tests for the analysis of internal erosion in a model of an embankment, in particular *piping* and *suffusion* phenomena. Material choices and design solutions have been made with the aim of improving several aspects of the instruments used in the literature, creating a versatile apparatus for various applications, allowing for:

- the analysis of various internal erosion phenomena;
- the use of models of different sizes;
- pressurised tests when high gradients are to be achieved;
- the installation of piezometers to directly measure pressures in the sample;
- the visual analysis thanks to the transparency of the walls;
- the creation of samples with inclined layers thanks to a rotational mechanism of the base of the box with respect to the horizontal;
- the possibility to easily replace filters according to the materials employed or the requirements of the test.

The first two chapters of this thesis are devoted to the description of the different forms of internal erosion and to the analysis of some of the experimental models available in the literature. In the third chapter the new model designed and implemented is presented examining construction details and the reasons for the choices made. The fourth chapter describes the material used, reports the particle size distribution curves of the different fractions available and presents the analyses carried out on the void ratio during the preparation of the sample for the subsequent tests. The fifth chapter analyses the vertical seepage tests carried out in a permeameter modified to be used with the material of interest, while the sixth chapter reports the tests carried out with the EPBox starting from the preliminary analyses to verify the instrumentation up to the horizontal seepage tests. The last chapter is devoted to conclusive considerations on the work carried out.

Chapter 1

Erosion in soils

The process of erosion consists in the removal of soil particles caused by an external action that may be due to atmospheric agents, subsurface and superficial water seepage or other factors. It can be subdivided into two different phases, which are the detachment of the single particle from the whole body and then its transportation. The movement occurs if the mobilising forces on the particle exceed those resisting the movement, thus causing the beginning of the phenomenon. It then proceeds until the particle is deposited, when the energy underlying the movement is no longer sufficient to keep it in a state of motion, unless the particle is completely washed off from the soil mass. The factors influencing the occurrence of erosion can be geometric, meaning soil properties such as average grain size, distribution and size of voids, and grain size distribution, hydraulic such as hydraulic gradient, flow direction and velocity, and mechanical, meaning density, layer inclination, cohesion and stress state.

There are two main categories that can be distinguished: superficial and internal erosion.

Superficial erosion is usually known as *weathering* and mainly relates to the action of wind, rain and snow on the portion of the soil in contact with the atmosphere. The surface is more affected when subjected to degradation by chemical elements (e.g. acid rain), so the combined effect of chemical and physical action must always be considered.

Internal erosion involves the inner part of the soil and the causes of the movement are mostly of a physical nature; however, some researchers (Lutz et al. 1934) have focused on the combined effect of chemical nature on the erosion processes, showing how this joint action can be one of the main factors influencing the stability of embankments. The investigation of this phenomenon is of great importance because the data collected showed that approximately 0.5% of embankment dams worldwide have experienced

failure due to internal erosion (Fell and Fry 2007).

A considerable volume of research has been published in the literature on the phenomenon of internal erosion and, considering that these works often derive from international and multidisciplinary studies, there can often be confusion in terms of definitions of the specific mechanism that is taken into account. Often several phenomena are gathered under the term of *piping*, which, although leading to similar end results, are triggered by different causes, and for this reason an understanding and distinction between them is fundamental.

There is a large amount of data collected over the years on the causes and modalities of the collapse of embankments or dams - both in earth and concrete - over time, but it is often difficult to trace the real causes of the event. In fact, with the collapse of the embankment, any evidence of what may have caused the disaster is also washed away. Therefore, from a statistical point of view, observing the records of the various events over time, it is necessary to note that these data must be associated with broader engineering considerations in order to have a better interpretation of the individual phenomena (Richards and Reddy 2007).

The most relevant problems due to *piping* are concentrated flows due to *backward erosion*, although historical data on dam collapses show that there are often other factors involved. In fact, a large part of them are due to internal erosion, inadequate sizing or lack of maintenance of the filters. From these data it appears that only 31.1% of *piping* failures are associated with the classical model of *backward erosion*, but this could be much less if the specifics of these failures were known. The majority of these events are attributed to mechanisms of *piping* along conduits, other structures and internal erosion (49.8%) into or along foundations or abutments (15%) or *piping* due to *tunnelling* (4.1%) (Jones 1981).

Based on the data collected, the most relevant phenomena in terms of number are those related to *piping* and diffuse phenomena such as *suffusion*. For this reason, the development of an apparatus such as the EPBox, capable of simulating these types of mechanisms, is essential to better understand their causes and the ways in which they occur.

The different types of internal erosion, are triggered by different factors and have different characteristics, which will be described in the following chapter starting with

the phenomena that can be studied by means of the apparatus designed in this thesis work and ending with a short analysis of two other types of internal erosion.

1.1 The piping phenomenon

1.1.1 Description of the process

The water infiltration movement which is responsible for the transport of material is established due to the difference in hydraulic head between the reservoir side and the countryside of the embankment. The infiltration of water can cause instability of the earth dam due to internal erosion processes. The material removal and transport begins at the foot of the embankment on the countryside and tends to extend, creating real channels which amplify, leading to the possible collapse of the structure.

"Pipes" can be defined as linear voids created by the flow of water in soil works. They can occur under all climatic conditions and vary from a diameter of a few millimetres up to several metres (Figure 1.1).

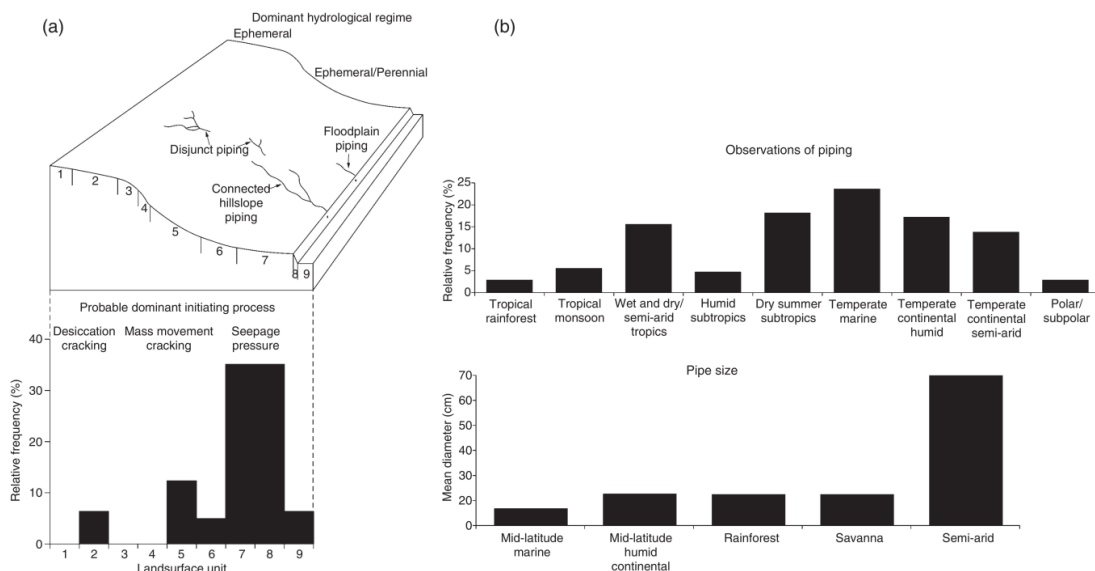


Figure 1.1. Geomorphic and climatic distribution of pipes: (a) frequency of *piping* in different landsurface units; (b) frequency and mean size of pipes in different climatic zones (Canocher and Dalrymple 1977, NULM classification)

It is often difficult to clearly define a distinction between these types of conduits and other macroporosity present in the soil. The substantial difference that can be

taken into account is that pipes, once generated, become preferential conduits that allow water to flow with ease (Figure 1.2). These conduits can also create an underground network of small tunnels that form a subterranean grid capable of creating ramifications of up to several metres in length.



Figure 1.2. Pipe development in laboratory tests (Van Beek, Knoeff, et al. 2011)

Once conduits of this type are created, due to micro collapses of their walls caused by continuous erosion, tunnels can be formed by the union of smaller pipes, further increasing the possibility of water crossing the ground. These openings are called *gullies*, and are often one of the main causes of embankment collapses (Jones 2004).

In cases where pipes run through the embankment, the traditional slope stability analysis based on material properties is no longer able to give a good indication of the risk of collapse. For this reason Karl Terzaghi (1922) drew the attention of the science of soil mechanics to this phenomenon, as it is the cause of numerous collapses in earth dams, hillslopes, riverbanks or cliffs.

The water flow velocity according to the Darcy law (1856), can be expressed as in (1.1):

$$v_s = -k_s i_s \quad (1.1)$$

With:

- v_s water flow velocity in the s direction;

- k_s hydraulic conductivity or coefficient of permeability;
- i_s hydraulic gradient in the s direction.

The hydraulic conductivity of soils depends on several factors: fluid viscosity, pore size distribution, particle size distribution, void ratio, mineral particle roughness and degree of soil saturation. The value of hydraulic conductivity varies widely for different soils (Table 1.1). The hydraulic conductivity of unsaturated soils is lower and increases rapidly with the degree of saturation (Das 2006).

Table 1.1. Typical values of hydraulic conductivity of saturated soils

Soil type	k (cm/s)
Clean gravel	$10^2 - 1$
Coarse sand	$1 - 10^{-2}$
Fine sand	$10^{-2} - 10^{-3}$
Silty clay	$10^{-3} - 10^{-5}$
Clay	$10^{-5} - 10^{-6}$

The importance of the role of the hydraulic gradient in the seepage phenomenon can also be explained by (1.2), in which i is related to the seepage forces F_s :

$$F_s = -\gamma_w i_s V \quad (1.2)$$

With:

- γ_w specific weight of water;
- V volume of soil.

The driving force increases with an increment of the hydraulic gradient, constituting the most important trigger in the developing of *piping*. The shape and dimension of the grains have an influence on the possibility of detachment, the microstructure of the soil on the dragging of the eroded material. If the erosion is localised in a limited zone, so-called "*pipes*" can be created, areas in which the removal of material leads to the formation of preferential channels that widen and propagate in the material to the point of possible collapse of the structure in the worst cases.

Once the particles begin their movement, the grains can only be transported if the voids are large and interlinked enough to allow their passage. If the particles do not find sufficient space, they are deposited and obstruct the pores of the soil with a phenomenon known as *clogging*. This is the case of *self-healing* of the soil mass.

The materials most susceptible to *pipining* are fine sands and silts, often with a gap-graded size distribution, where the finer particles can be moved easily within the pore network of the coarser grains matrix. The process can occur in the foundation soil, in the body of the embankment, or also at the interface between soil and the structure (Figure 1.3). Specifically, the EPBox is a useful device for studying this phenomenon along the interface surfaces between the material and the walls of the box, which are the areas where *pipining* is most likely to develop.

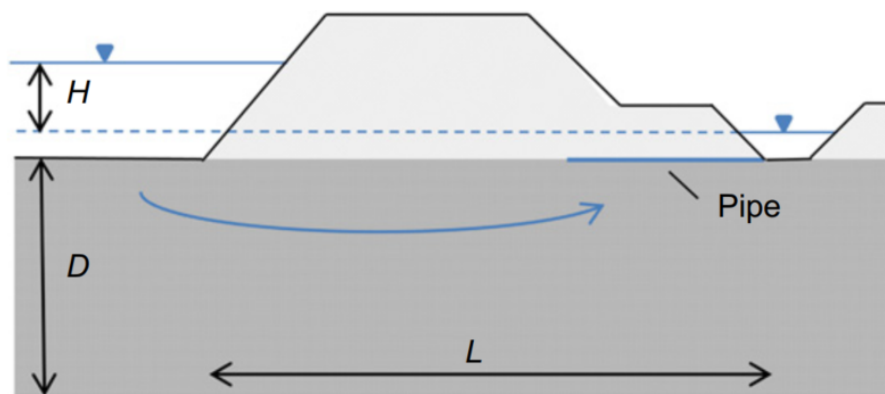


Figure 1.3. *Pipining* in the interface between a dyke and the soil (Van Beek, Van Essen, et al. 2015)

The difference in water level between the inner and outer side of the river results in greater criticality during periods of flooding, when the watercourses reach a height that could cause *pipining*; in fact, the average hydraulic gradient is proportional to this difference (denoted by the letter H in Figure 1.3).

The signs that the process is occurring can be noticed in the countryside close to the embankment: in fact, it is possible to see the presence of "sand boils" in the spots where the water begins to flow to the surface, creating holes with accumulation of fluids, with solid particles in suspension if material transport is taking place. This is the evidence of whether the process is also acting with the removal of soil or only with the passage of water.



Figure 1.4. Large "sand boil" at the base of the landside of the levee on Coutts Island Road, New Zealand (Green and Cubrinovski 2010)

1.1.2 Historical analytical approaches

From the beginning of the 1900s onwards, a greater awareness of the phenomenon of *piping* began to develop, partly as a consequence of the collapse of the Narora dam on the Ganges river in India in 1898 (Richards and Reddy 2007). It was precisely in India that Bligh developed a theory in 1910, following this event, that describes the *piping* phenomenon from an analytical point of view and how it is triggered.

Through the *line of creep theory* he identified a potential connection between the length of the seepage path and the tensile forces capable of moving soil particles. This method is derived from experimental observations made to evaluate the probability of occurrence of the *piping* phenomenon at the interface between soil and structure.

What Bligh observed is that the flow occurring at the contact surface between soil and structure does not follow a Darcian flow rule, but is governed by a cubic law typical of planar openings, in which the width of the opening plays a key role. The flow path followed is not Darcian either, however the flow rate follows Darcy's law in which the discharge rate, and consequently also the flow velocity, is directly proportional to the hydraulic head and inversely proportional to the length of the seepage path. According to Bligh's theory, the length of the seepage path has to be calculated as the sum of the vertical and horizontal distances measured along the interface between structure and soil (Figure 1.5). The aspect of this theory according to which the flow occurs across the boundary surface between the two has generated

Table 1.2. Bligh's line of creep recommended values for *piping* stability (Richards and Reddy 2007)

Class	Soil	Required c
A	Fine silt and sand	18
B	Fine micaceous sand	15
C	Coarse sand	12
D	Gravel and sand	9
E	Boulders, gravel and sand	4–6 (increased to 6–9 in 1913)

discussion in the early 1900s, because according to other researchers the flow takes place as intergranular (Lane 1934).

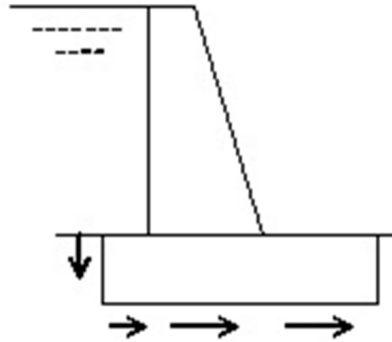


Figure 1.5. Vertical and horizontal distances at ground-structure contact (Richards and Reddy 2007)

The equation that governs Bligh's theory is as follows:

$$L = cH \quad (1.3)$$

With:

- L flow length (calculated as the sum of vertical and horizontal length);
- c percolation factor;
- H hydraulic head across the structure.

Regarding the percolation factor c , Bligh developed guidelines to identify a safety coefficient for percolation from his equation and relating it to dam failure events, while classifying the soil into five different classes as shown in Table 1.2.

Lane in 1934, based on Bligh's studies, used the term *piping* to describe the process of the removal of soil particles along the dam-foundation soil contact. He also provides a clear distinction between the flow that occurs at the soil-structure contact and the one within the granular medium. Lane refines the *line of creep theory* by taking into account the anisotropy of soils and the conditions governing the flow of water in stratified soils.

The equation of Lane's theory known as the *weighted creep method* is as follows:

$$Ln = cH \quad (1.4)$$

With:

- Ln maximum length of seepage path that can be considered on the safety side;
- c safe weighted creep ratio.

The relationship is similar to Bligh's (1.3) but the seepage path is approached differently. Lane indeed considers an anisotropic flow and introduces a reduction of the seepage path length by 30%. On the basis of equation (1.4) in conjunction with studies on more than 200 dams, the author provides the values of the c coefficient for twelve different soil classes (Table 1.3). It is thus observed that the risk of *piping* increases with the hydraulic gradient and decreases inversely with the length of the seepage path. This method is still in common use, especially when applied at soil structure boundaries.

1.1.3 Backward erosion

In the wider category of *piping* the specific process called *backward erosion* can be described in detail, being frequently observed.

This phenomenon is triggered from the bottom of the structure at the countryside, through a progressive mechanism in which, following the opposite direction to the outgoing flow, soil particles are removed until a pipe is formed that may reach the water basin. Once the flow has found a preferential path, the phenomenon becomes quite similar to that described above generally as *piping*. The particles are progressively removed from the soil matrix by drag forces produced by the intergranular infiltration flow. The mobilising forces are balanced by the shear strength of the grains and the

Table 1.3. Lane's weighted creep recommended values for *pip*ing stability (Richards and Reddy 2007)

Soil	Required c
Very fine sand or silt	8.5
Fine sand	7.0
Medium sand	6.0
Coarse sand	5.0
Fine gravel	4.0
Medium gravel	3.5
Coarse gravel and cobbles	3.0
Boulders with some cobbles and gravel	2.5
Soft clay	3.0
Medium clay	2.0
Hard clay	1.8
Very hard clay	1.6

weight of the soil particles. The drag force that causes this type of erosion is directly proportional to the velocity of the flow between the grains. Moreover, the erosive forces are highest where the stream of water is concentrated at a single exit point and, once the soil particles are removed by erosion, the magnitude of the erosive forces increases due to the greater concentration of the flow and the lack of resistance considering that the grains have been dislodged. This mechanism is representative of *backward erosion pip*ing. *Backward erosion* is generally triggered where the ground surface allows an opening to be formed.

Another fundamental element of the phenomenon are the cracks caused by desiccation, which are commonly used by water, either meteoric or from any reservoir to find an easy seepage path. The openings are filled and are also kept open by filtering water, following preferential paths given for example by tree roots, burrows dug by animals or in the surroundings of installed artificial conduits.

Earth embankments are generally designed and constructed in such a way that *pip*ing formation is limited, for example by the use of special filters designed to counteract the issue. Foundation soils, on the other hand, are more susceptible to the phenomenon because they are less treated and therefore it is necessary to consider the erosion process in detail in this context. In addition, it is difficult to monitor what is happening in the subsoil and, once there is evidence that the process has taken place, it may be too advanced for any action to be taken. The main factor is lithography and in particular the presence of an aquifer confined by a layer of cohesive material.

The formation of the pipe generally occurs due to an increase in pressure in the layer of sand that generates a fracture within the layer of cohesive material, determining a preferential path that the flow of water can undertake to emerge easily. The particle removal mechanism is triggered on the downstream side of the structure, at the fracture and at the interface between the two soil layers, where the flow is concentrated and the mobilising forces are at their peak. Once the removal of particles takes place, the pipe develops in the direction opposite to the movement of the water until it reaches the upstream side of the structure; the layer of cohesive material forms the upper limit of the pipe. A hydraulic conduit is formed in which the velocity of the water tends to increase, accelerating the phenomenon: the pipe progressively increases in diameter, compromising the stability of the structure. The main evidence of the process is the leakage of "sand boils" and the presence of water at the downstream side of the pipe.

Backward erosion consists of four phases: **infiltration**, **erosion and pipe formation**, **pipe extension** and **collapse**. Taking a simple stratigraphy into account, the four characteristic phases of the phenomenon will be analysed below.

The process starts with a first **infiltration** phase triggered by the difference in hydraulic head between the upstream and downstream reservoirs. The water flows through the foundation soil until it reaches the downstream side at an exit point, which may be present naturally if the portion is constituted by coarse-grained material and there is no fine-grained soil limiting the free upflow of the water (Figure 1.6) or if there is an artificial channel crossing the cohesive layer (Figure 1.7) or a natural fracture.

On the other hand, if the exit point is not already present, the rising of water is possible when the pressure value of the water within the sandy state exceeds the weight of the overlying fine-grained soil layer, thus causing local fractures and allowing the water to escape (Figure 1.8).

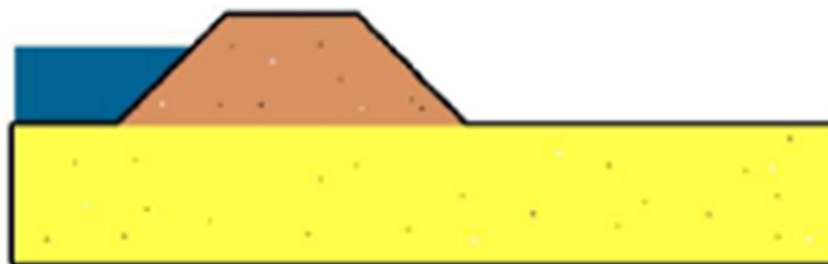


Figure 1.6. Embankment on a sandy layer (Van Beek, Knoeff, et al. 2011)

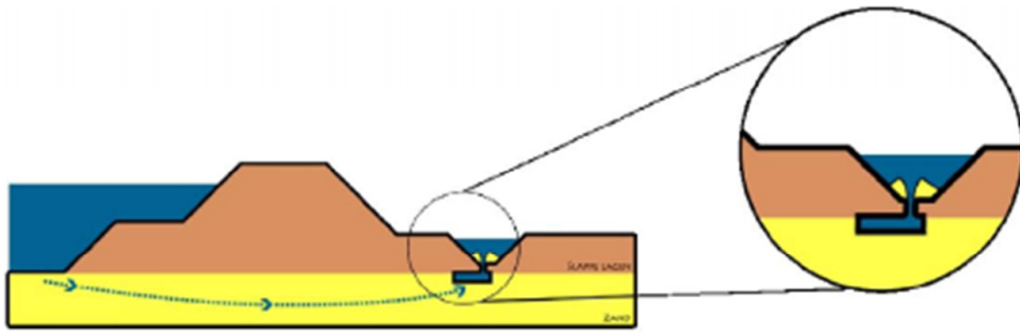


Figure 1.7. Embankment on a cohesive layer but with the presence of an artificial channel crossing it (Van Beek, Knoeff, et al. 2011)

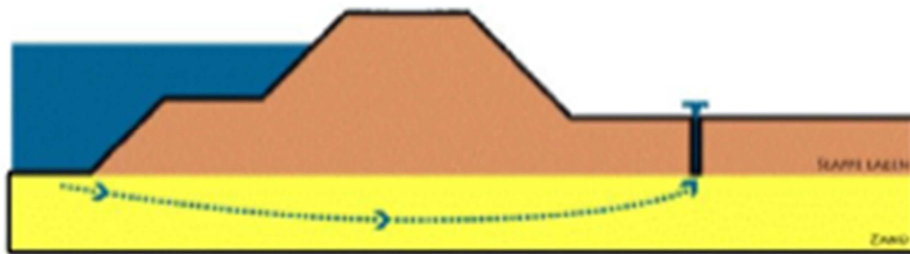


Figure 1.8. Local fracture in the cohesive layer (Van Beek, Knoeff, et al. 2011)

Once the fracture has been generated, the flow is concentrated at the outlet area and the seepage rate increases. The sand particles begin to be removed by **erosion** when the mobilising forces exceed the resisting ones.

If the portion of the sand layer is fluidised, the value of the effective force becomes positive again, because the water can flow out more easily. If the flow velocity is high enough to drag the finer soil particles with it and deposit them on the surface, so-called "sand volcanoes" (Figure 1.9) are formed, from which sand bubbles emerge and increase in size. During this phase, **pipe formation** occurs at the interface between the two layers of soil, with the shallow one acting as a roof and allowing the pipe to remain intact.

The most critical periods for the generation of this type of phenomenon are the prolonged floods of the watercourses, during which there is a particularly high difference in hydraulic head between upstream and downstream reservoirs and seepage occurs with greater forces (1.2), having more potential to move the fine particles and erode them.

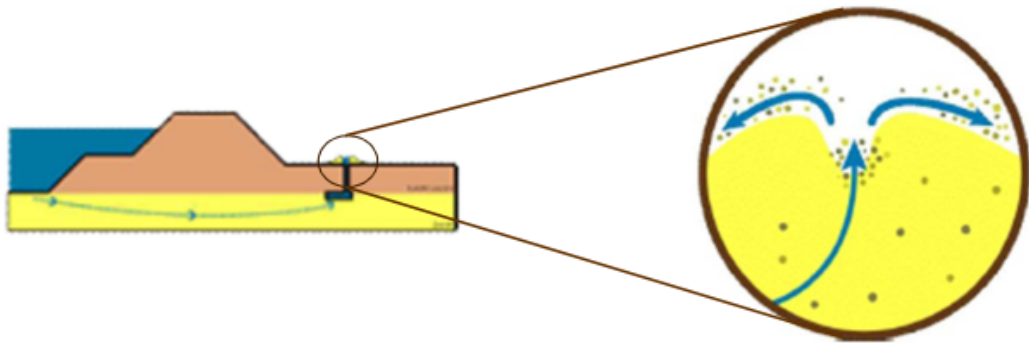


Figure 1.9. Formation of the "sand volcanoes" (Van Beek, Knoeff, et al. 2011)

A critical gradient is identified as that value for which the mobilising and resisting forces are equivalent, thus leading to a limit value that allows the pipe to lengthen. If the value of the gradient is higher than it, the dragging forces exerted by the water on the bottom of the pipe remove the grains so that a **pipe extension** occurs (Figure 1.10). Therefore there exists an upstream reservoir level such that the gradient exceeds the critical level and this height can be considered as the one at which the phenomenon takes place.

From recent literature it has been stated that *piping* is common even if the hydraulic gradients are not very large. In fact, generally values less than 1.0 had been considered safe, but there are nowadays some instances of phenomenon of *piping* occurred even with gradients as little as 0.17.

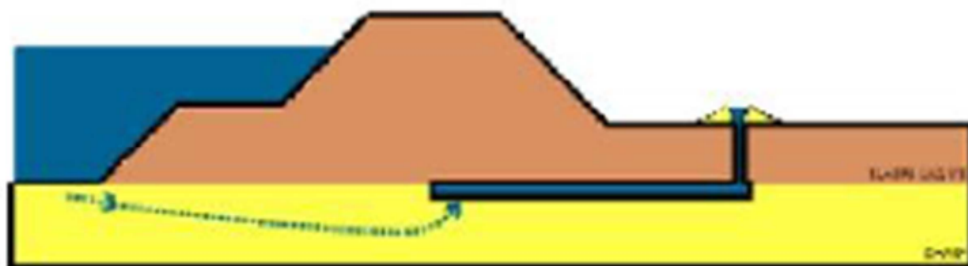


Figure 1.10. Development of a pipe (Van Beek, Knoeff, et al. 2011)

Laboratory studies have demonstrated that the hydraulic head required to enlarge the pipe is lower than that required to trigger the phenomenon, due to the fact that the laws governing the two mechanisms are different.

Initially the water flow follows a Darcian mechanism, but once the pipe is formed, the hydraulic of the phenomenon can be represented by the Poiseuille equation:

$$k = \frac{32S}{\pi\mu} \quad (1.5)$$

With:

- k hydraulic conductivity or coefficient of permeability;
- S section of the pipe;
- μ viscosity of the fluid.

When the pipe grows large enough to directly connect the upstream reservoir with the downstream reservoir, a flow of water is established so high that there is no resistance from the grains and erosion increases as a result.

Shields' theory identifies the incipient motion condition of a soil grain, both in the case of laminar and turbulent flow (Figure 1.11). It is based on the definition of the parameter Φ given by the ratio of the drag force exerted by the water on the soil and the immersed weight of the grain (Shields 1936).

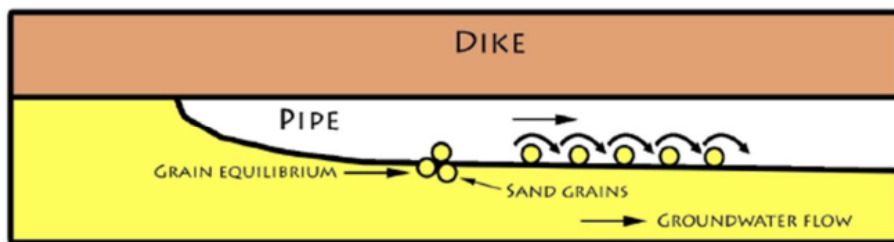


Figure 1.11. Motion initiation as a result of the drag force (Van Beek, Knoeff, et al. 2011)

The critical drag action τ is defined by:

$$\tau = \Phi(\gamma_s - \gamma_w)d \quad (1.6)$$

With:

- γ_s specific weight of grains;
- γ_w specific weight of water.

- d diameter of grains.

Considering the total number of grains, the shear stress exerted by the water on the grains can be calculated by introducing the parameter η (White 1940):

$$\eta = \frac{Nd^2}{A} \quad (1.7)$$

With:

- N number of particles;
- A area involved in the shear stress.

The drag force acting on the single particle is then given by:

$$F_s = \frac{\tau d^2}{\eta} \quad (1.8)$$

The *correction factor* α takes into account that the point of application of the force F_s is slightly displaced from the centre of the grain. The *angle of repose* ω is also introduced, which is the angle between the line of action of the weight force and the line passing through the point of contact between the particle and the underlying grains acting as support (Figure 1.12).

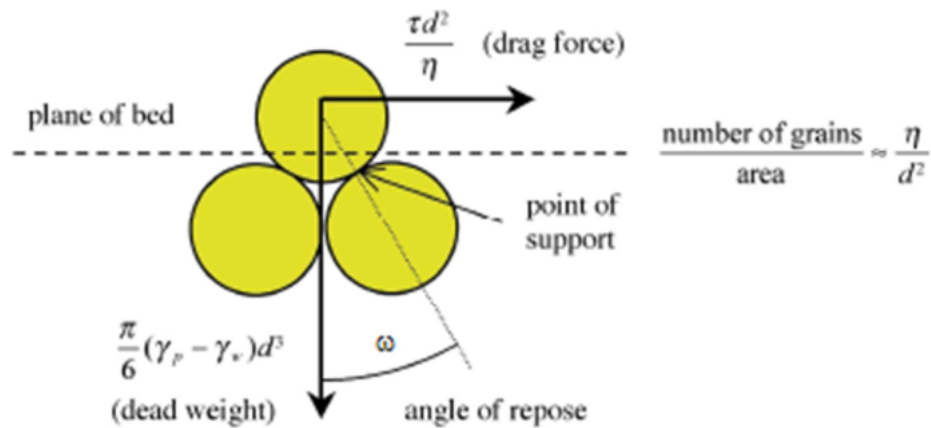


Figure 1.12. Forces acting on the particle according to the White theory (Van Beek, Knoeff, et al. 2011)

The particle is in equilibrium if the drag force is balanced by the frictional force between the grains due to the weight of the particle. The shear stress is then defined by:

$$\tau = \alpha \eta \frac{\pi}{6} (\gamma_s - \gamma_w) d \tan(\omega) \quad (1.9)$$

With the increasing of the dimension of the pipe, the water tends to erode more and more material, resulting in the **collapse** and the sinking of the structure above it (Figure 1.13, Figure 1.14). This phenomenon can act also in a short timeframe (6-12 hours) providing little warning signs and therefore becoming even more critical.

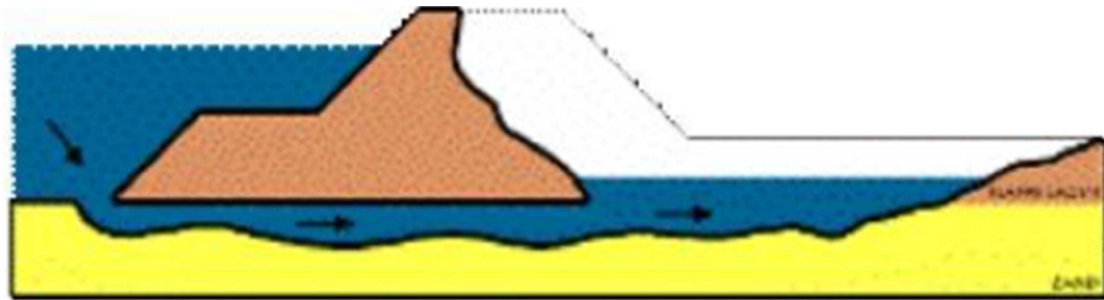


Figure 1.13. Collapse of the levee (Van Beek, Knoeff, et al. 2011)

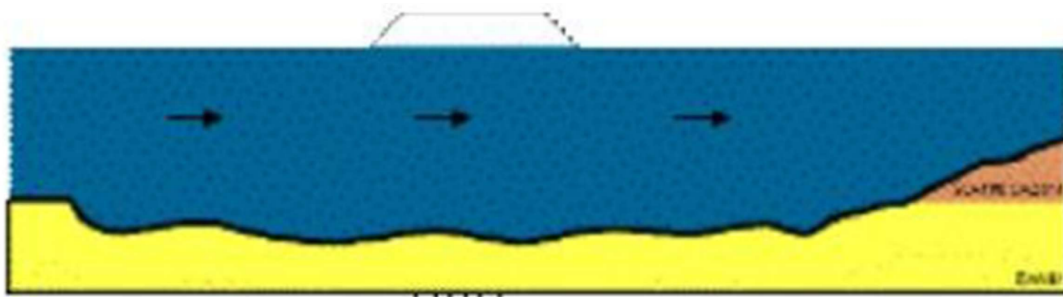


Figure 1.14. Sinking of the levee (Van Beek, Knoeff, et al. 2011)

1.2 Suffosion and suffusion

The term *suffosion* describes the gradual migration of fine material into a rigid matrix of coarse material, which is thus brought to local collapse. This phenomenon results in a framework of granular material with zones of high hydraulic conductivity that can

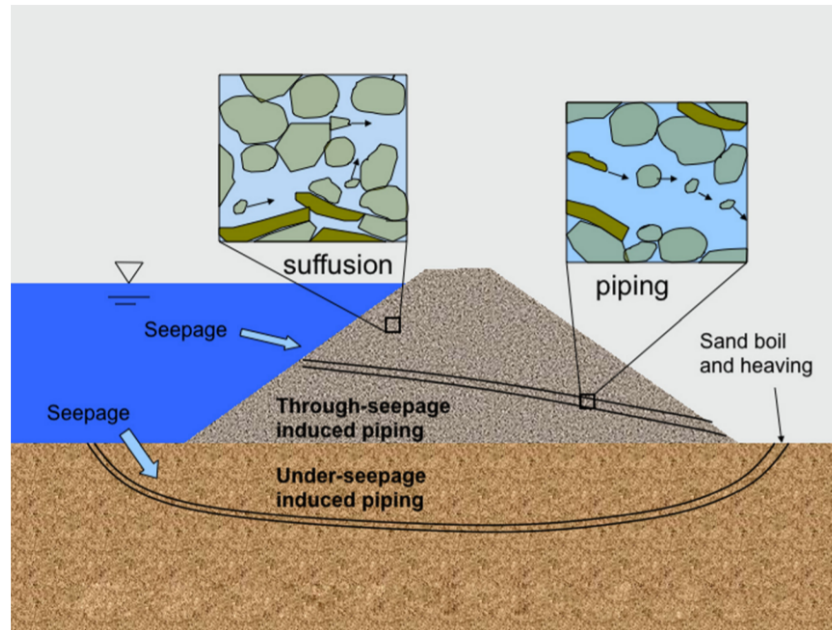


Figure 1.15. *Piping* and *suffusion* phenomena (Xiao and Shwiyhat 2012)

lead to the collapse of the soil skeleton itself. With non-cohesive materials this results in zones where water easily flows through the material and the seepage forces are consequently increased. The concept was introduced by Eastern European researchers and can result in a much slower process than what is generally observed with *piping* Jones 1981. In fact, *suffosion* can be associated with long-term effects of seepage, resulting in an increasing amount of outflow over time. The gradual loss of fine material in a material supported by a rigid solid skeleton is called *suffusion*. The seepage-induced mass loss does not induce a variation in volume and the hydraulic conductivity increases. *Suffusion* usually can take place if the matrix of soil is sufficiently coarse to allow the movement of fine particles through the openings between coarser grains. As will be described in more detail in the following chapters, the type of material used for the EPBox tests has been chosen to be well suited to the investigation of this phenomenon, with a matrix of coarser grains forming the solid skeleton through which the water flows, removing some of the finer material. If this leads to the collapse and loss of stability of the structure then it is termed *suffosion*, observed with mass loss that occurs with a reduction of volume and a consequent change in the hydraulic conductivity.

The process differs greatly from *piping* in that the latter is a phenomenon in which preferential water flow pipes are formed with a localised erosive action, whereas *suffusion* is a distributed effect that acts on the finer particles while leaving the structure of the coarse portion intact (Figure 1.15).

1.3 Other erosion mechanisms

1.3.1 Internal erosion

The term internal erosion is also used to refer to a specific phenomenon that has a mechanism similar to *backward erosion* with drag forces that remove soil particles. The difference is that in the case of internal erosion the flow occurs through fractures in the cohesive materials or along voids at the interface between soil and structure. Internal erosion does not follow the dynamics of intergranular flow and the hydraulic laws governing it are different from *backward erosion*: rather than being initiated by Darcian flow at an exit point, internal erosion is triggered by the erosive forces of water along a pre-existing planar opening. Therefore, it can be expected that internal erosion would begin according to the cubic law of flow for planar openings. In the case of internal erosion the tensile force acts along the entire length of the fracture, whereas for *backward erosion* the phenomenon is mainly localised at the exit point. Due to the nature of the hydraulic conductivity at the soil-structure boundary, fluid velocities may be more erosive for a given hydraulic gradient due to higher velocity flows. In addition, since hydraulic conductivity tends to be slightly higher at the interface, this is often the first location where increasing hydraulic gradients can manifest themselves through erosion.

1.3.2 Tunnelling or jugging

Tunneling or *jugging* refers to the erosion that occurs within dispersive soils due to precipitation. Dispersive soils are those in which the mineralogical constitution and microstructure result in repulsive forces between the fine grains greater than attractive forces when they come into contact with water. As a result, in the presence of water the finer grains separate from the soil aggregate and are therefore more easily subject to erosion. As several Australian and New Zealand researchers have explained (Jones 1981), this phenomenon occurs in the unsaturated zone of the soil. In fact, rainwater infiltrates the openings already existing in the soil, thus eroding the finer fraction of the grains. The phenomenon occurs with a high risk of collapse of the earth structures, similar to the effect of animal burrows or cavities induced by the plant root apparatus.

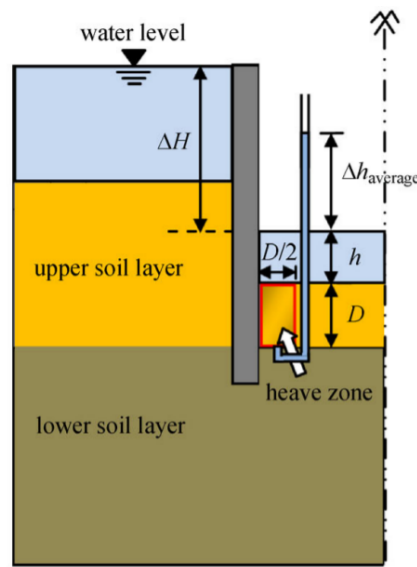


Figure 1.16. Heave zones lifted by pore water pressure in cohesionless soils where upper layer is less permeable than lower layer (Koltuk et al. 2019)

1.3.3 Heave

The phenomenon of *heave* was discussed by Karl Terzaghi (1922), who was studying the effect of the phenomenon in sheet pile cofferdams. As reported by Terzaghi, *heave* occurs when the underpressures acting in a permeable zone beneath a semi-permeable one are relatively high. A significant aspect of *heave* is that if fluid pressures in the pervious zone increase, as during a flood, a point can be reached where the uplift at the base of the semipermeable barrier exceeds the vertical effective stress of the overlying barrier (Figure 1.16).

Failure requires seepage velocity sufficient to remove individual soil particles. This phenomenon occurs when the pore water pressure developed by the seepage flow is enough to lift up the less permeable base, causing the failure by *heave*.

Chapter 2

Literature review of experimental tests

The aim of this chapter is to study how some devices and models have been developed in the literature for the analysis of internal erosion, manifested by different processes. In particular, attention has been paid to the materials used, the physical quantities taken into account, the measuring instruments used and the structure of the apparatus.

The devices impose a hydraulic gradient on a soil sample (which can be of various sizes, from a small scale to a full-scale model) positioned between an upstream and a downstream reservoir. Tests are carried out with an increasing head difference between the two reservoirs, eventually leading to the failure of the sample.

2.1 Purposely designed laboratory test

2.1.1 A tiltable model for internal erosion investigation

The effect of the direction of flow on internal erosion is very relevant. Within the same earthen embankment there may be regions where there is a flow of water directed as gravity, but also others where the flow is differently directed (Figure 2.1). For this reason, an apparatus capable of changing the relative angle between the vertical and the flow direction was developed to analyse the effect of internal erosion on samples consisting of bentonite and rock flour. In particular, having used gap-graded samples the specific phenomenon examined is *suffusion* (Pachideh and Hosseini 2019).

In order to analyse the effect of flow direction and inclination of the soil layers,

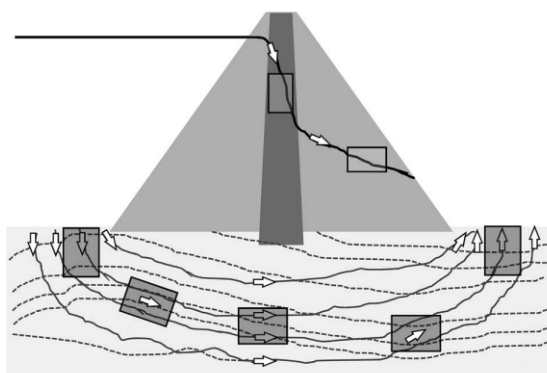


Figure 2.1. Direction of flow in different areas of an earth embankment (Pachideh and Hosseini 2019)

a two-dimensional apparatus with the possibility to rotate the sample was designed and developed. By rotating the sample at angles between 0° and 180° with respect to the vertical direction, the infiltration conditions of the water can be changed with respect to the direction of gravity while maintaining the load and pressure conditions. In order to monitor and record the data and control the testing process, a special computer software called Soil Erosion Software (SES) was designed and developed for this device. The main components of the device consist of device frames and a sample container, a water supply and pressure control system, a loading system, monitoring instrumentation, and a system for controlling and collecting the eroded mass (Figure 2.2, Figure 2.3).



Figure 2.2. Overview of the tiltable apparatus developed for internal erosion studies (Pachideh and Hosseini 2019)

The device consists of two rigid steel structures, one containing the sample container, hydraulic jacks, and input control valves, with the possibility of being rotated,

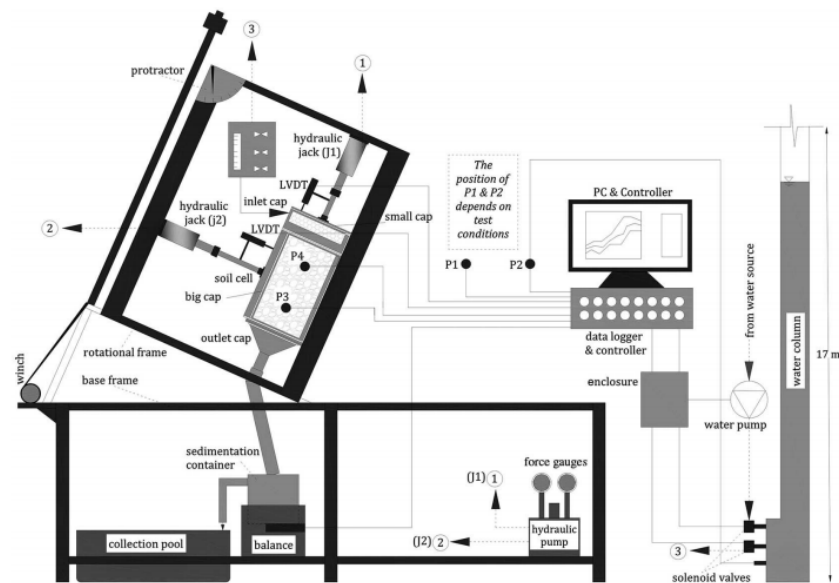


Figure 2.3. Schematic representation of the apparatus (Pachideh and Hosseini 2019)

and the other acting as a base and support for the structure above. The sample container has a base of 140 mm by 210 mm and a height of 400 mm. The ratio of length to width is approximately two, so that the container is long enough to observe possible erosional pipes and particle movement during the test. The smallest size of the box determines the maximum diameter of the soil particles, as the experimental evidences observed during the tests showed that the ratio between the diameter of the particles and the smallest size of the box must be less than about 0.2. For the experiments the author used a ratio of 0.14. The box containing the sample is divided into four sections, namely an inlet cap (small), big cap, sample cell, and outlet cap (Figure 2.4). The inlet cap is usually filled with sand so that the input is uniformly applied to the sample, the sample is placed in the sample cell, while the shape and type of the outlet cap are chosen according to the relative angle between the sample and the horizontal. The load cell is connected to the base by means of a hinge, which allows the upper part to be rotated by an angle between 0° and 90° , but with suitable modifications it can be rotated up to 180° (condition for which the flow is in the opposite direction to gravity).

The pressures are set by imposing the height of the inlet water column and applying an average gradient to the sample. A pipe with a diameter of 110 mm and a height of 17 m (equivalent to a pressure of 1.7 bar) was used for the water input. A water inlet valve with a capacity of 10 L/min was inserted at the base of the pipe, and the same valve was used for the discharge unit. In addition, a pump with a capacity of 4 bar was added so that in the case of a pressure drop the desired quantity can be

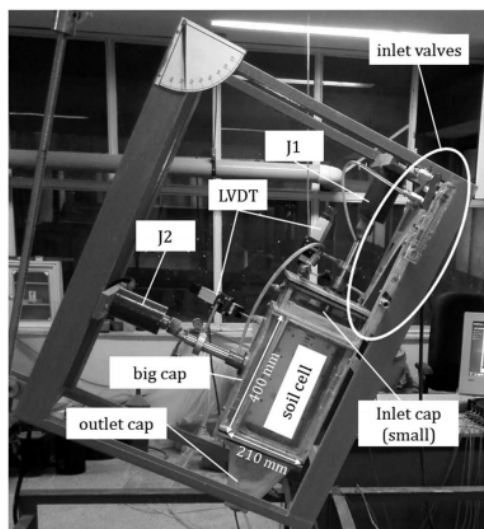


Figure 2.4. Sample container components and loading frame (Pachideh and Hosseini 2019)

generated and maintained, as well as in the case of applying higher gradients than those provided by the tube alone. The data of pressure, weight of the eroded mass and deformation of the sample are measured by means of electronic sensors, connected to a data logger and transferred to a computer, which records and monitors the progress of the test using the dedicated SES software.

Since one of the most important consequences of internal soil erosion is the change of the gradient acting on the soil, it is important to measure the water pressure and thus the gradient at any point. Here, four pressure sensors were used, with two sensors monitoring the gradient and two sensors placed inside the soil sample. The position of each of the sensors can be changed depending on the type of sample or the test angle. In this device, one plexiglass side of the container has been perforated to allow the sensors to be mounted in any position. A thin tube with an approximate length of 70 mm is also mounted inside to measure the water pressure in the centre of the sample.

The load is applied using two hydraulic jacks with a maximum displacement of 70 mm on two faces of the sample. Each jack is connected to a load plate, applying a force to the sample from two directions.

A special container was created to record the eroded mass data, consisting of a sedimentation basin, a cylindrical base and a load cell. The sedimentation basin consists of three cylinders with different diameters and heights located one inside the other. The outflow enters from the outlet into the central cylinder, then into the

outer cylinder and then into the outlet pipe. Thus, with a high probability (with an error of less than 10%), it can be said that all soil particles suspended in the outflow during a test will be deposited and collected. By increasing the amount of sediment in the sedimentation container, the force applied to the load cell also changes. The amount of particles in the outflow as a function of time can be analysed by their weight. The remarkable point in this respect is that before the start of the test, the entire sedimentation container is filled with water; therefore, after the particles have settled, changes in the load cell force will indicate changes in particle weight. The only weakness is that it will not be possible to record the amount of particles removed at any one time or to show how the size of the eroded particles has changed over a period of time.

Soils with the possibility of internal erosion are generally gap-graded. Therefore, conventional and standard methods of sample preparation cannot be used for these soils. The most important reason for this is the segregation of the grains during sample preparation. For this reason, a new method called *ideal moisture* was introduced. The method consists of reducing grain segregation during specimen preparation and compaction by adding moisture to the soil. In this method, the soil sample is prepared in a moisture that is in its most *ideal* condition compared to that found in nature. Therefore, if a sample is made in ideal moisture, it would be closer to the field conditions with regard to the arrangement of fine and coarse particles in the soil structure.

The fine soil fraction is of the rock flour and bentonite type, while the coarse aggregates (sand and gravel) are riverbed materials, with a dry density of an average of 1.7 g/cm^3 . In order to make a better simulation in the laboratory, the ratio of the size of the largest aggregate (19 mm) to the smallest size of the sample container (140 mm) was taken to be about 0.14. The tests were aimed at investigating the effect of flow direction with respect to gravity and layer direction on internal erosion *suffusion* by using filters with a mesh size equal to 2.38 mm. Therefore, a total of twelve tests were performed for soils with two different types of fine grains, as can be seen in Figure 2.5.

The input flow has been set in increasing steps of the gradient until a given value is reached and maintained constant for a given period of time, for a total of 13 steps. Three types of gradient were identified for each test. i_t erosion threshold gradient, a gradient whereby due to the seepage forces in the voids between the large particles, the finer particles start to be moved, i_t erosion occurrence gradient, a gradient whereby

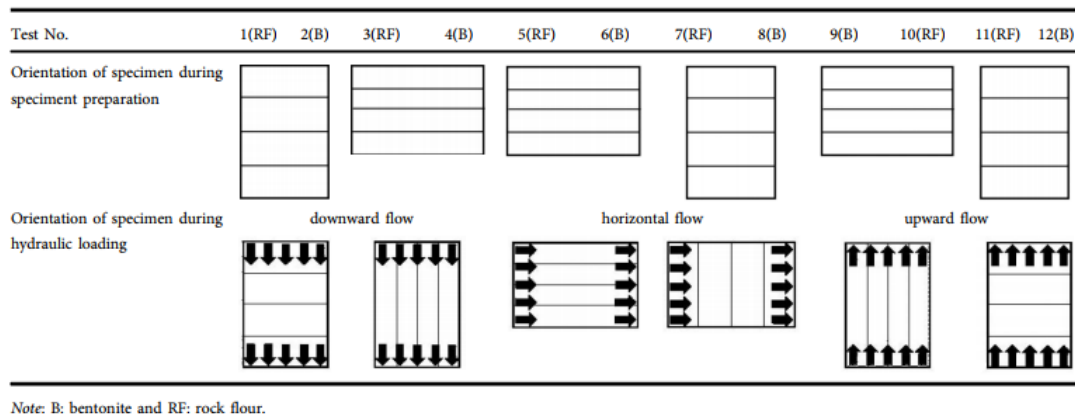


Figure 2.5. Different modes of testing (Pachideh and Hosseini 2019)

the flow of water causes the fine particles to detach and move into the spaces between the coarse soil structure, with the formation of micropipes and pipes in the soil, with the occurrence of bubbles on the surface in the case of vertical flow, and i_d erosion development gradient, for which the pipes formed expand in width and are more diffused throughout the sample. Values of specific discharge have been associated with each gradient in the results, and have been reported also the the eroded mass in terms of percentage for each test.

From the results obtained it was observed that in the case of upward flows, the time interval between the threshold and development of erosion is higher than in downward flows, although the threshold gradient in downward flows is less than in the upward ones. It is noted that the more rapid the initiation of erosion, the greater the outlet specific discharge. In general, erosion gradients are higher in upward flows and lower in downward flows, while in horizontal flows it has an intermediate value. This means that the higher the angle between the direction of flow and the direction of gravity, the greater the erosion gradient.

With regard to the eroded mass in the upward flow tests, since the particles were displaced and deposited on the upper surface of the specimen and were not transferred to the outlet, the exact measurement of the weight of the eroded mass was not possible. Furthermore, in almost all cases, for soils with fine fractions of the same type, the weight percentage of the eroded mass is higher in the case of layers parallel to the inflow than in the case of layers perpendicular to the inflow. This confirms precisely the effect of the inclination of the layers on the phenomenon of internal erosion. Through visual observations during the tests, a dependence of the pipe shape on the inclination of the soil layers was noticed. In samples where the

layers are parallel to the flow direction the pipes are generally generated as straight lines following the shape of the layer (Figure 2.6 on the right), whereas in the case perpendicular to the flow, the pipes have broken line shapes and change their path (Figure 2.6 on the left).

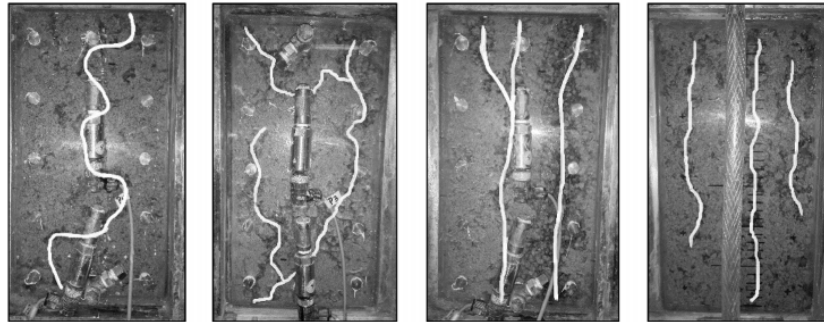


Figure 2.6. An example of the shape of the pipes in the tests (Pachideh and Hosseini 2019)

2.1.2 True-triaxial piping test apparatus

Richards and Reddy (2012) have designed a new true-triaxial *piping* test apparatus (TTPTA) with the purpose to monitor the triggering factors of *piping* under different stress and seepage conditions. The system allows the study of *backward erosion* and *suffusion* for different soil types, both cohesive and non-cohesive.

The equipment consists of a cubic cell in which the samples are placed and then subjected to confining pressure, with seepage controlled by varying the seepage rate. The device is complex (Figure 2.7) and its main element is the true-triaxial cell (Figure 2.8). It is 120 mm x 120 mm x 150 mm in size and allows control of the pressures in the three perpendicular axes. The hydraulic head in the cell is monitored with a precision differential pressure gauge, while the water pressures are measured with transducers. The pore pressures are controlled by pressurised upstream and downstream tanks and the flow through the apparatus is governed by a flow transducer. During the consolidation phase the compression is applied to the sample with air bladders and neoprene pads, sealing all the openings and allowing the isolation of the chamber before the seepage test. The TTPTA is only able to simulate the stress conditions of relatively small to medium scale embankment models, due to the limited pressures that can be reached by the load cells.

The flow out of the TTPTA is monitored by measuring voltage readings of a flow

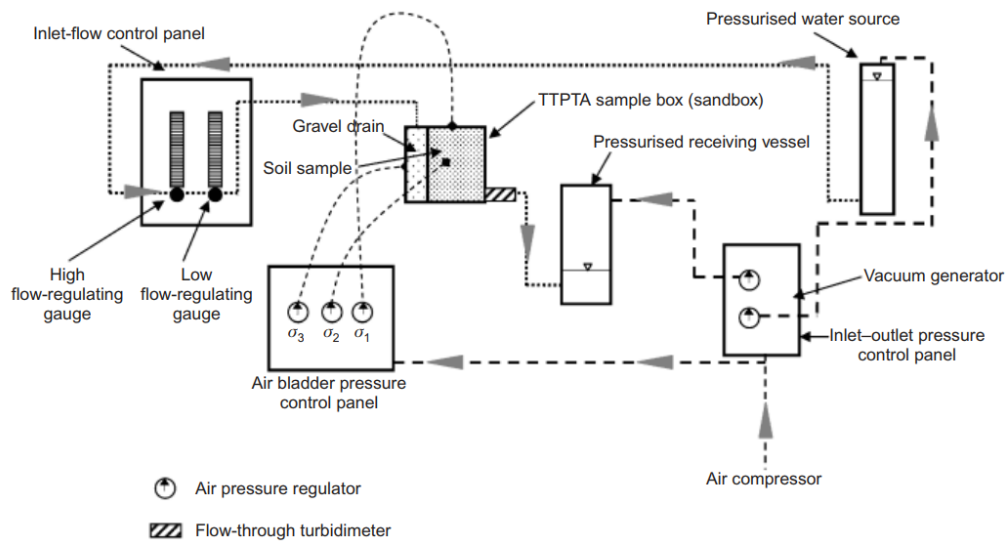


Figure 2.7. Components of the TTPTA (Richards and Reddy 2012)

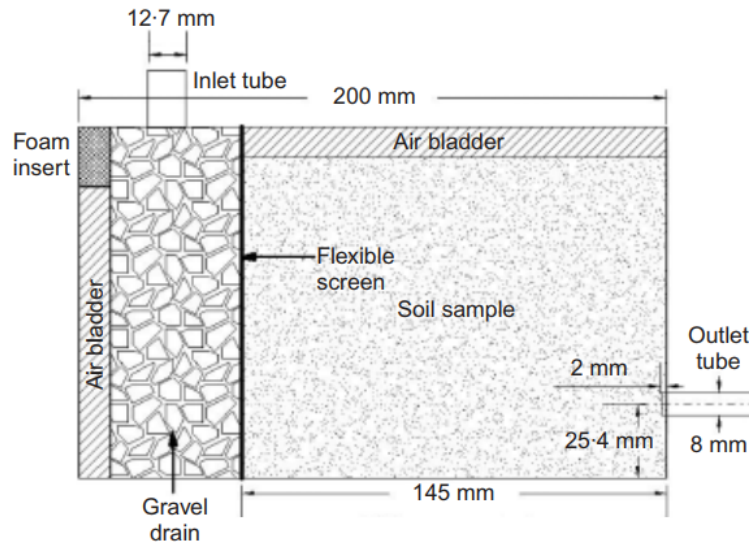


Figure 2.8. Detail of sample box of the TTPTA, with a third air bladder in the plane of the page (Richards and Reddy 2012)

turbidimeter of size 880 nm installed on the outlet port. High voltage measurements indicate that the outlet water is free of turbidity, while lower readings indicate that more particles are leaving the cell.

If the reading is zero it means that relatively large amounts of soil have been removed at the same time. If this occurs very quickly it can be interpreted as the movement of the coarser fraction of the sample, indicating the beginning of *backward erosion*. *Suffusion*, on the other hand, can be interpreted by the reading of a voltage value that gradually begins to decrease, with a small portion of the fine soil detaching from the matrix and being eroded.

The flownet within the sample (Figure 2.9) represents the flow condition in the sample and remains constant for homogeneous and isotropic sample, resulting in being dependent on the geometry of the sandbox and not on the material used.

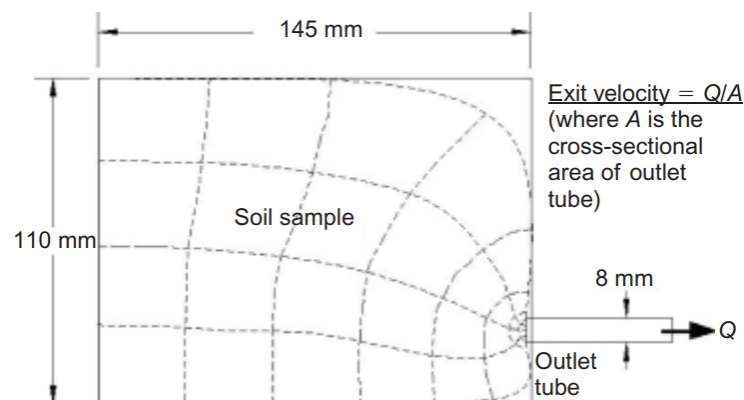


Figure 2.9. Flownet through isotropic soil samples (Richards and Reddy 2012)

The material used for the preliminary tests was sieved to remove the coarse matter and maintained at a field moisture condition. Before being placed in the apparatus, it was mixed to obtain a uniform and isotropic sample. Each sample was prepared in three layers carefully compacted to obtain the same density throughout the volume. Once in position, the soil was saturated and air was removed before proceeding with consolidation. After this stage, the upstream and downstream reservoirs were fixed at a certain pressure so that the hydraulic head and, consequently, the gradient were also fixed. Through the flow transducer the seepage test was initiated until *pipng* was reached. The testing phase was carried out with a uniform sand to ensure the repeatability of the test.

The TTPTA provides the critical velocity, meaning the seepage velocity at which *pip*ing occurs. This variable is a good predictor of *pip*ing, better than void ratio or gradient. In fact, the velocity is given by the combination of hydraulic conductivity and gradient, meaning that it takes into account the role of both of them at the same time.

Eight sets of experiments were conducted using different soils and testing conditions. For the first six, a uniform commercial sand was used, for the seventh a laboratory mixed soil, and for the last set of tests, field samples from four different dams in the central USA were employed (Figure 2.10).

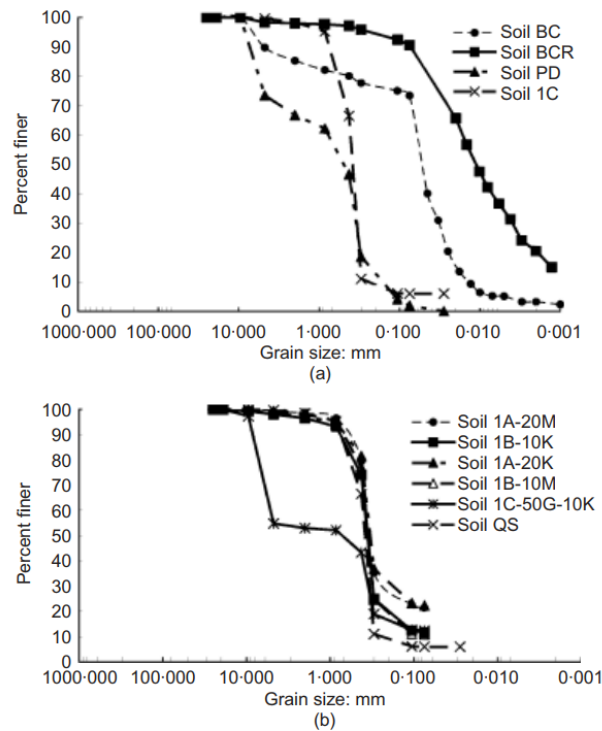


Figure 2.10. Grain-size distribution of (a) field soils and (b) mixed soils prepared by mixing commercial uniform sand (QS) with kaolin (K), montmorillonite (M), or gravel (G) (Richards and Reddy 2012)

The initial void ratio e_0 was used as an approximation of field conditions, as well as the dry unit weight γ_d , which were reported for every test, derived from measurements made on each soil type of the specific gravity. The samples were slightly compacted to simulate the *in situ* conditions of uncompacted foundation soils or poorly constructed dams.

The first three set of tests followed the stress conditions reported in Figure 2.11a,

while the last five using stresses as indicated in Figure 2.11b.

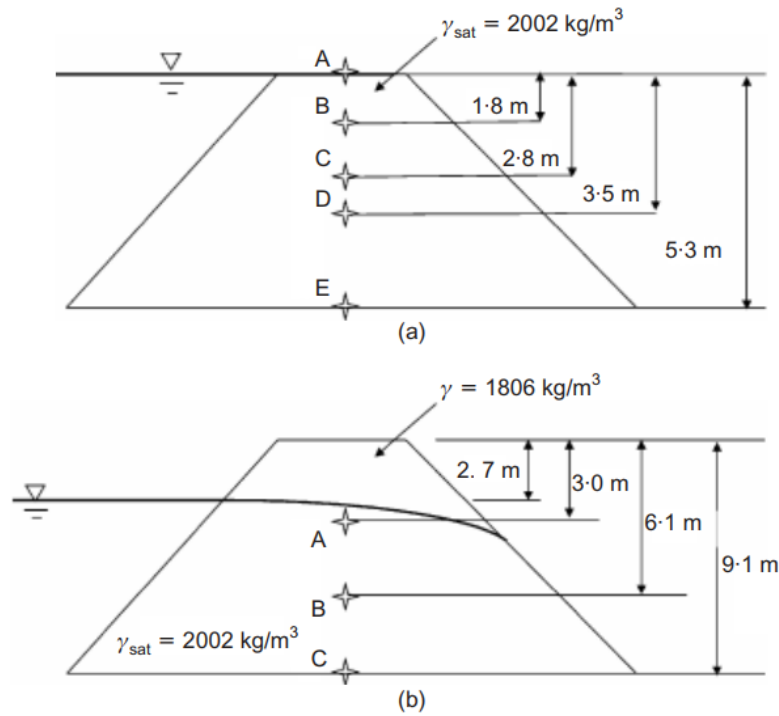


Figure 2.11. (a) General stress states (A, B, C, D, E) for initial tests; (b) general stress states (A, B, C) for subsequent tests (Richards and Reddy 2012)

The critical velocity v_{crit} is calculated from the Q_{crit} through Darcy's equation:

$$v_{crit} = \frac{Q_{crit}}{A} \quad (2.1)$$

With:

- A cross-sectional area of the outlet pipe.

For the assessment of stress conditions, values for p' and q' were computed, where:

$$p' = \frac{\sigma'_1 + \sigma'_2 + \sigma'_3}{3} \quad (2.2)$$

$$q' = [(\sigma'_1 - \sigma'_3)^2 + (\sigma'_2 - \sigma'_3)^2 + (\sigma'_1 - \sigma'_2)^2]^{(1/2)} \quad (2.3)$$

When p' resulted in negative values, it were established conditions for hydraulic fracturing.

The first three series of tests were performed changing the stress state condition and the effect on the seepage velocity required to trigger *pipiing*. The fourth was

Table 2.1. Summary of test series (Richards and Reddy 2012)

Test series	Test parameter*
1	Magnitude of confining stress ($K = 0.5$)
2	Shape of stress ellipsoid or minor/intermediate principal stresses ($K = 0.5, 0.33, 0.25$)
3	Effective stress (pore pressure)
4	Seepage direction ($\hat{c} = +10, +7.5, 0, -7.5, -10$)
5	Initial void ratio
6	Rate of increase in seepage rate
7	Behaviour of cohesive and non-cohesive laboratory-mixed soils
8	Behaviour of cohesive and non-cohesive field soils

* Series 1–6 were conducted with laboratory uniform sand (QS).

conducted to understand the effect of the direction of seepage, the fifth the role of compaction or initial void ratio, the sixth the effect of seepage rate increase and the last two were performed on a laboratory mixed soil and field samples. A summary of the tests is provided in Table 2.1.

A relationship was found between the effective mean confining stress (p') and the critical seepage velocity. Actually only the principal component of it affects the initiation of *piping* in low plasticity soils, while there is no correlation between it and the other two principal stresses. The critical seepage velocity increases with an increase in the maximum principal stress providing a greater stabilising effect on *piping*.

Regarding the relationship with the seepage direction, it was found that the critical velocity is significantly lower when the vector has an angle of at least 10° below the horizontal. Higher compaction results in an increase in seepage velocity, whereas no relation was found with respect to the rate of increase in seepage.

In the kaolin mixed soils with low-plastic fines *suffusion* was the first phenomenon observed, occurred at lower velocities than the ones required for *backward erosion*. Once *suffusion* took place, it progressively transformed into *backward erosion*. Soil mixed with montmorillonite with high-plastic fines had a different behaviour, failing by concentrated leak erosion, rather than by *backward erosion* or *suffusion*.

Regarding the two field sandy soils tested, the phenomenon observed was dependent on the quantity of fines present, while for clayey and silty ones there was always a concentrated leak erosion process.

2.1.3 Suffusion experimental investigation

An apparatus for studying *suffusion* was developed by Xiao and Shwiyhat (2012). It consists of a triaxial cell modified in a way to allow the passage of water and the collection of eroded material in a special container maintained at atmospheric pressure (Figure 2.12).



Figure 2.12. *Suffusion* experimental triaxial cell (Xiao and Shwiyhat 2012)

Special pressure gauges connected to an A/D converter are inserted into the equipment to display the test data in real time. Moreover, a volume change unit (VCU) was installed to monitor the total migration of the confinement water into and out of the triaxial cell, thereby monitoring the total volume change of the specimen.

The cell has a cylindrical internal section with dimensions 5.1 cm in diameter and 10.44 cm in height, inside which the properly compacted sample is placed. The specimen inside the triaxial cell is then saturated and consolidated. A procedure that can be used to speed up the saturation process is to inject carbon dioxide to free the sample from bubbles, since this gas dissolves in water in a shorter time than simple air. The base of the triaxial cell has been modified to maintain atmospheric pressures and ensure easier collection of eroded material, thanks to the conical shape of its inside (Figure 2.13).

During the seepage phase, loads are imposed for fixed time intervals and known volumes of water. The hydraulic gradient is applied by imposing a certain pressure value at the top of the sample and leaving the pressure at the bottom equal to the

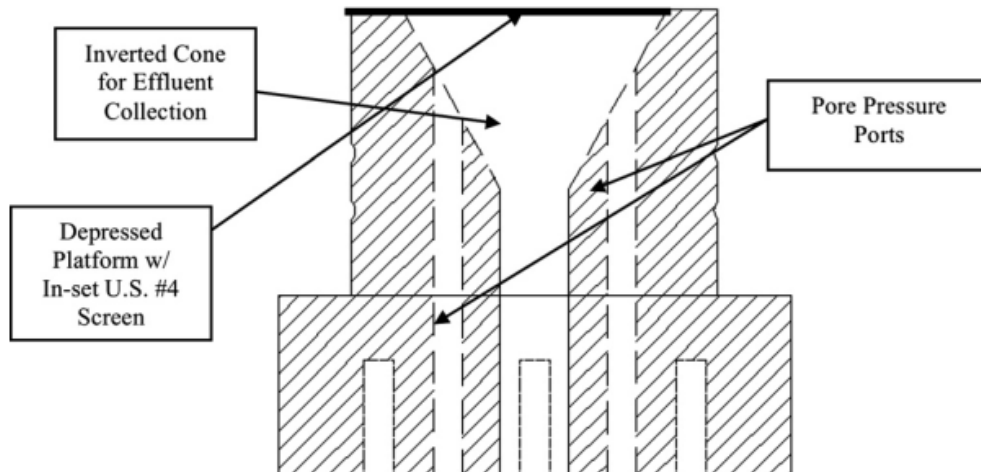


Figure 2.13. Modified base of the triaxial cell (Xiao and Shwiyhat 2012)

atmospheric pressure. By using triaxial cells it is possible to apply different values of confining pressure in order to study the dependence of erosion on the state of confinement of the sample.

The water and the eroded material are conveyed into an outlet reservoir underneath the equipment and collected in a graduated container. The hydraulic conductivity value is obtained by measuring the volume of water and soil removed. The contents of the graduated cylinder are weighed and sieved in order to determine the quantity of eroded material and its particle size distribution in relation to the volumes of water used.

The test ends when no further material is eroded from the cell. Following the seepage test, a triaxial compression test may also be performed to study the change in mechanical response of the sample after erosion.

The experimental results provide evidence that *suffusion* can affect the physical and geomechanical properties of soils. Although the effects are apparently minor in small-scale tests, the duration of time over which the phenomenon occurs can be much greater in the field.

In the presence of *suffusion*, changes may occur in hydraulic conductivity, shear strength characteristics and volume (for example settling, turning into a *suffosion* phenomenon). Hydraulic conductivity decreases as *suffusion* progresses and the re-

duction in k varies by up to two orders of magnitude. The degree of reduction is highly dependent on the internal clogging that occurs. With regard to the changes in compressive strength, different results are obtained depending on the sample examined. Volume changes show approximately one third to three quarters of a percentage reduction for the soil samples tested.

2.2 Assessment of erodibility properties

The study of soil erosion within cracks was also carried out in literature through the use of the Hole Erosion Test (HET) and the Slot Erosion Test (SET). Erosion characteristics were assessed from the erosion rate index, which measures the rate of erosion, and the critical shear stress, which represents the minimum shear stress able to remove a soil particle from the solid skeleton. The erosion rate is dependent on the characteristics of the material used in terms of both properties and composition, while the critical shear stress depends mainly on the grain size and cohesion of the material. Knowledge of these characteristics is important because it allows to better understand the possibility of failure of a fractured embankment due to *pip*ing phenomena.

The erodibility of a soil can be described by two aspects: the rate of erosion when a given hydraulic shear stress is applied to the soil and the ease with which the soil starts to erode.

From the tests performed (Wan and Fell 2004) it was estimated that there is a linear relationship between the erosion rate and the hydraulic shear stress expressed by:

$$\dot{\epsilon}_t = C_e(\tau_t + \tau_c) \quad (2.4)$$

With:

- $\dot{\epsilon}_t$ rate of erosion per unit surface area of the slot/hole at time t (kg/s/m²);
- C_e proportionality constant named coefficient of soil erosion (s/m);
- τ_t hydraulic shear stress along the slot/hole at time t (N/m²);
- τ_c critical shear stress (N/m²);

C_e has been obtained from numerous HETs or SETs tests and is a small number in the order of 10^{-1} to 10^{-6} s/m. Since $-\log(C_e)$ is more often used in analysis of

correlation and representation of results, it is more convenient to use the Erosion Rate Index (I) defined by:

$$I = -\log(C_e) \quad (2.5)$$

I varies from 0 to 6. A small I implies a soil which is more rapidly erodible.

2.2.1 Hole Erosion Test

In HET the soil specimen is compacted in a mold usually employed for the standard compaction test. The concentrated leak is simulated by perforating a 6 mm-diameter hole along the longitudinal axis of the sample, having a maximum length of 117 mm. The sample is placed in a cylindrical container positioned horizontally and confined by two wire nets at the two side ends; a 20 mm long stratum of gravel is placed in the left chamber of the box to allow seepage and at the same time support the soil sample (Figure 2.14).

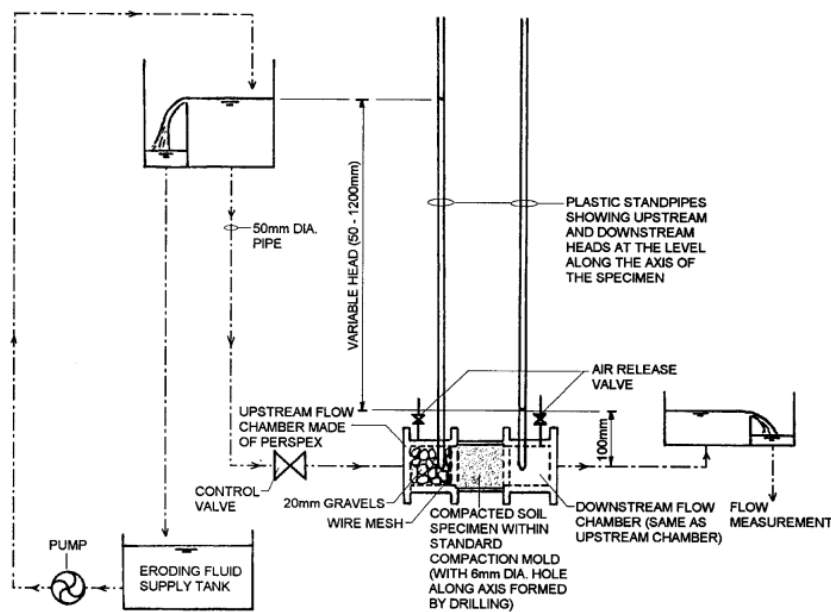


Figure 2.14. Schematic drawing of the HET apparatus (Wan and Fell 2004)

The difference in hydraulic head between the upstream and downstream reservoir has been set from 50 to 1200 mm. The upstream level is increased until the erosion process takes place and then held constant throughout the test. The water pressure upstream and downstream of the sample is indicated by the height of water reached

within the piezometers inserted immediately before and after the soil sample. The flow rate is used as an indirect measurement of the diameter of the hole drilled at the beginning of the test.

The hydraulic shear stress along the cavity can be expressed as:

$$\tau_t = \rho_w g s_t \frac{\phi_t}{4} \quad (2.6)$$

With:

- τ_t hydraulic shear stress on the surface of the preformed hole at time t (N/m²);
- ρ_w density of the eroding fluid (kg/m³);
- g gravity acceleration;
- s_t hydraulic gradient across the soil sample at time t (m);
- ϕ_t diameter of the preformed hole, assumed to remain circular, at time t (m).

The rate of erosion per unit surface area of the slot at time t ($\dot{\epsilon}_t$), is provided by:

$$\dot{\epsilon}_t = \frac{\rho_d}{2} \frac{d\phi_t}{dt} \quad (2.7)$$

With:

- ρ_d dry density of the soil (kg/m³).

The diameter ϕ_t of the pipe at time t can therefore be estimated from:

$$\phi_t = \left(\frac{16Q_t f_{Lt}}{\pi \rho_w g s_t} \right)^{1/3} \quad (2.8)$$

or

$$\phi_t = \left(\frac{64Q_t^2 f_{Tt}}{\pi^2 \rho_w g s_t} \right)^{1/5} \quad (2.9)$$

With:

- f_{Lt} and f_{Tt} friction factors relating shear stress to the mean flow velocity;
- Q_t flow rate at time t (m³/s).

If the conditions of flow are laminar it can be used (2.8), whereas (2.9) is for turbulent flow.

During the test s and Q are measured at given time intervals (10-20 s), while the dimension of the diameter of the pipe is imposed at the beginning of the test and measured at the end of it. By approximating the results obtained with a best-fit straight line represented by (2.4) the value of C_e can be computed for each test (Figure 2.15).

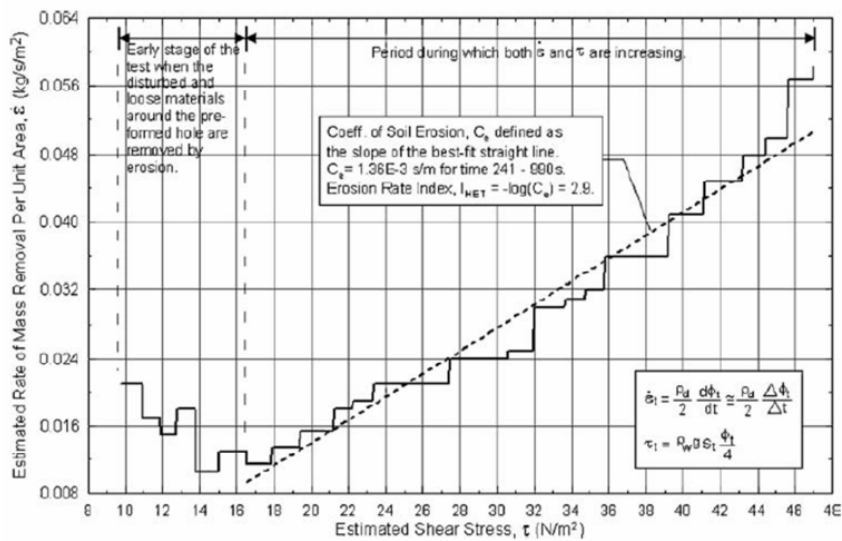


Figure 2.15. Estimation of erosion rate per unit area as a function of shear stress (Wan and Fell 2004)

2.2.2 Slot Erosion Test

In the SET, a soil sample is compacted and placed inside a rigid rectangular aluminium box. The box is 150 mm wide, 100 mm deep and 1000 mm long and is closed with a plexiglass cover (Figure 2.16).

The sample of material employed is compacted inside the box. The compaction step is carried out by layers of a predetermined thickness, predetermined mass and specific water content.

The soil sample is supported laterally inside the box by wire mesh and a 20 mm layer of gravel, as is the case with the HET; the right-hand part, on the other hand,

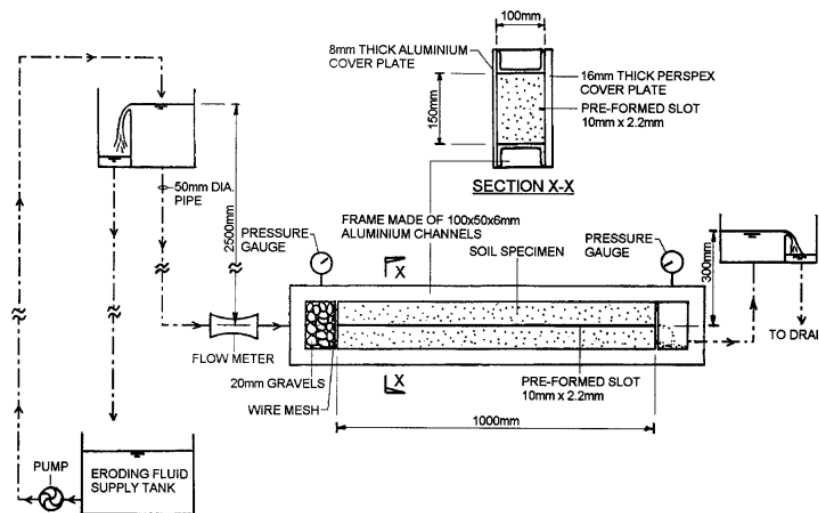


Figure 2.16. Schematic drawing of the SET apparatus (Wan and Fell 2004)

forms a reservoir for collecting the eroded material.

To initiate the erosion process, a slot of 10 mm width all along it and 2.2 mm height is created at the top of the sample. The slot is visible through the transparent wall so that the evolution of the erosion process can be monitored during the test. The process of water seepage is then initiated by imposing a hydraulic gradient; two tanks are used for this purpose, filled to 300 mm for the downstream one and 2500 mm for the upstream one; these values were defined by trial and error, testing different soil samples.

At regular time intervals of approximately 10-20 seconds the following are monitored: the pressure difference, using pressure gauges installed one at the beginning of the box and one at the end of the sample, the flow rate, evaluated with flow measuring devices placed in the right-side of the box and the volume of eroded material collected downstream. The evolution of the pipe inside the soil sample is also monitored by means of digital images.

The test is considered completed before the slot widens to the edge of the box or before the flow rate exceeds the values measurable during the test. The plexiglass cover is then removed and the depth of the eroded sample is measured using a suitable gauge. The sample taken at the end of the test is weighed and its water content is determined.

Knowing the diameter of the hole at the beginning and at the end of the test, the

hydraulic gradient and the effluent flow rate, it is possible to estimate the shear stress with which the erosion process starts and the erosion rate of the soil. A constant cross-section of the sample along its length as well as the shear strength and the wetted perimeter are introduced as simplifying assumptions; furthermore, the flow resistance is provided only by the soil surface in contact with the created crack, considering that of the plexiglass cover negligible.

2.2.3 Results

The results obtained from different soil samples, which were subjected to both HET and SET, show that the erosion rate is strongly influenced by the water content with which the soil is compacted. In most of the samples tested, those compacted with a higher water content showed greater resistance than those compacted with a lower one. In terms of the critical shear stress τ_c of different specimens, no particular connection with the soil properties is apparent. The HET results on the samples show the general trend that coarse-grained soils have lower initial critical shear stress (τ_0) values than fine-grained soils, and that the value of a fine-grained soil increases as its erosion rate index increases (Figure 2.17).

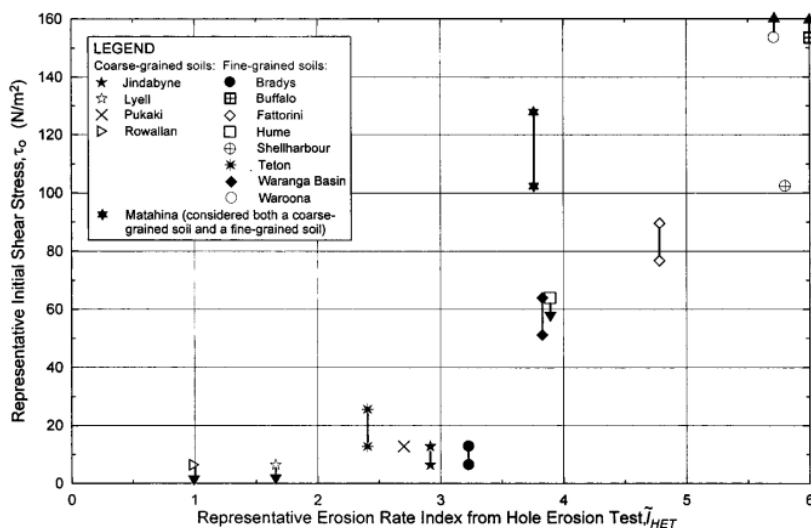


Figure 2.17. Initial shear stress versus erosion rate index (Wan and Fell 2004)

The results of both HET and SET under identical conditions and conducted on the same soil specimen are considered well reproducible and comparable. Both tests are characterised by relatively long preparation and execution times and the erosion process is time-dependent. The HET is simpler and more economical as it uses a

smaller soil sample size than the SET. On the other hand, the SET has two major advantages: firstly, due to the presence of the plexiglass cover, it is possible to observe how the drilled groove evolves, and secondly, the considerable length of the sample contributes to the stability of the grains against the water pressure exerted upstream and downstream of the sample.

2.3 A real scale test

In order to validate the results obtained at the small and medium scale, it can be beneficial to have a full-scale model available. At the University of Delft in the Netherlands, studies were conducted which led to the development of the model at IJkdijk in the Northeast of the Netherlands (Van Beek, Knoeff, et al. 2011). Two large basins measuring 30 x 15 m were prepared, filled with two different types of sand, with a d_{50} of 150 μm and 200 μm , referred to as "fine sand" and "coarse sand" respectively (Figure 2.18). The sand was placed in layers and densified until it had a relative density of at least 50%, after which it was saturated.

A clay embankment with a height of 3.5 m and a slope of 1:2 was built on top of the sand by densification of small clay units, resulting in an embankment with a 15 m long infiltration path (Figure 2.19).



Figure 2.18. Filling of the basin with sand and construction of the levee (Van Beek, Knoeff, et al. 2011)

In the downstream part, an overflow was created to keep the reservoir level constant at a height of about 10 to 20 cm below the sand layer. The level of the downstream reservoir, on the other hand, can be increased to a height of 3 m and kept constant

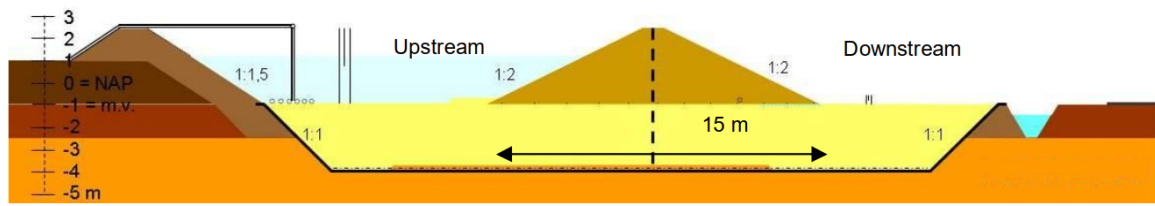


Figure 2.19. Cross-section of the experiment (Van Beek, Knoeff, et al. 2011)

Table 2.2. Testing program (Van Beek, Knoeff, et al. 2011)

Test nr.	Sand type	Monitoring equipment	Objective
1	Fine sand	Low disturbance techniques	Validation of model and process / Testing monitoring techniques
2	Coarse sand	No additional monitoring	Validation model and process
3	Fine sand	No additional monitoring	Validation model and process
4	Coarse sand	High disturbance techniques	Testing monitoring techniques

by a pump system capable of discharging $150 \text{ m}^3/\text{h}$.

To monitor pipe formation, multiple rows of pore pressure gauges were installed between the sand and clay layers, and fibre optics were placed to measure temperature and strain difference. Monitoring wells were set up to measure the head difference and water pressure in the two reservoirs, with a flow meter connected to the overflow unit.

Four tests were performed in order to fulfill the three objectives of the project: the validation of the calculation model, investigation of the failure process and testing of the monitoring equipment. Considering that some of the monitoring techniques used were invasive and could interfere with the validation of the model, it has been defined a program using monitoring equipment more and more invasive as shown in Table 2.2. The fourth test indeed was considered by the authors as too disturbed to be considered as not influent on the analysis of the process.

Each test was performed increasing the head difference with 0.1 m every hour until seepage took place. If material transport was observed, the increase in hydraulic head was postponed until the phenomenon had ceased, although due to time constraints this rule was not always respected. If sand craters formed in the downstream reservoir, they had to be removed manually to avoid changing the hydraulic gradient.

The *piping* process was divided into the classical four stages, starting with seepage and ending with collapse (1.1.3).

Initially, only seepage without material transport was observed, which was useful for

Table 2.3. Relative density and hydraulic conductivity obtained by the first three tests (Van Beek, Knoeff, et al. 2011)

Test nr.	Sand type	Relative density [%] ¹⁾	Permeability [m/s] ²⁾
1	Fine sand	60	8E-5
2	Coarse sand	75	1.4E-4
3	Fine sand	60	8E-5

determining the hydraulic conductivity of the sand layer and verifying that the state of saturation was adequate. The relative density and hydraulic conductivity levels obtained are reported in Table 2.3.

Erosion has already appeared at gradients between 0.007 and 0.09 with traces of sand observed in the downstream reservoir with a diameter of approximately 10-30 cm. These spots appear even without a visual movement of sand, but they mean that transport is taking place within the foundation soil, but without affecting the state of pore pressures.

Once the gradient of 0.1 was exceeded, sand boiling was observed, with the opening of pipes but without the accretion of a crater due to the transport and redeposition of the eroded material. With the further increase in hydraulic head, the formation of new pipes and the growth of existing pipes was observed, with the crater rising (Figure 2.20).

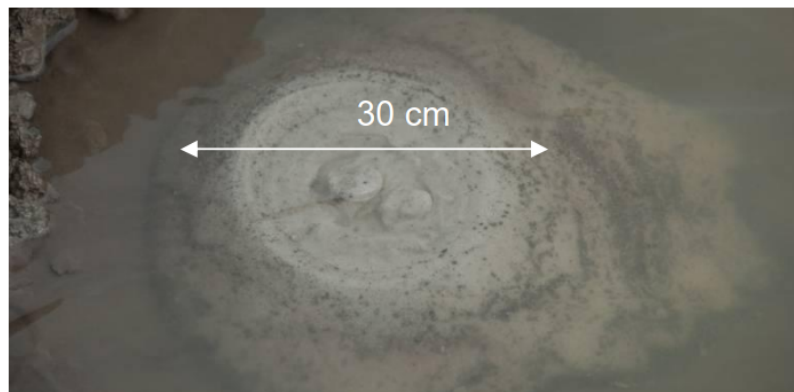


Figure 2.20. Crater of sand increasing (Van Beek, Knoeff, et al. 2011)

The amount of erosion remained constant (0.5 kg/h) throughout the duration of the application of a given hydraulic head. As the hydraulic head increases, the amount of eroded material also rises. The creation of a new pipe is observed by means of a local decrease in pressure, as shown in (Figure 2.21).

As soon as the channel becomes long enough to reach the upstream reservoir from the downstream reservoir, the process of channel widening begins. The initiation of

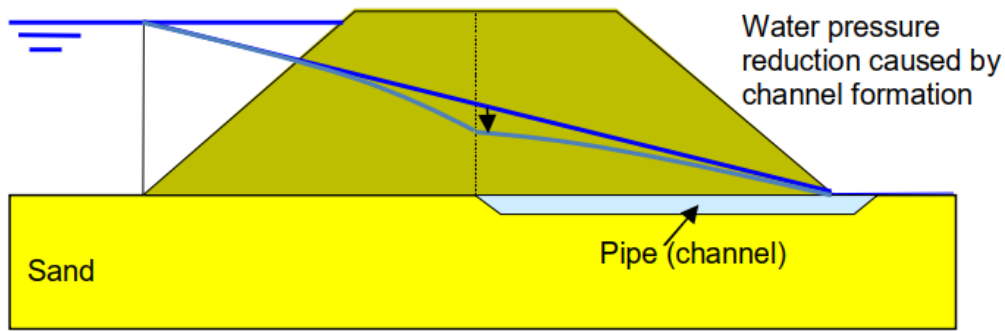


Figure 2.21. Local decrease of water pressure (pale blue line) caused by formation of pipes compared to initial water level (blue line) (Van Beek, Knoeff, et al. 2011)

the process cannot be observed in the behaviour of sand boils because the amount of eroded does not change initially as indicated by Figure 2.22. Instead, an increase in pressures can be observed because the widened channel provides less hydraulic resistance (Figure 2.23).

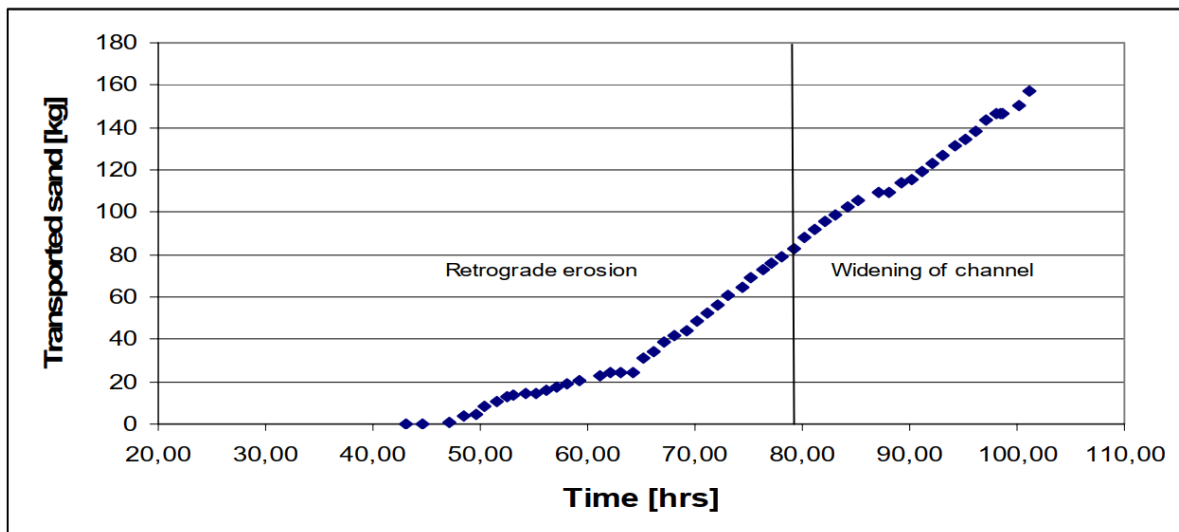


Figure 2.22. Cumulative amount of transported sand in test 3 (Van Beek, Knoeff, et al. 2011)

As the channel widens, an increase in erosion is then observed (Figure 2.24). After that, the flow may lead either to the collapse of the structure having created a cavity in it, or the embankment may deform and close the channel causing a decrease of transported material. Actually this second phenomenon leads to a subsequent re-opening of the channel and a new collapse may occur.

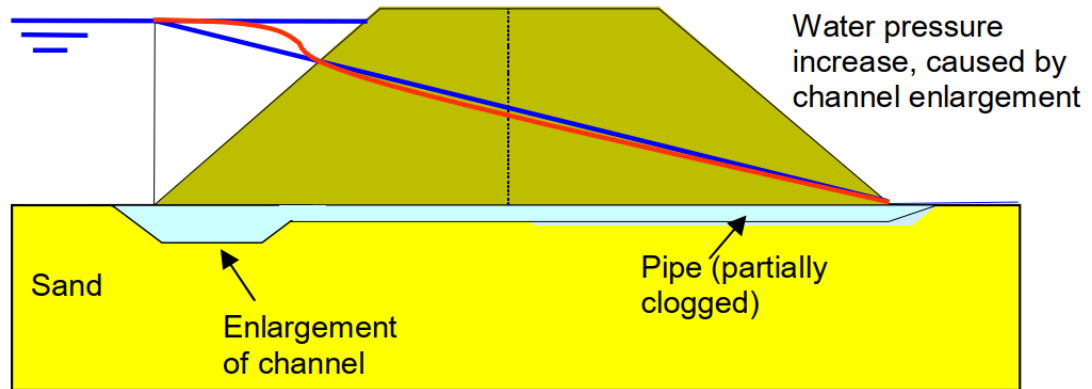


Figure 2.23. Change of water pressure in the sand as a result of channel enlargement (red line) compared to initial one (blue line) (Van Beek, Knoeff, et al. 2011)



Figure 2.24. Widening of the channel with a consequent increase in the eroded material (Van Beek, Knoeff, et al. 2011)

Collapse occurs with an increase in turbulent flow and material transport. Openings begin to appear on the surface of the embankment and part of the toe is eroded (Figure 2.25). The amount of water flowing from upstream to downstream is so great that the first level cannot be maintained constant and consequently the gradient drops. In reality, this decrease does not take place and the consequences are therefore even more devastating than those observed in the test.



Figure 2.25. Collapse of the levee (Van Beek, Knoeff, et al. 2011)

2.4 Summary and remarks

By means of a literature review of some models and devices developed, the features of what has been achieved by other authors have been highlighted so as to take as an example those considered effective and improve their weaknesses where possible, as summarised below.

A tiltable model was employed to investigate the effect of flow direction on internal erosion (*suffusion*) using a gap-graded material. The sample can be rotated and the data are recorded using special software developed specifically for this equipment. The limitations in material collection are that it is not possible to measure in real time the amount of eroded particles or their particle size distribution. Measurement problems have been encountered in the case of vertical flow due to the sedimentation of eroded particles on top of the sample in the case of vertical seepage tests. Internal erosion triggering data are obtained in relation to the angle of inclination of the flow

with respect to the vertical. The size of the sample is strictly related to the size of the cell in which it is placed.

The TTPTA is a different machine to the previous one, but it is also designed to monitor the factors that trigger *piping*. It is not able to be rotated and therefore does not allow the influence of flow direction to be assessed. It employs turbidity readings to measure the amount of eroded material present in the outlet.

Suffusion investigations can also be carried out in a triaxial cell to evaluate the influence of the confinement state of the sample on erosion. The volume difference of the sample and the amount of eroded material is measured, as well as the hydraulic conductivity by measuring the volume of water removed. At the end of the seepage test, a triaxial compression test is performed to evaluate the change in mechanical response of the sample after the removal of material.

HET and SET are useful for estimating erodibility as a soil characteristic, but are not used to assess how the phenomenon arises and develops. In HET, the sample is drilled along its longitudinal axis and it is measured how its diameter changes during a seepage test. The shear stress on the surface of the cavity and the erosion rate are obtained, while the pressure upstream and downstream of the sample is measured by means of piezometers. In SET, the sample is longer than the previous one and a slot is created above it. The process starts with the imposition of a hydraulic gradient and is also monitored visually through the transparent walls. Measurements of pressure, flow and eroded material are collected.

The real scale model is useful for validating the results obtained with smaller ones. Through this test, the initiation and development of seepage phenomenon can be observed in a manner similar to that which would develop on the field. To monitor pipe formation, pore pressure gauges were installed and fibre optics were placed to measure temperature and strain difference, whereas monitoring wells were set up to measure the head difference and water pressure in the two reservoirs.

The new device has been designed allowing for the analysis of various internal phenomena such as *suffusion* and *piping* (but also a HET and SET could be performed in it), pressurised tests with high gradients, different sizes of samples, measurement of pressures, visual inspections thanks to the transparency of walls, positioning of the sample with inclined layers and filters that can be easily replaced.

Chapter 3

The EPBox

The equipment already discussed in the literature and described in the previous chapters has limitations due in general to the lack of possibility of varying the characteristics of the tests in terms of shape and size of the sample, stratification in the reconstruction of the soil and seepage path. Machinery often constrains the shape and size of the sample without guaranteeing a possible modification of length and thickness as required, as well as the seepage path takes place in most cases in a direction parallel to the layers. Bearing these restrictions in mind, the Erosion-Piping Box (EPBox) that has been developed aims at overcoming them, to obtain a single machine that allows different types of tests to be carried out in different conditions (Figure 3.1).

In particular, the new device allows to:

- analyse various internal erosion phenomena;
- use models of different sizes;
- perform pressurised tests when high gradients are to be achieved;
- install piezometers to directly measure pressures in the sample;
- perform visual analysis through the transparency of the walls;
- create samples with inclined layers thanks to the possibility of rotating the base of the box with respect to the horizontal;
- replace filters according to the materials employed or the requirements of the test.

Thanks to the support equipped with a mechanical gear, the box can be inclined up to 90° during the sample reconstruction phase so as to allow the deposition of

the soil layers with a prescribed inclination angle with respect to the box base. The tests can be purely horizontal with a completely saturated sample or with a free water surface and seepage not parallel to the horizontal, imposing in both cases the difference in hydraulic head between upstream and downstream by modifying the level of the tanks. The box also has the possibility of being pressurised in order to reach high gradients.

A system of pressure measurement by piezometers has been devised over the lateral surfaces of the apparatus to ensure that this quantity is monitored during the course of the tests, in order to assess along all directions of the sample how the pressure regime is modified over time. In this way, it is possible to evaluate empirically whether the pressures applied to the sample are in accordance with theory. Furthermore, the material chosen as the main body of the apparatus is transparent plexiglass, and consequently during the test in addition to the measurements that can be taken it is always possible to observe the behaviour of the sample and how erosion is acting on it.

In accordance with the possibility of varying the type of test and its characteristics, the equipment has been designed with the idea of being able to modify the filters, also in relation to the type of material used for the test. In fact, the device leads to a versatility and numerous possibilities of modifiable options depending on the type of test to be carried out in relation to the phenomenon being studied. It is possible to reconstruct a small-scale model of an embankment, provided that the geotechnical characteristics of the sample (degree of saturation, relative density and grain size) are chosen appropriately.

3.1 Functioning of the system

The general operating scheme can be described with an upstream and a downstream reservoir by which a hydraulic head difference, and therefore a gradient, is applied to the sample between them. This scheme is common to most of the physical models of horizontal seepage in the literature. The model consists of a box in the form of a rectangular parallelepiped inside which are the tanks, the filtering walls and the sample, with a cover in order to close the volume. The box is equipped with appropriately sized holes for connection to a system for supplying water to the tanks and collecting the eroded material and excess fluid. To work more easily on the box, it is kept lifted from the ground by means of a steel support, which allows also horizontal movements

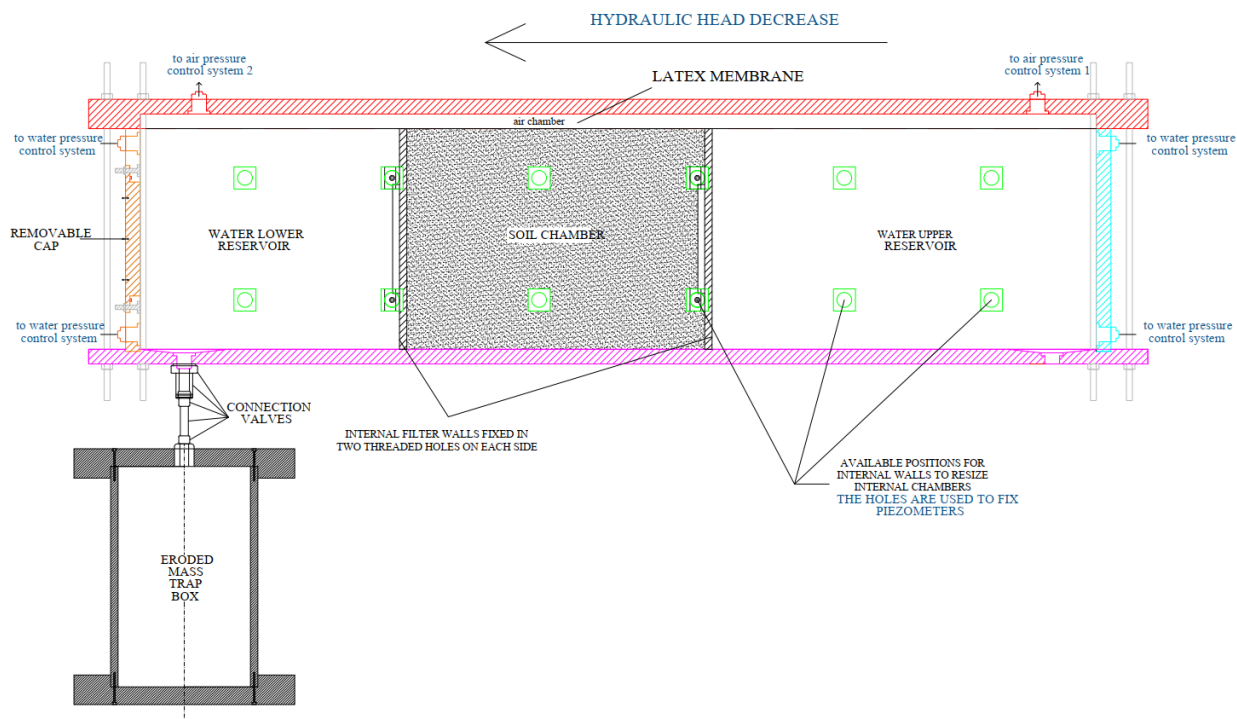


Figure 3.1. General look of EPBox

thanks to wheels at the base and permits a rotation for the reconstruction of the sample.

3.2 The box

The box has a length of 130 cm with an internal section of 30 cm in width and 34 cm in height, with a panel thickness of 2 cm (Figure 3.2).

The sample has a rectangular prismatic shape and its size in length varies according to the positioning of the filters: 20, 40, 60 or 80 cm. Moreover, the position of the specimen is not fixed, but can be chosen closer to the upstream or downstream reservoir or in a central position according to the type of test to be performed; the height of the sample can also be modified, starting from a minimum level linked to the position of the piezometers on the side panel and a maximum equal to the height of the box itself (Figure 3.3).

The body of the box was made from slabs of polymethylmethacrylate (PMMA, also known as plexiglass), assembled together. The choice of this material was motivated by the intention of guaranteeing the transparency of the apparatus so that the performance of the test could be observed on the inside, but having a low density



Figure 3.2. The EPBox on its support

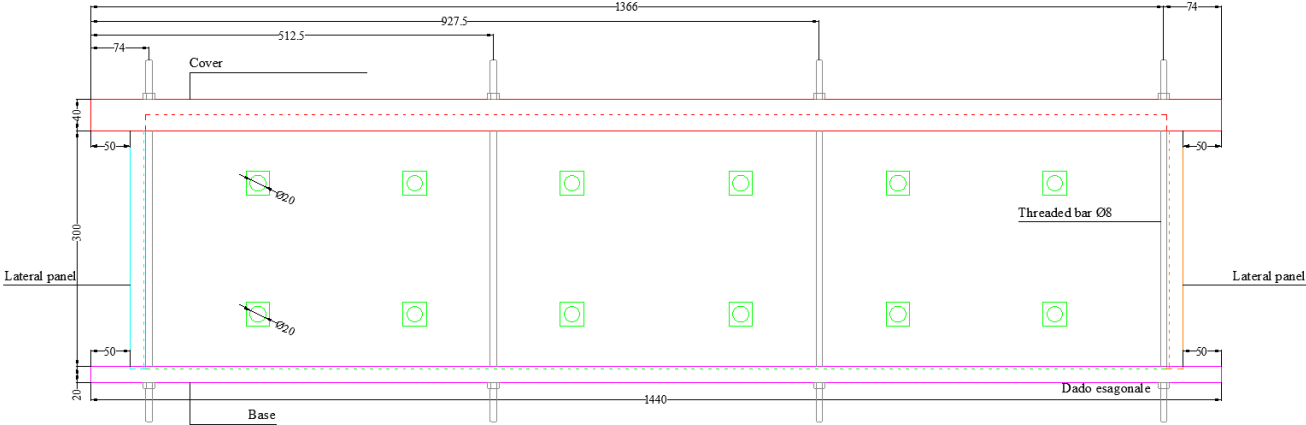


Figure 3.3. Technical drawing of the EPBox, lateral view

and good ease of fabrication. Compared to the main commercial alternatives on the market, such as glass and PVC, PMMA has a lower density (its density is half of that of glass and only slightly lower than PVC), is more resistant and elastic and therefore is well suited to mechanical processing, such as threading, and it is possible to make solid gluing, equivalent to welding. Where the material is subject to cutting operations, it can be smoothed and polished to ensure transparency even where it could be damaged by processing. From an economic point of view, plexiglass is more expensive than PVC, but the former is less sensitive to environmental factors such as light and temperature, which can cause degradation such as yellowing of the material and therefore a loss of transparency. On the surface, plexiglass is more susceptible to scratches than other materials, but the problem can be remedied by removing them with specific maintenance products or by avoiding the use of harder materials in direct contact with the surface (Celada and Magno 2013). In particular, when choosing the screws and tools required for the connections and installation of the measuring instruments, plastic materials such as nylon or PVC were chosen. In addition to this, to further preserve the PMMA surface, silicone flat gaskets were added to avoid direct friction between the screws and the plexiglass surface.

The slabs are joined using specific adhesives for this material that dissolve the surfaces in contact and induce subsequent polymerisation, creating a bond comparable to a weld so that it can withstand high stresses. In addition, in order to make the joints even more resistant to certain stresses that could be critical for their integrity, the two assembled slabs have an interlocking system that provides greater adhesion in addition to gluing alone (Figure 3.4).

3.3 The cover and the removable cap

A rectangular shaped cover is placed on the top of the box which, when positioned, allows an air chamber to develop above the sample and thus apply pressure to the air so that it is transmitted to the fluid. The cover is made of transparent plexiglass so that the inside of the box can be viewed even when it is closed. The box is made watertight thanks to a latex membrane positioned as a gasket, as well as separating the air from the water and thus allowing the division between the two fluids during pressurisation and when carrying out the test. The cover and the base of the box are provided with 12 through holes of 8 mm diameter to allow the locking of the box: through the openings there is a threaded nylon bar tightened with plastic nuts in

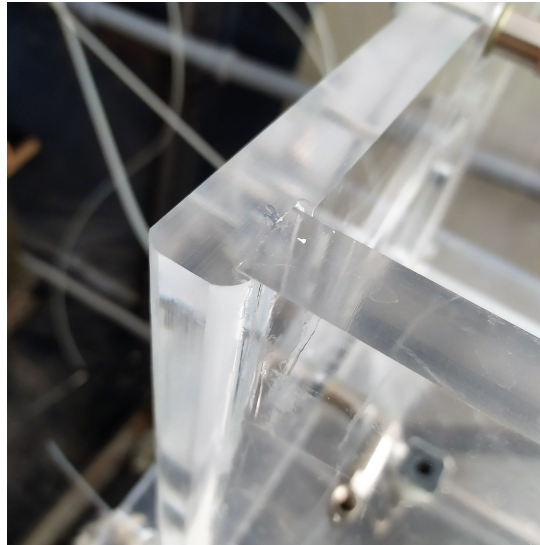


Figure 3.4. Corner of the box and highlight on the interlocking system where the two slabs are glued

order not to damage the PMMA surface so that the adherence between the cover and the membrane is guaranteed. Hexagonal nuts are used for the bottom closure, while butterfly nuts are used for the upper one, making it easier to open and close without the need for special keys or tools (Figure 3.5).

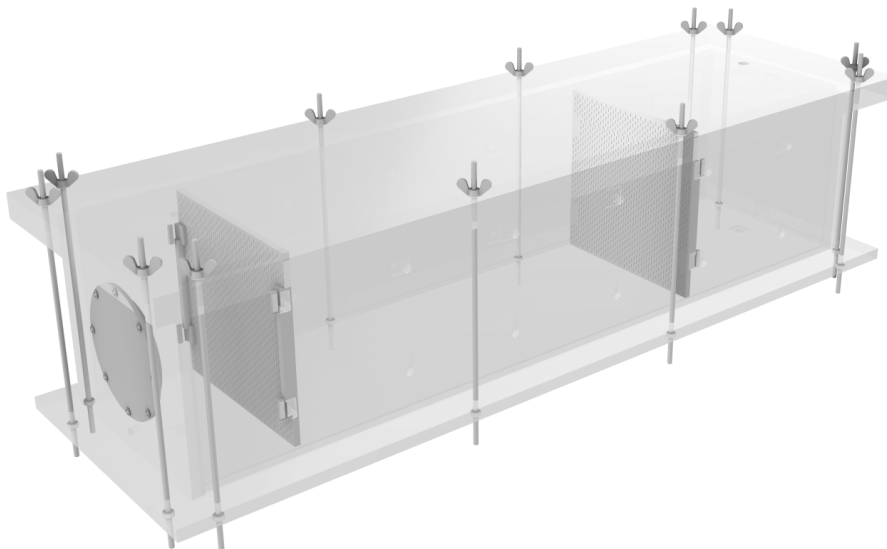


Figure 3.5. Box with cover positioned on the top

The cover is only necessary in the case of pressure tests or reconstruction of the sample with a vertical box, so in the other cases it was decided not to use the cover to allow immediate access from above.

To fill the box vertically, a removable cap on the lateral panel having diameter equal to 15.5 cm internally and 20 cm externally was designed (Figure 3.6). Its function is to allow access to the inside of the box and to insert the material in such a way that the deposition of the layers can take place perpendicularly to the box base, that is the direction of flow, or at a certain angle of inclination as desired, and not parallel as is the case with most devices of this type in the literature.

In order to guarantee the hydraulic impermeability of the surfaces of the removable cap and of the box in contact, a specific slot has been designed on the removable cap in order to position a rubber ring seal (OR 3650) so that the pressure given by the compression of the cap against the surface does not allow the passage of water.

To fix the removable cap to the box, 8 grey PVC M6 screws of 3 cm length are used, positioned in the same number of pass-through holes in the removable cap and in the side panel, also equipped with a small O-Ring to prevent the passage of water (OR 2037) (Figure 3.7). The screws are tightened by nylon nuts with a silicone gasket in between to avoid damage to the surface.

Special care must be taken when closing the removable cap because the O-Rings may be less effective: in fact, the silicone gaskets do not allow the nuts to push against a rigid surface and consequently the pressure exerted by the rubber ring may not be sufficient to prevent the passage of water, especially at high pressures. To overcome this problem, a thin protective film can be applied to the surface of the removable cap, so that in any case the bolts are in direct contact with a more rigid surface than silicone.

3.4 The filters

The filters have the function of delimiting the volume inside which the soil sample (or material simulating the behaviour of a terrain) to be used for the test will be placed and at the same time allowing the water flow. They consist of two rectangular plates with dimensions coinciding with the internal section of the box. The flow of water is ensured by a series of small openings of a geometry chosen during the design phase to be positioned vertically so that they form a filtering wall. The filter is designed so that the coarser material is not removed from the sample by water seepage, while the fine particles can be removed by the action of erosion. The movement of the largest part inside the sample without erosion could lead to a lowering of the sample with a consequent change in the void ratio or a variation over time in the distribution of the composition of the material in terms of the percentage of coarse, medium and fine

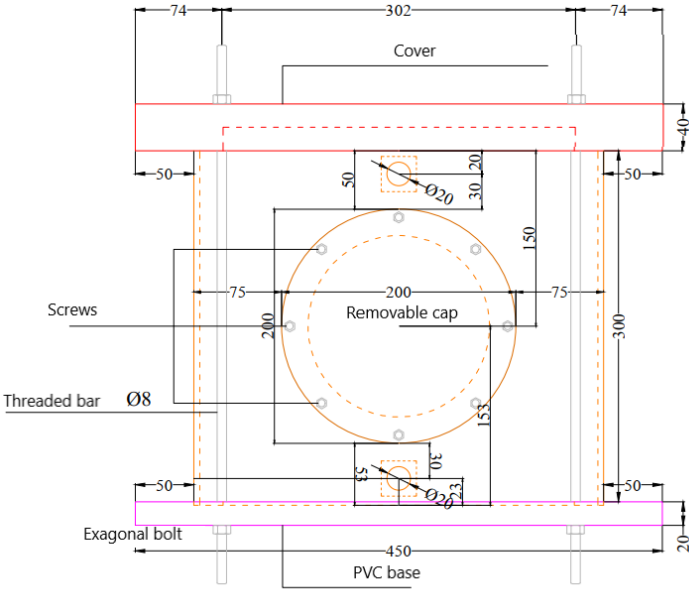


Figure 3.6. Technical drawing of the removable cap (mm)

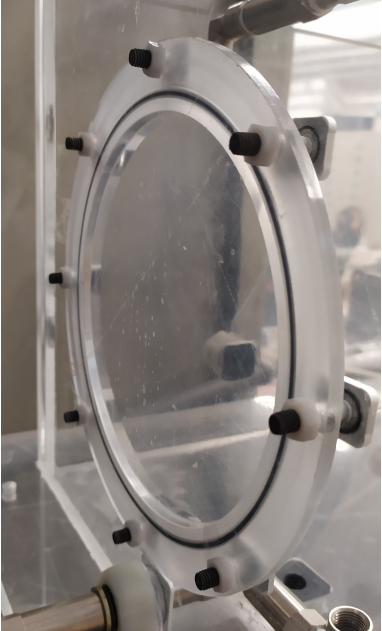


Figure 3.7. Detail of the removable cap with its O-Ring put in place

particles.

In particular, having chosen 2 mm as the diameter of the large particles of the material used, the filter was sized by choosing a smaller opening in order to stop their washout. Various hypotheses were considered concerning the arrangement and geometry of the holes on the plates, all of which were valid from the point of view of functionality, but had a substantially different impact in terms of ease of processing and, consequently, costs.

In their thesis, Celada and Magno opted for a plexiglass plate to be screwed to the side panels in order to block it, with circular holes made by laser instrumentation with a diameter of 1.5 mm and a centre-to-centre distance of 1.8 mm, close together in groups of four. This layout prevents the holes from being occluded, in fact when a sphere with diameter of 2 mm closes a hole, the adjacent hole cannot be closed (Figure 3.8). The problem in making this type of filter is that it is difficult to find machinery suitable to create the holes, and consequently the costs increase, weighing on the possibility of realising other pairs of filters with a low economic impact.

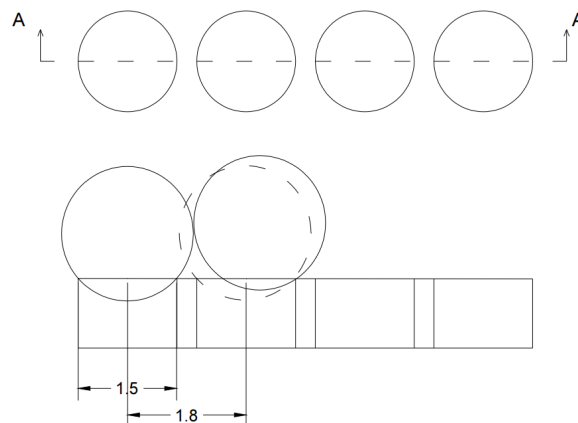


Figure 3.8. Details of the filter employed by Celada and Magno 2013 (mm)

Therefore, considering the need to create filters that are easy to replicate but equally resistant and effective, slotted steel plates were chosen, which are easily available and convenient from an economic point of view, with openings wider than the reference 2 mm. By overlapping two plates with the same geometry, but slightly displaced from each other, it is possible to obtain smaller slots.

The gluing between the two slabs must be carried out bearing in mind that the

glue must be water-resistant and must not generate filaments that would close the thin openings that are created, but guaranteeing perfect adhesion and absence of gaps where the eroded fine particles may be trapped. The ideal solution was therefore identified as an ultra-resistant quick-setting spray glue not soluble in water, applied to one of the two surfaces. The plates are then superimposed and loaded with some weights to help the glue adhere (Figure 3.9).

An alternative to glue has been identified as welding, but acting at localised points could lead to deformation of the slab and an imperfect adhesion, guaranteed instead by a glue applied uniformly over the surface.

The material of which the filters are made must be water resistant and not susceptible to rust or other factors due to contact with moisture. If a material with these characteristics is not available or, for economic considerations, it is far more convenient to use a material that could be corroded by water, there are various types of products on the market that make it possible to waterproof surfaces. For instance with a spray a thin film can be applied to protect them from the action of water, but it must be noted that the geometry of the plate is complex and therefore the film must be sprayed from various directions and in a sufficient number of layers so that the surface is evenly covered without leaving any parts that could allow rust to attack the material (Figure 3.10).

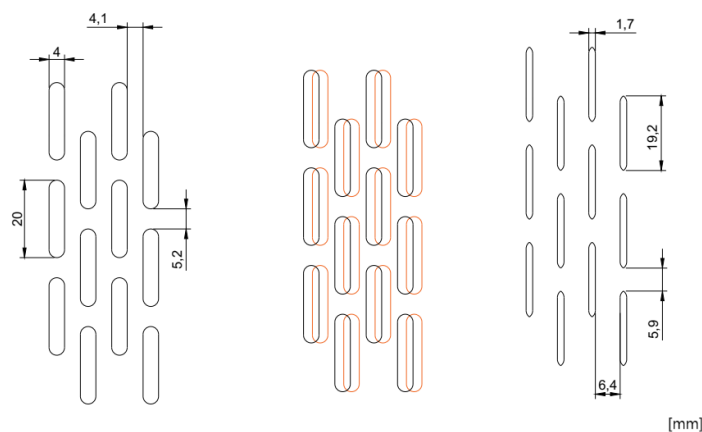


Figure 3.9. Filter realised by superposition of the two slotted slabs

The filters are fastened to the box by a pair of rails made from plastic "C-profiles" - cut to the same height as the inside of the device - which are in turn attached to the head of PVC screws to be positioned inside the holes in the box. The profile can be joined to the screws in different ways: by gluing (for example using the same

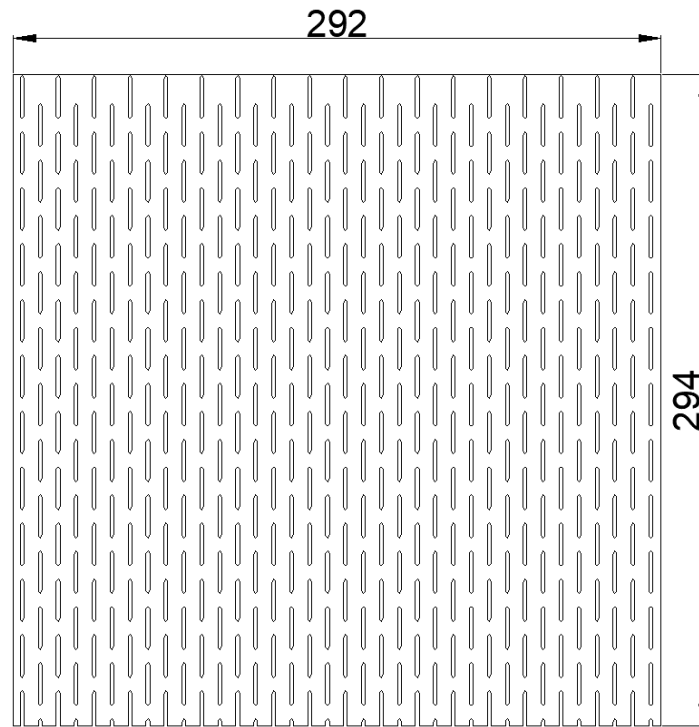


Figure 3.10. Technical drawing of the filter used (mm)

glue used to join the two staggered slabs for the filter), by nailing or by means of special screws with a small hole, which will be described in more detail in the next paragraph, so as to drill the profile and tighten it directly onto the screw (Figure 3.11).

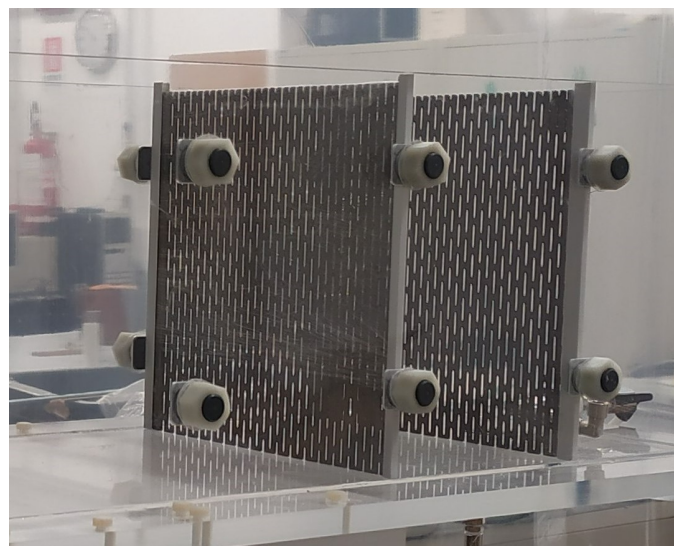


Figure 3.11. Filters positioned into the box with their supports

If the thickness of the profile is too small, the simplest and quickest solution is gluing, which was adopted as a first attempt in this thesis. Following the acknowledge-

ment of a weak seal of the glue with respect to the thrust of the water acting under high hydraulic gradients, especially because of the small contact surface on which the glue is placed, a different solution was conceived using L-shaped angle profiles cut, drilled and then screwed onto the PVC screws heads in such a way that the seal was guaranteed by the same principle adopted previously, but with greater rigidity given by the screwing (Figure 3.12).



Figure 3.12. L-shaped angle profiles used as rails to fix the filters

3.5 The holes and screws

In order to allow hydraulic connection, installation of measuring instruments, water isolation, and other functions, a series of holes of different diameters have been prepared. Together with the holes, a set of PVC screws has also been designed for specific functions, with different structure.

The holes are provided with a circular through opening, which will be occupied by the threaded portion of the screw, passing from side to side and allowing the placement of a bolt on the opposite side. The square-shaped screw head with rounded corners disappears completely thanks to a cavity above the through-hole, thus leaving the inner wall smooth without any protruding parts, which could create deviation of the water streamlines (Figure 3.13, Figure 3.14).

A threaded part of the screw then emerges from the outside of the box, onto which a nut can be screwed (also made of plastic, in particular the material used for this purpose has been identified in nylon due to its availability and low cost) so that the

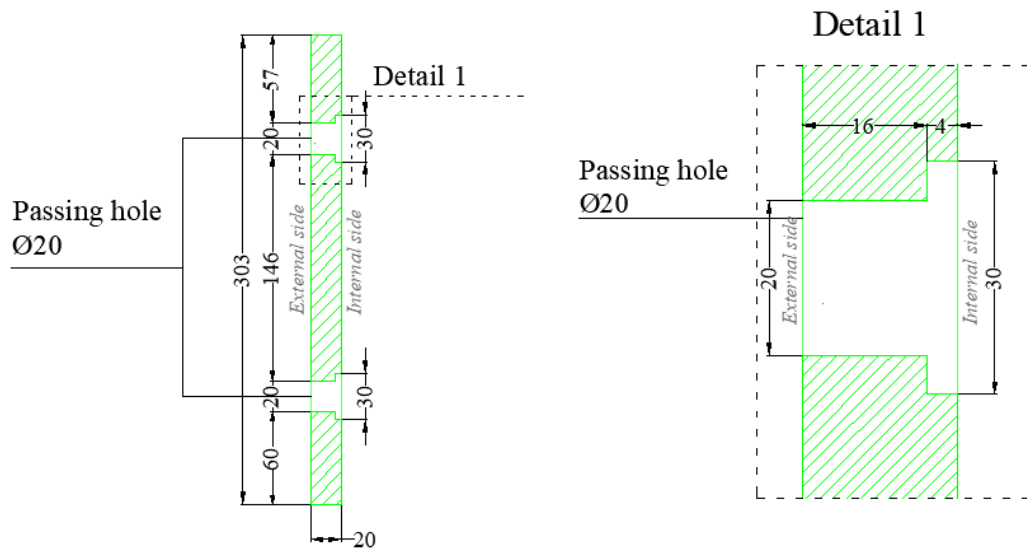


Figure 3.13. Technical drawing of passing holes

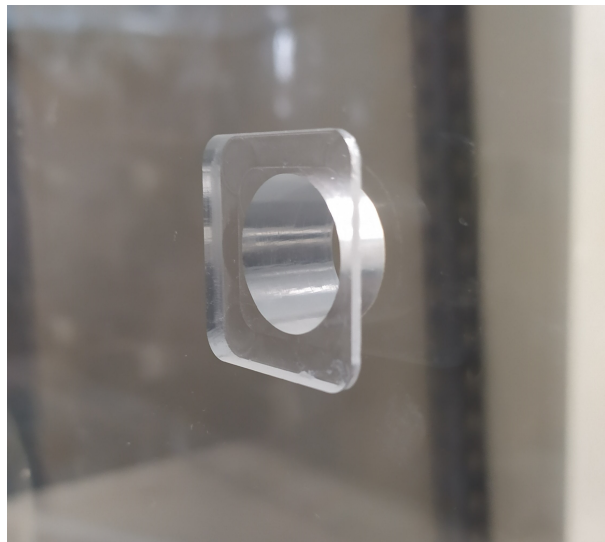


Figure 3.14. Hole with cavity for the positioning of the squared screw head

two ends can be tightened transversely against the wall of the box and to guarantee the hydraulic seal without the leakage of fluid. It is not necessary to use any type of spanner on the inside of the box as the groove used to hide the head of the screw also has the function of locking it (Figure 3.15).



Figure 3.15. Grey screw bolted with a white nut and with the addition of a circular silicon protection gasket

In order to prevent the nut from scratching the plexiglass wall during screwing and causing damage, as mentioned in the previous paragraphs, silicone gaskets have been designed which are both very effective and low cost. The flat gaskets can also be produced independently if a punching machine is available which can make holes of different sizes from a single sheet of this material. Rings can be made with an internal diameter slightly larger than that of the threaded part of the screw and large enough to cover the full width of the nut thickness (Figure 3.16).

The screws are made of grey PVC, a resistant material that cannot be deteriorated by water as well as, for example, stainless steel, but the use of a plastic material does not risk damaging the plexiglass surface or scratching it; moreover, since they are custom-made through mechanical processing in the laboratory, the use of a plastic material guarantees easier production.

All PVC screws are provided with a circular groove, which goes against the plexiglass wall where a rubber ring seal is placed. This ensures a watertight seal by deforming when compressed by the action of the nut on the thread (Figure 3.17). The nut is able to act effectively in spite of the presence of the external protective



Figure 3.16. Gaskets for screws M20 and M4

silicone gasket. In Table 3.1 and Table 3.2 are respectively shown the holes present overall on the box, removable cap and cover, and the types of screws available with the respective functions (Figure 3.18).



Figure 3.17. Cavity on the screw and its O-Ring

Table 3.1. Dimension and quantity of holes

Box		Removable cap		Cover	
Diameter [mm]	Number	Diameter [mm]	Number	Diameter [mm]	Number
8	22	6	8	8	12
20	30			20	2

Table 3.2. Type of screws

Id	Type	Function
<i>Vite 1</i>	Threaded hollow	Hydraulic connections
<i>Vite 2</i>	Threaded hollow	Measurements with piezometers
<i>Vite 3</i>	Blind hole	Locking of filters
<i>Vite 4</i>	Solid	Hydraulic impermeabilization
<i>Vite M6</i>	Solid	Locking of removable cap

3.6 The PVC base and the steel support

The lower part of the box is fixed to a white rectangular PVC base which, in turn, is firmly anchored to a C40 steel support equipped with wheels to facilitate movement (with respective locking system to prevent unwanted shifting). By using ten M8 screws and nylon bolts, the PVC base with a length of 50 cm and a width of 45 cm (Figure 3.19), is joined to the steel support. On the upper part of the structure there is a steel board with six M6 threaded holes that guarantee a solid seal between the PVC base and the support thanks to stainless steel screws. Support for the box is provided by a tilting shaft made of C40 steel. The tilting of the box is entrusted to a system of two motor reducers coupled together, in an aluminium box with oil-bath worm gears with manual lever control in order to avoid safety problems in current or pneumatic applications. The double gear system ensures the safety of the instrumentation during use, as it does not allow the box to tilt or oscillate, which could compromise experimental procedures. The double reduction gear system also offers the convenience of having a transmission ratio of 1:448, so that 112 revolutions must be applied to the lever to make a 90° rotation. The pendulum structure is appropriately fixed to a system consisting of rolling bearings with a steel structure equipped with four rubberised aluminium swivel wheels mounted on bearings, two of which have a lever brake system.

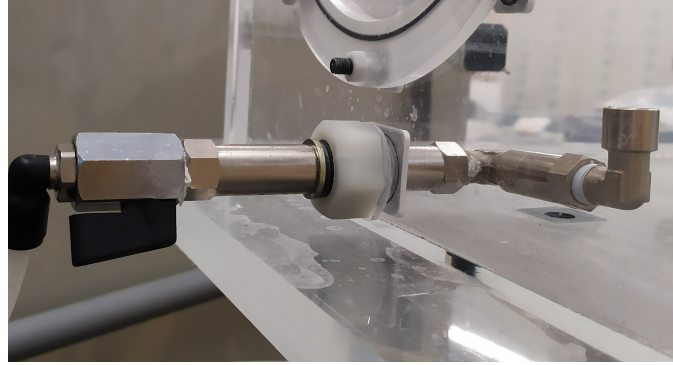


Figure 3.20. Detail of the hydraulic connection in the upstream reservoir

to a piping system that allows water disposal (Figure 3.21). The same process takes place downstream, where a discharge system guarantees a sufficient outflow to maintain a constant level. The continuous overflow system was designed with a vertical pipe screwed onto a 90 degree elbow fitting, available in different lengths depending on the water levels to be maintained during the test (Figure 3.22).

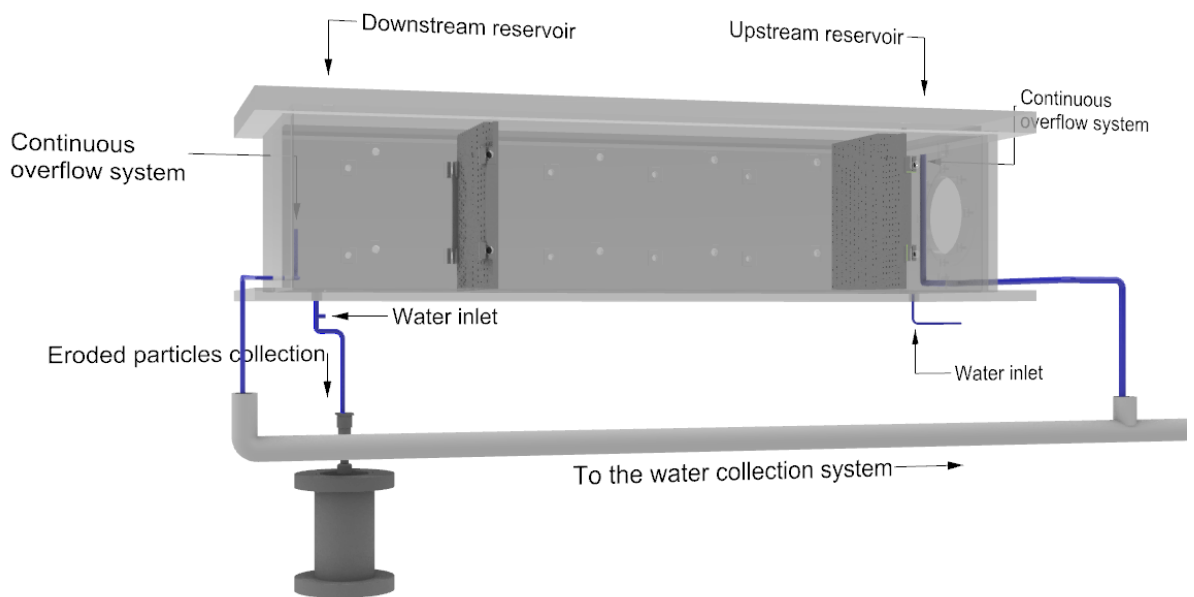


Figure 3.21. System of inlet and disposal of water, to balance the equilibrium of upstream and downstream reservoirs

If the length of the chosen sample allows it, meaning that at least three rows of screws are available (two for fixing the filters and one free in the middle of the sample), piezometers can be used to measure the water pressures in the sample during seepage and their distribution along the sample volume. For the piezometers transparent rigid tubes with a graduated scale can be used. These instruments are attached to polymer



Figure 3.22. The continuous overflow system

fittings and bolted to type 2 screws and their watertightness is guaranteed by a ring gasket in the instant fittings. In order to prevent the tube from being clogged by material that could be transported in, it is necessary to place a paper or fabric filter in the part in contact with the sample.

3.8 The trap box

Once the sample saturation procedure has been completed, the downstream hole positioned at the bottom no longer has a water input function and is therefore used as an opening for collecting the eroded material. The material removed by the seepage process in the sample is deposited at the base of the downstream reservoir and, by means of gravity, is slid into a trap box placed in hydraulic continuity with the box in which the test is carried out. The cap of the trap box was drilled with a diameter of 22 mm and an automatic fitting was screwed on with a bolt on the opposite side to ensure a good hydraulic seal (Figure 3.23). The material collected during the test can then be sieved and weighed once the container has been emptied and rinsed. When a measurement of the amount of eroded material is to be carried out, it is sufficient to close the tap placed as connection between the trap box and the EPBox in order to maintain the hydraulic continuity of the system and there is no change in pressures (Figure 3.24). In addition, when the trap box is connected again and the tap is opened, it is put in place already filled with water so that there is no rapid discharge of water from the downstream tank.



Figure 3.23. Trap box employed for collecting the eroded material

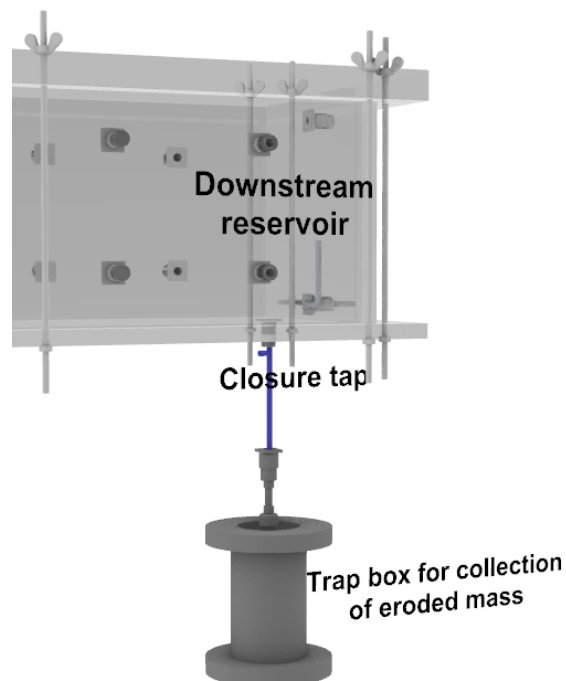


Figure 3.24. Schematic connection between the downstream reservoir and the trap box

Chapter 4

Materials

4.1 Selection of the material

The material used for the first set of experimental test had been reconstructed in the laboratory in order to obtain a material with a critical composition from the point of view of erosion. In fact, the finer part of gap-graded soils is more subject to the action of dragging when water flows into the soil and is less likely to be deposited during movement given their shape and size (Figure 4.1).

Glass, a material with a specific weight comparable to that of sand, was used in the laboratory to reconstruct a sample similar to a real soil sample. Glass is also a particularly advantageous material because it does not induce phenomena as swelling or shrinkage.



Figure 4.1. Picture of the material employed

The behaviour of the glass beads depends on their size gradation, their arrangement and the friction between particles. As deformations take place in these materials, external forces can cause internal changes to their structure, caused by spheres slipping, rolling and interlocking. These changes produce a different response of the material in terms of mechanical behaviour and also seepage. Understanding this material behaviour is very important in order to perform and interpret laboratory tests in the best possible way.

Based on the commercially available particle size classes of glass beads and referring to the classification according to the AASHTO (American Association of State Highway and Transportation Officials) system (Table 4.1), the diameters reported in Table 4.2 were chosen.

Table 4.1. Classification of particle size for common natural materials

Material type	Diameter D of particles
cobbles	$D > 75mm$
gravel	$2mm < D \leq 75mm$
sand	$0.075mm < D \leq 2mm$
silt	$0.002mm < D \leq 0.075mm$
clay	$D \leq 0.002mm$

The selection of these diameters allows the reconstruction of a material with a coarser part (class A) that constitutes the solid skeleton, being the limit between sand and gravel, allowing the finer particles (class B and C) to be eroded, to flow with water and to be transported through the filters. The first fraction instead, does not pass through the openings and is not considered as a removed material but only displacements and dislocations take place. In fact, it is supposed that the phenomenon studied at these gradients involves mainly the finer fraction of the soil. The larger diameter fraction constitutes a rigid structure through which the

Table 4.2. Diameter of glass beads chosen

Class	Range of diameter (mm)
A	2
B	0.57-0.70
C	0.07-0.11

Table 4.3. Values of G_s for different classes of material

Class	G_s [-]
A	2.54
B	2.45
C	2.48

passage of water erodes the finer particles resulting in the *suffusion*, which is one of the phenomena for which the EPBox is designed. The water dislodges the particles within the sample by transporting them downstream if the flow has sufficient drag force.

4.2 Material characterisation

In this section the process of classification of the material used for the tests will be described, with particular reference to the determination of the grain specific weight and the grain size distribution curve, reporting part of the results obtained in previous studies, with the integration of additional information related to the velocity of deposition and geotechnical parameters. Since the material used in this thesis is the same as that employed in 2013, it was not considered necessary to repeat the basic characterisation tests and the results obtained will therefore be reported.

4.2.1 Grain specific weight

For the determination of the specific weight γ_s , the procedures indicated in the ASTM D854 standard were used, by means of a calibrated pycnometer. The method consists of evaluating γ_s at a given temperature, based on the difference in weight between a mass of soil and a mass of de-aerated distilled water occupying the same volume inside the instrument.

Then the specific gravity is obtained dividing γ_s by the specific weight of water γ_w :

$$G_s = \frac{\gamma_d}{\gamma_w} \quad (4.1)$$

The values obtained for the three different fractions, with reference to a value of γ_w equal to 0.995 g/cm^3 , are reported in Table 4.3.

Considering then a specimen reconstructed with a different percentage of each material fraction (for example 60% class A, 20% class B and 20% class C), a G_s derived from the weighted average of the specific gravity values according to the amounts of each fraction, can be considered.

4.2.2 Grain size distribution curve

The second important property of the soil is its grain size distribution curve, meaning the distribution of the diameters of the particles generally expressed as cumulative percentage. For its determination two parallel procedures are required: sieving and sedimentation.

The first was carried out according to the standard ASTM D 422, by using sieves up to the minimum diameter of 0.075 mm. Below this value, once the G_s is known, a sedimentation procedure is required. The principle is based on Stokes' Law, according to which particles of equal size immersed in a liquid fall with the same velocity, which remains constant over time. By measuring the different densities of the suspension at fixed time intervals, it is possible to determine the quantity of that is still in suspension and the quantity that has been deposited on the bottom.

The results are plotted in Figure 4.2, Figure 4.3 and Figure 4.4.

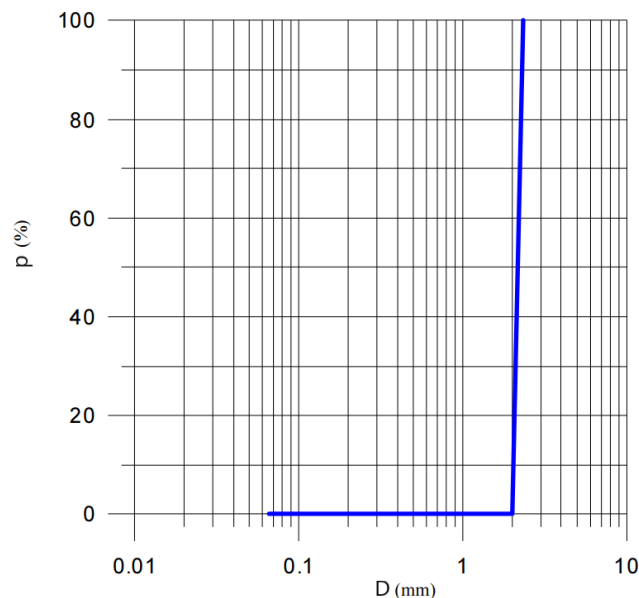


Figure 4.2. Grain size distribution curve class A

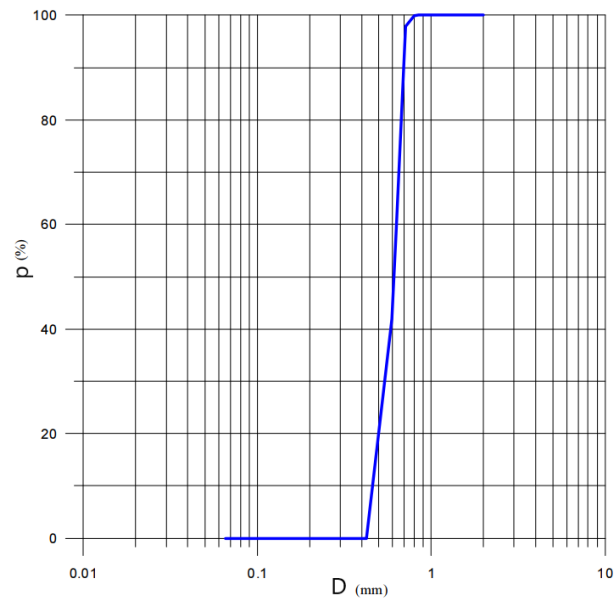


Figure 4.3. Grain size distribution curve class B

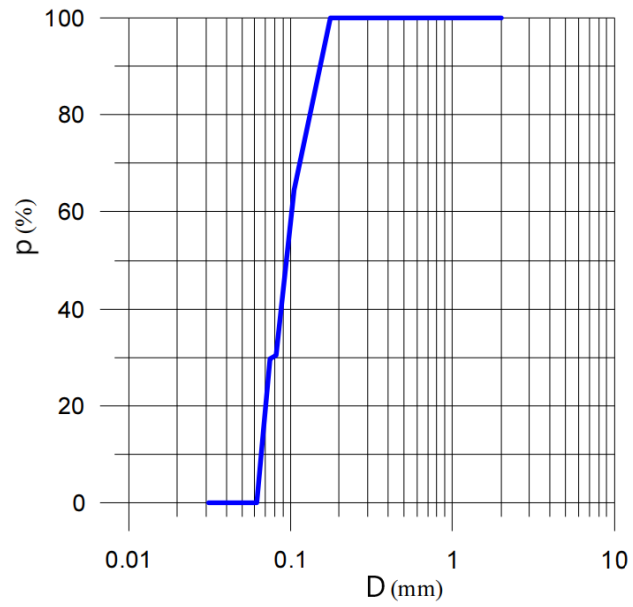


Figure 4.4. Grain size distribution curve class C

If the particle size distribution curve is vertical, the sieved material is uniform. The results show that the distribution is uniform, but the uniformity coefficient C_u can be used to obtain an estimate of the uniformity of the material. C_u is defined by:

$$C_u = \frac{D_{60}}{D_{10}} \quad (4.2)$$

With:

- D_{60} diameter corresponding to the 60% of finer fraction;
- D_{10} diameter corresponding to the 10% of finer fraction.

C_u equal to 1 is the minimum value of the parameter and, as the value rises, the non-uniformity of the sample increases as reported in Table 4.4.

The analysis of the grain-size distribution curves shows C_u values below the value of 2 and therefore the soil can be considered as uniform (Table 4.5).

4.2.3 Velocity of deposition

In order to verify that the material eroded by seepage actually deposits on the base of the box during the test and does not remain in suspension, it was necessary to determine another fundamental parameter of the soil, namely the velocity of deposition of the particles.

This characteristic of the soil, and in particular of the smaller particles that tend to remain in suspension, is fundamental because, if they were present in the most superficial part of the downstream reservoir, they would be washed off through the continuous discharge pipe and not collected as eroded particles.

In reality, to prevent this problem, a very fine-meshed geotextile was used, glued to a funnel (useful for increasing the surface area of contact of the drain with the water and thus its discharge capacity), which was fixed to the top of the pipe used as the drain. However, in high gradient tests where the quantity of water flowing is

Table 4.4. Classes of uniformity of soil

$C_u \leq 2$	Uniform soil
$2 < C_u \leq 15$	Slightly non-uniform soil
$C_u > 15$	Highly non-uniform soil

Table 4.5. Values of C_u obtained in the tests

Class of grain size	D_{60} (mm)	D_{10} (mm)	C_u (-)
A	2.15	2.01	1.07
B	0.63	0.47	1.34
C	0.10	0.066	1.51

Table 4.6. Time of deposition of the sample

# test	t of deposition (s)
1	19
2	18
3	18
4	19
5	17

particularly significant this can lead to a problem. In fact, since the geotextile has to retain particles up to 0.07 mm in diameter, even the water cannot pass easily and consequently the drain may not be able to discharge all the excess water to keep the downstream level constant. For this reason, checking that the particles settle to the bottom in a short time is a guarantee for the use of continuous drains without any kind of filter.

A test was therefore carried out to verify the fast deposition of particles to the bottom.

To do this, a graduated cylinder with a capacity of 1000 mL and a height of 35 cm (Figure 4.5) was filled with water and a small sample of 60 g of material containing equal quantities of class A, B and C fractions was poured on top. The time required for the smallest particles to settle to the bottom was then measured with a stopwatch and found to be less than 20 seconds (Table 4.6).

It can be concluded that by placing the sample sufficiently far from the point where the continuous discharge is placed, the event that some of the material remains in suspension and is washed off is unlikely to occur.



Figure 4.5. Graduated cylinder employed for the test

4.3 Preparation of material for the tests

4.3.1 Grain size distribution

For the tests, it is necessary to identify a material composition that can correctly suit the phenomenon to be analysed. In particular, having chosen filters with apertures of 1.7 mm, *suffusion* was observed in which only the finer part was eroded by the seepage with a structure composed of coarser material remaining relatively intact.

With this in mind, the percentages of the three classes were chosen:

- 60% class A;
- 20% class B;
- 20% class C.

The grain size distribution curve of the sample chosen with this composition is reported in Figure 4.6.

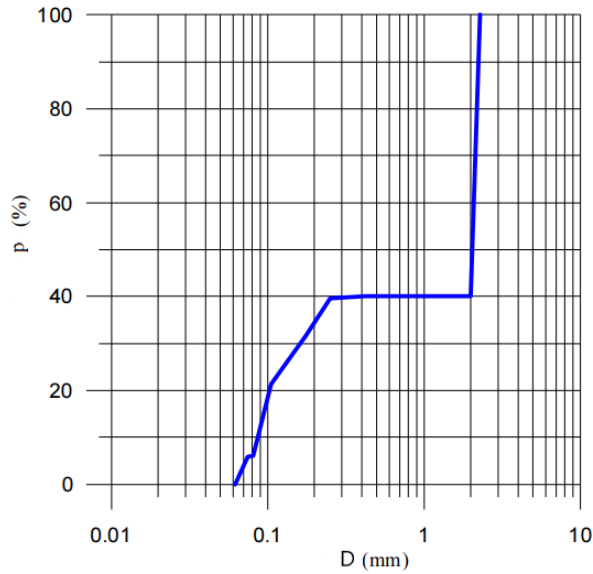


Figure 4.6. Grain size distribution of the sample employed for the tests

The value of specific gravity $G_{s_{mean}}$ was derived as average value weighted on the percentages of the three fractions:

$$G_{s_{mean}} = G_{s_A} \cdot 0.6 + G_{s_B} \cdot 0.2 + G_{s_C} \cdot 0.2 \quad (4.3)$$

The value obtained is equal to 2.51 and the density ρ_s of grains is equal to 2.50 g/cm^3 .

4.3.2 Void ratio

The maximum void ratio e_{max} and the minimum void ratio e_{min} of a sample of fixed volume V were estimated experimentally.

The procedure consists in the determination of e by weight measurements once the volume has been chosen, with one sample in a loose state (e_{max}) and one in a compacted state (e_{min}) trying to reach minimum and maximum compaction conditions. The procedure was repeated twice, once for a dry sample and once with a wet sample (water content $w = 8\%$). The volume selected is 200 cm^3 , in a transparent glass container on which a reference height has been marked.

The procedure consists of filling the volume of 200 cm^3 and weighing the mixture in the container. Once the weight is obtained, the density is calculated using the following formula:

$$\rho_d = \frac{m}{V_T} \quad (4.4)$$

With:

- m mass;
- V_T volume of the sample.

The porosity n is expressed as:

$$n = \frac{V_v}{V_T} \quad (4.5)$$

and the void ratio e as:

$$e = \frac{V_v}{V_s} \quad (4.6)$$

With:

- V_s volume of the solids;
- V_v volume of the voids.

Then, given ρ_d and ρ_s it is possible to obtain n :

$$n = 1 - \frac{\rho_d}{\rho_s} \quad (4.7)$$

From the porosity, e is given by:

$$e = \frac{n}{1 - n} \quad (4.8)$$

The preliminary operation was to measure the void ratio of the glass beads assembly in a dry condition by first combining the three fractions and then placing them in the volume. Initially, a void ratio corresponding to the material in a loose state was determined, with the mixture poured from a low height without shaking the container.

The test was then carried out with compacted material, by placing layers of decreasing thickness on top of each other and compacting each stratum with a falling hammer to achieve the highest possible compaction index. The sample reconstruction procedure is based on the procedure introduced by Ladd. This method is based on the

Table 4.7. Results of void ratio on dry material

	Loose	Compacted
ρ_d [g/cm ³]	1.89	1.99
n [-]	0.25	0.21
e [-]	0.33	0.26

consideration that the minimum energy required to compact the soil layers decreases linearly from bottom to top (Ladd 1978). This is because each time the mixture of the new layer is deposited on the previously compacted layer, the blows given with the hammer contribute to the further compaction of the underlying layers, causing their height to decrease. The hammer used is made of plastic with a metal end, and has a circular shape that well fits with the geometry of the container, facilitating compaction especially at the boundaries.

The results obtained are reported in Table 4.7. The effect of compaction induces a limited variability range of void ratio between 0.26 and 0.33.

Following this, the distribution of the fine and coarse fractions was monitored through the transparent container. As it can be appreciated in Figure 4.7, the material belonging to classes B and C was deposited at the bottom of the sample as a result of the compacting blows, resulting in a lack of homogeneity in density between the upper and the lower parts of the sample.



Figure 4.7. Effect of grain separation of the fine and medium particles from the coarser ones for highly compacted samples

Taking into account the principles presented in the previous paragraph, it was decided to repeat the procedure under wet conditions to overcome the problem of separation between the different components.

To assess the amount of water m_w to be added to the dry mass m_d , the water content

Table 4.8. Results of void ratio on wet material

	Loose	Compacted
ρ_d [g/cm ³]	1.94	1.95
n [-]	0.23	0.22
e [-]	0.29	0.28

w was considered:

$$w = \frac{m_w}{m_d} \quad (4.9)$$

The water content was decided after some visual trials on the material, selecting a value equal to 8% as optimal for the purpose.

The results are reported in Table 4.8. The values of e are very similar in both the compacted and the loose cases. This may be due to the fact that the compaction procedure is already partly carried out by the water, meaning that an additional pounding does not lead to a different result in terms of e . Moreover, the similarity in the results obtained in the compacted and loose condition can be related to the composition of the material. In fact, it might be hard to reconstitute different compaction states of a material with such a relatively balanced composition of the three fractions. When examining the material after compaction, there is no separation between the fractions and consequently the problem encountered when performing the procedure with dry material appears to be solved (Figure 4.8).



Figure 4.8. No separation observed on the compacted sample in wet condition

The value of e taken into account when preparing the samples for the seepage tests is 0.29, considering the material poured without compaction. An initially wet condition was chosen considering that the first phase after the selection of the sample volume is the saturation. By introducing a material already partially saturated and mixed, the further effect of water in terms of compaction and separation of the fine particles from the coarse ones is minimised.

Chapter 5

Vertical seepage

5.1 Purpose of tests with permeameters

The aim of the first series of tests is to measure hydraulic conductivity k in a traditional way, by means of vertical seepage. In addition, by increasing the gradient i it is possible to verify the triggering of internal erosion phenomena such as vertical *piping* and *suffusion*, also measuring the amount of material eroded over time.

A permeameter is an apparatus employed in the laboratory to measure the hydraulic conductivity of a material, and there are several of them depending on the type of test to be performed. Usually a permeameter can be used for a narrow range of orders of magnitude due to physical limitations related to the application of the hydraulic gradient or the required flow rate. Since hydraulic conductivity values vary up to 14 orders of magnitude in nature, different types of permeameters are needed to evaluate the hydraulic conductivity of different soil types, for example a coarse sand or a clay.

There are different tests aimed at measuring the hydraulic conductivity of a material under different conditions of duration, in laboratory or in field. A brief analysis of the standard equipments was carried out and a basis was gained for appropriate modifications of the available device. The most common method is the one based on a constant head condition, but there are also different methods such as falling head, constant flow, constant volume variable head, and constant head constant volume test (Germaine 2009). Here, the constant head condition was used, since it is the easiest method to implement and utilise.

The constant hydraulic head test is used to measure the hydraulic conductivity of

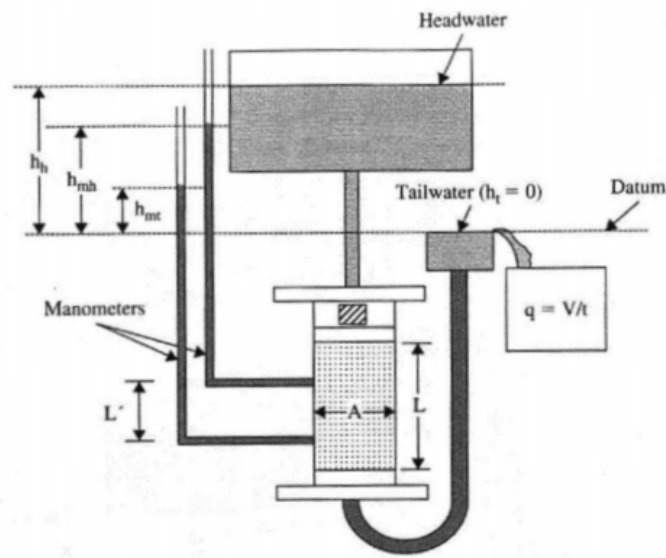


Figure 5.1. Schematic diagram representing a constant hydraulic head test (Germaine 2009)

a sample for a given void ratio which is assumed to remain constant throughout the duration of the test. A hydraulic gradient is applied by means of an upstream and a downstream reservoirs placed at different heights, as schematically shown in Figure 5.1. The outflow is measured and the hydraulic conductivity k can be calculated, using Darcy's law:

$$k = \frac{Q}{iA} \quad (5.1)$$

With:

- k hydraulic conductivity [m/s];
- Q flow rate through the specimen [m^3/s];
- i hydraulic gradient [-];
- A area of flow [m^2].

The Darcy's equation (5.1) only applies once the flow has reached the steady state. The gradient can be measured locally by means of piezometers installed at two points of the sample set at a given distance (L' in Figure 5.1), or related to the whole sample by evaluating the hydraulic head difference between upstream and downstream, and considering the entire length of the specimen inside the permeameter (L in Figure 5.1).

5.2 Tests in permeameter

To carry out vertical seepage tests, a permeameter was used that consists of a plexiglass cylinder and a base filled with a coarse material with high hydraulic conductivity. Water fills the device from a tank placed at a given height. The water flows through the sample and spills into a tank to collect the seeped water. This instrumentation normally allows for the measurement of the hydraulic conductivity of the material, and has been suitably modified to also permit the collection of the material eroded during the course of the test.

5.2.1 The device employed

In the vertical seepage tests, a cylindrical plexiglass permeameter was used, applying a constant head to a sample of glass beads. The level of water in the upstream reservoir was set at a height Hm from the point identified as reference height $z = 0$, with a continuous inflow of water kept constant by a spillway that removes excess water. Through a flexible tube, a seepage process is then set up from the upstream to the downstream reservoir, in which the level of water is maintained at a constant height Hv by a hole that allows the discharge of the flowing water (Figure 3.18). The volume of water corresponding to the downstream reservoir in traditional permeameters is placed directly above the sample, as the eroded material is collected by the same overflow that keeps the downstream water level constant.

The base of the permeameter was filled with coarse material so that the pressure drop in the first part of the path is minimised. Above the coarse material a metal grid enclosed between two sheets of filter paper was placed to prevent the fine material used in the test from entering the base and obstructing the passage of water.

The plexiglass cylinder is 42 cm high and has a series of holes that permits to set the level of water above the sample to five different measures. The upstream reservoir one instead is fixed to a support that can be raised up using a connecting pipe of sufficient length. The internal part of the device has a diameter of 10 cm and equipped with a piezometer. In fact, although coarse material was inserted into the base of the permeameter so as not to reduce the applied gradient, it is useful to monitor the actual pressures at the base of the sample. The piezometer has been realised with a transparent tube and protected with a geotextile at the tip to avoid any obstruction.

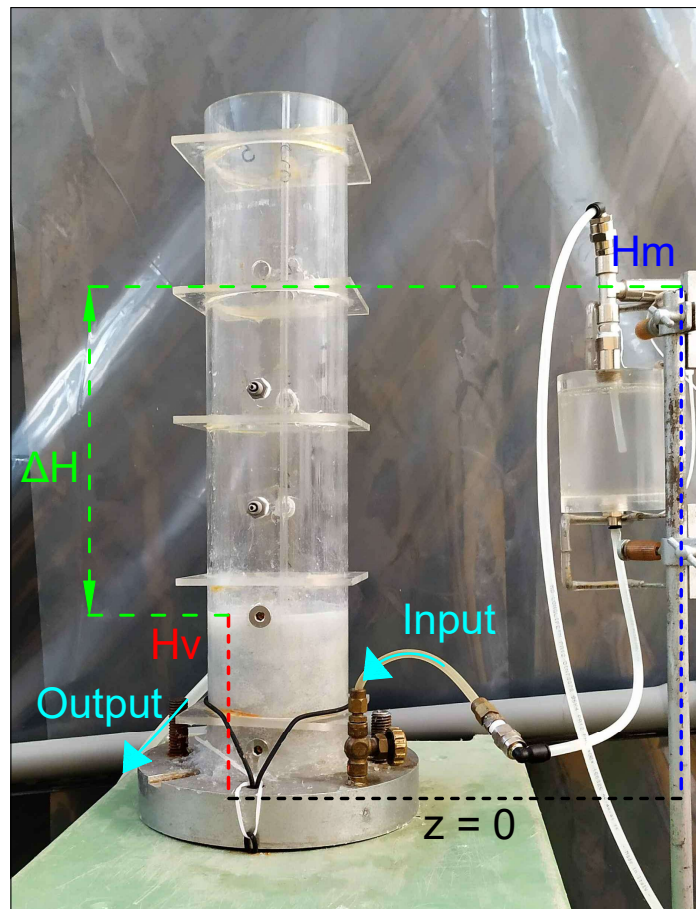


Figure 5.2. The permeameter employed for the tests

5.2.2 The material

The material used for the test has the gradation described in paragraph 4.3.1, with percentages of the three fractions of class A, B and C corresponding to 60%, 20% and 20% respectively. The sample height is 9 cm, the void ratio e is 0.29, and the initial water content w is 8%.

Once the sample was placed in the permeameter and an initial saturation phase was carried out, a settlement of the sample of 0.5 cm was observed, thus modifying the void ratio initially measured. In fact, the value of e to reach the value of 0.22.

With the vertical seepage test it is expected that the eroded material belongs to the two lower diameter classes and that the class A material may be displaced but

not removed, since the seepage force of the water is not sufficient to keep the coarser particles in suspension. The appropriate sieves were then set up to separate the two fractions of medium and fine material once the eroded beads had been collected, checking also if class A particles have been eventually removed.

5.2.3 The setup of the test

The test was carried out in two different sessions, one with a lower set of gradients, also used to verify the reliability of the instrumentation, and a second with the aim of achieving high gradients until soil boiling was established in the sample. The list of gradients applied in the two sessions are reported in Table 5.1.

Table 5.1. List of gradients for the tests

First set	Second set
i [-]	
0.15	0.05
0.27	0.16
0.33	0.32
0.46	0.47
0.63	0.80
	1.09
	1.32
	1.65
	1.89

The first phase of the test consists in placing the upstream tank at the same height of the downstream outlet in order to saturate the sample without introducing any seepage process. This step must be carried out slowly without disturbing the sample.

Once the saturation stage is completed, the H_m level is increased until the prescribed gradient is obtained. If the entire hydraulic head difference ΔH was dissipated within the sample of height l , the gradient would be expressed by the following relation:

$$i = \frac{\Delta H}{l} \quad (5.2)$$

The upstream hydraulic head is measured by means of the piezometer and during the course of the test it is possible that the level of water in it changes from the initial one, so it is necessary to monitor it to report any changes in the hydraulic gradient.

The water flowing out of the spillway of the downstream reservoir is collected in a graduated cylinder and at given time intervals, after having separated the glass beads from the water, the weight of the outflow is measured. The flow rate is then calculated using the Darcy equation to determine the value of k for that time interval.

The eroded material is collected in the cylinder, then poured into a series of sieves and weighed to determine what fraction of the medium and fine beads have been removed from the sample. If the gradient is not sufficient to keep the beads in suspension so that they flow out of the spillway, a stirring rod can be used to agitate the water above the sample to hold them in suspension and prevent settling. In fact, a volume of water corresponding to 2 cm above the sample was designated to observe the behaviour of the particles once eroded.

5.3 Test results

5.3.1 First set

To evaluate the hydraulic conductivity of the glass beads assembly in undisturbed conditions, the first set of tests was carried out with gradient values lower than the critical gradient, which is the value that, according to Terzaghi's principle, nullifies the effective stresses at the base. The critical gradient i_c is given by:

$$i_c = \frac{\gamma'}{\gamma_w} = 1.17 \quad (5.3)$$

With:

- γ' effective weight of the glass beads [kN/m^3];
- γ_w specific weight of water [kN/m^3].

To better understand how the hydraulic gradients chosen are distant from the critical one, the safety factor F_s (Table 5.2) is computed for each test:

$$F_s = \frac{i_c}{i} \quad (5.4)$$

The hydraulic conductivity is evaluated with equation 5.1. The trend observed in the various tests is common, with a higher initial value of k and a regular decrease in some cases, such as the ones corresponding to $i = 0.15$, $i = 0.27$ or $i = 0.63$. In the cases with $i = 0.33$ and $i = 0.46$ on the other hand, some irregularities can be observed, which can be ascribed to experimental uncertainties. At such low gradients, the base may get clogged or air bubbles may form in the small tube connecting the upstream reservoir to the sample, thereby altering the measured hydraulic conductivity value. Special attention should also be given to the piezometer, which is embedded within the sample and can create a preferential seepage path along its outer surfaces. The level readings in the piezometer are also subject to variation, so care must be taken to ensure that there is no clogging at the base of the tube that could compromise the determination of the gradient.

From a comparison carried out on a logarithmic scale of k , it is possible to note a decrease in the initial values of k as the gradient increases, with the exception of the test with i equal to 0.33. As the test progresses, a decrease in k common to all five tests is observed, eventually stabilising on hydraulic conductivity values lower than 10^{-4} m/s (Figure 5.3). The decrease in hydraulic conductivity observed over time can be explained as the effect of the flowing water that tends to dislodge fine and medium particles that settle with time, creating non homogeneities in the density.

Table 5.2. F_s for the first set of tests

i [-]	Fs [-]
0.15	7.80
0.27	4.33
0.33	3.55
0.46	2.54
0.63	1.86

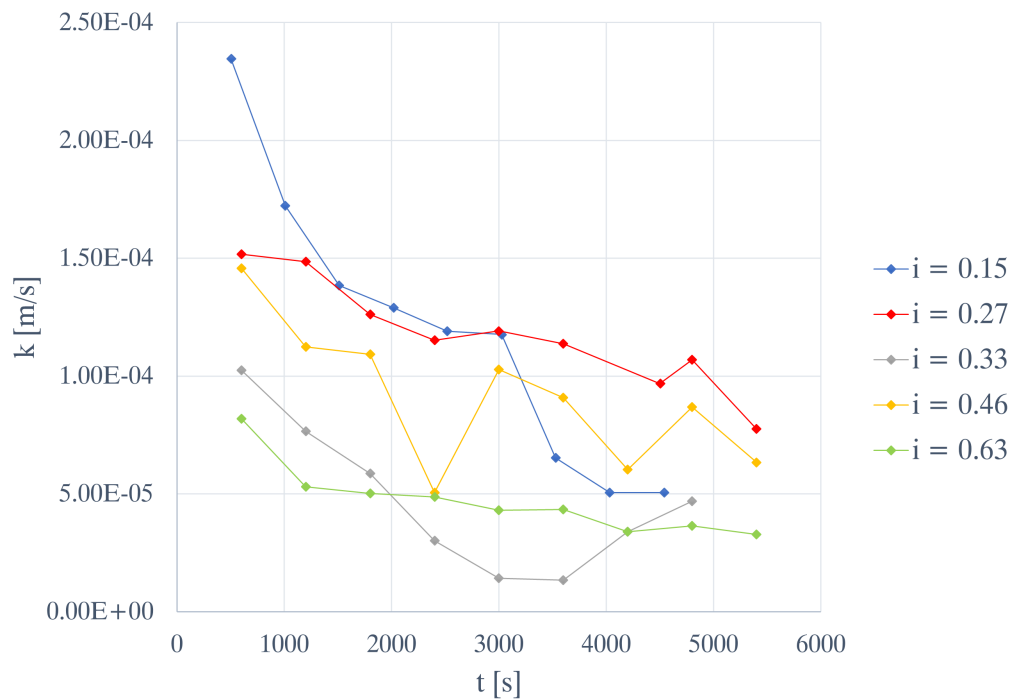


Figure 5.3. Hydraulic conductivity tests with i from 0.15 to 0.63

A comparison has then been carried out considering Figure 5.4 in which the values are reported considering the last three measurements carried out assuming to have completed the initial transient phase, after more than one hour from the beginning of the test. From the results it is noted that the gradient values of 0.15, 0.33 and 0.63 have provided k values around $3.5 \cdot 10^{-5}$ m/s. The other two tests, on the other hand, provided much higher k values, leading to two possible considerations: in the case three cases of lower k , a clogging phenomenon of the base or pipe for the input or output of water may have occurred, or in the case of higher k , a preferential flow path may have originated. The flow is not in a steady state condition, so a longer test duration would have been required to provide a better interpretation of the results. In addition, the flow generates particle displacement and density change for high t , with an increasing effect with i . For this reason it is likely that k decreases with time and in tests with higher i , the initial values of k are lower.

No relevant quantities of eroded material were collected in the first two tests, likely because no particularly high values of k were reached. Only for the last three a small quantity of material eroded from the sample was noticed. From the results reported in Figure 5.5 a small quantity of glass beads is removed only for gradients higher than 0.33. Initially there is more material of class B, but in the fourth and fifth tests the trend is inverted with more class C material. No glass beads of class A were collected.

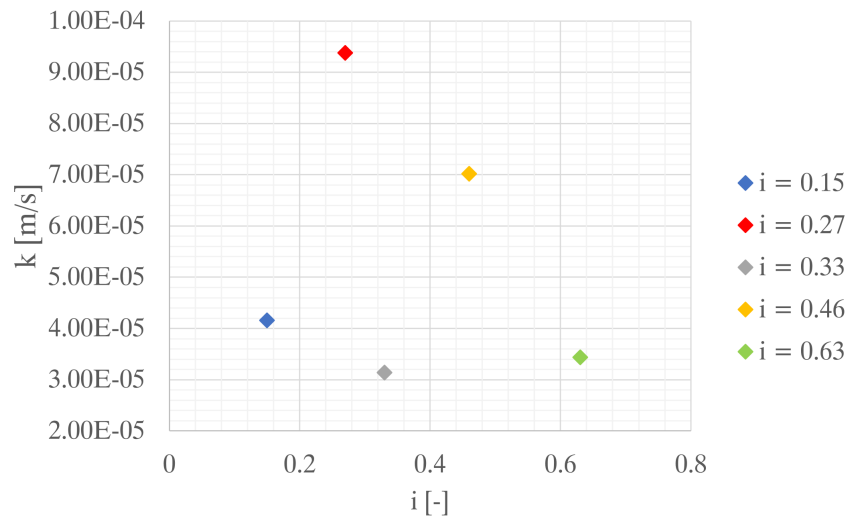


Figure 5.4. Mean values of the last three measurements of k for each test

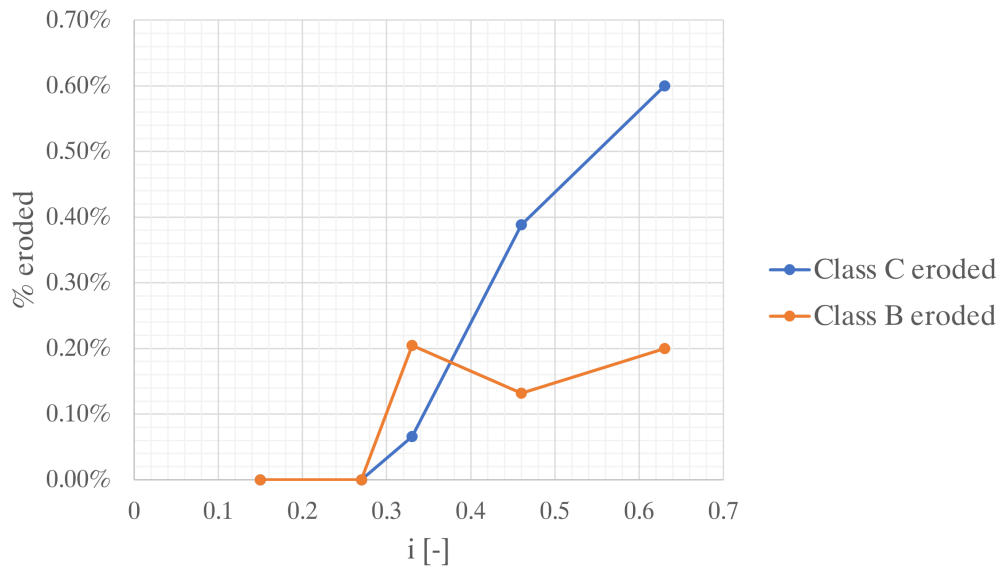


Figure 5.5. Eroded mass measured in the first set of tests as percent over the total

The main effect of seepage in these tests results in a displacement of the finer particles which are subsequently transported to the superficial layer. To investigate this phenomenon, small quantities of material were taken at different sample heights and sieved to reconstruct their grain size distribution. The results obtained are shown in Figure 5.6: the fine particles have been moved from the lower layer to be deposited in the more superficial one thus creating an intermediate layer (-6.5 cm) richer in large particles (class A) and an upper layer richer in fine particles (class C) with respect to

the initial distribution.

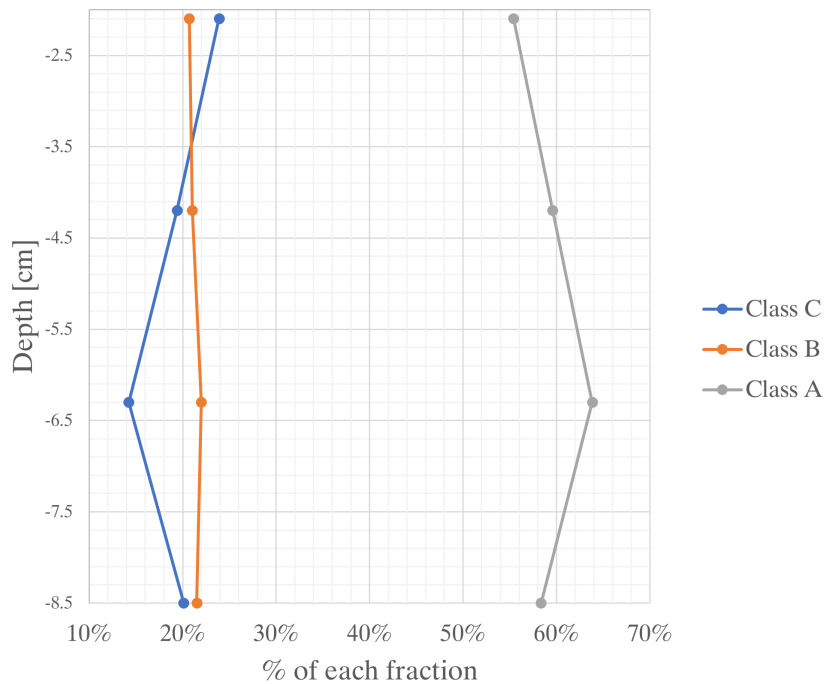


Figure 5.6. Particle size distribution along depth in the first set of tests

5.3.2 Second set

Once the preliminary operations carried out in the first set of tests were completed, further significant tests were carried out to reach and go beyond i_c . The critical gradient was in fact determined with the (5.3).

The sample was reconstructed using the same methodology as before and the critical gradient was reached by means of small increments in order to monitor in detail the progress of erosion as the upstream hydraulic head increased. The tests were conducted with nine different gradients from 0.05 to 1.89. The initial void ratio of 0.29 decreases because of the saturation phase that induces a settlement of 0.5 cm of the sample. The new void ratio was found to be the same as in the previous case and equal to 0.22.

Especially for low gradients, a rapid decrease in hydraulic conductivity with time has also been observed in this case. The phenomenon occurs in a more pronounced way and with a tendency towards an asymptotic value in the cases with a lower gradient, while for those with a gradient above or around the critical value different

behaviours can be observed, which can be explained by a large flow rate input. As a consequence, the measurement is more difficult due to the velocity with which the collection tank is filled, often causing irregularities in the water outflow probably due to air bubbles that tend to clog the output pipe.

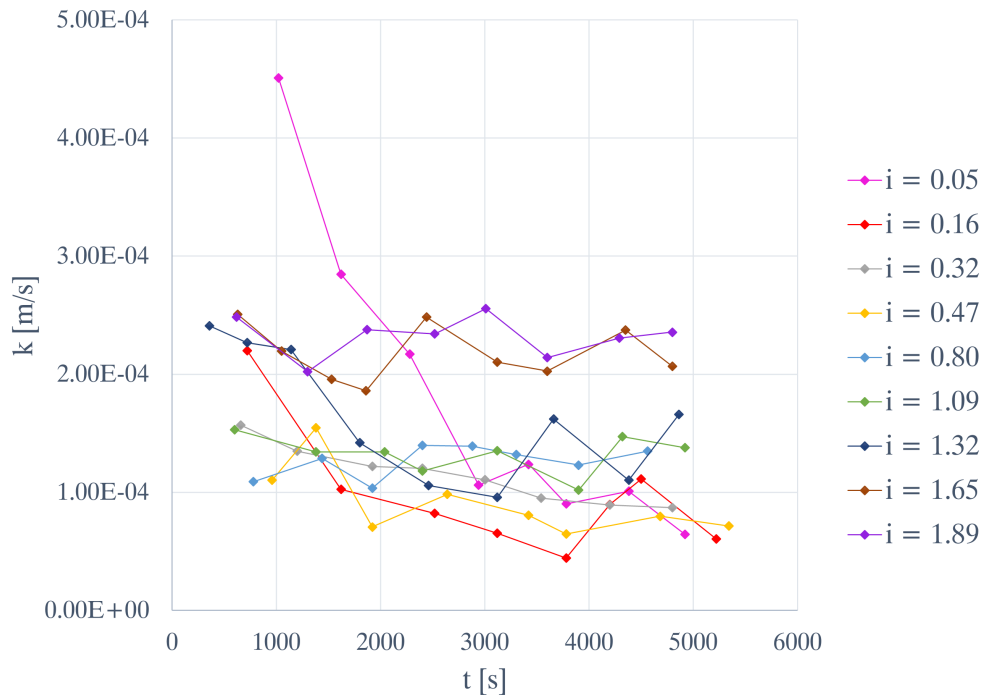


Figure 5.7. Hydraulic conductivity tests with i from 0.05 to 1.89

During the tests with a gradient higher than the critical one, some phenomena such as the release of bubbles were observed. In particular, starting from the test with $i = 1.32$ soil boiling was observed. Furthermore, at the beginning of the test with hydraulic gradient equal to 1.65, a considerable flow of material out of the sample was immediately noticed.

An analysis carried out by comparing the different variations of k over time shows that at the beginning of the first test with lower gradient, the highest hydraulic conductivity value was observed, probably due to the fact that during the placement of the material and the saturation phase preferential channels remained along the walls which allowed the water to flow more rapidly. As the test continued, the re-arrangement of the material led to lower hydraulic conductivity values. The value of k then increased with the gradient due to the pipes that were created inside the sample, which caused the flow to pass more easily. Excluding the first part of the first test, it can be observed that the hydraulic conductivity for values of i around

the critical value are slightly above 10^{-4} m/s, up to $2.3 \cdot 10^{-4}$ m/s with the maximum gradient. For high values of i the flow stops being laminar, therefore Darcy's law does not govern the process anymore.

Compared to the previous tests, the consistency of the results obtained in this case leads to the conclusion that they are more reliable than those obtained in the first tests because more familiarity has been gained with the instrumentation, especially in managing the measurement methods of the outflow and in controlling the level in the piezometer. As can be seen from Figure 5.7, the values obtained for low gradients do not differ too much from those achieved previously.

Observing the average values obtained from the last values recorded for each test, it can be appreciated that a linear correlation exists between the hydraulic conductivity and the hydraulic gradient. In fact, as i increases, k also increases and the data are arranged along a straight line with an intercept slightly lower than $5 \cdot 10^{-5}$ m/s. This effect is due to the fact that as the gradient increases, the sample is subject to the formation of pipes, leading to higher values of k . In addition, the more fine soil is removed from the sample, the easier the skeleton of coarser material is permeated. No change in the correlation between i and k is observed after the critical gradient is exceeded.

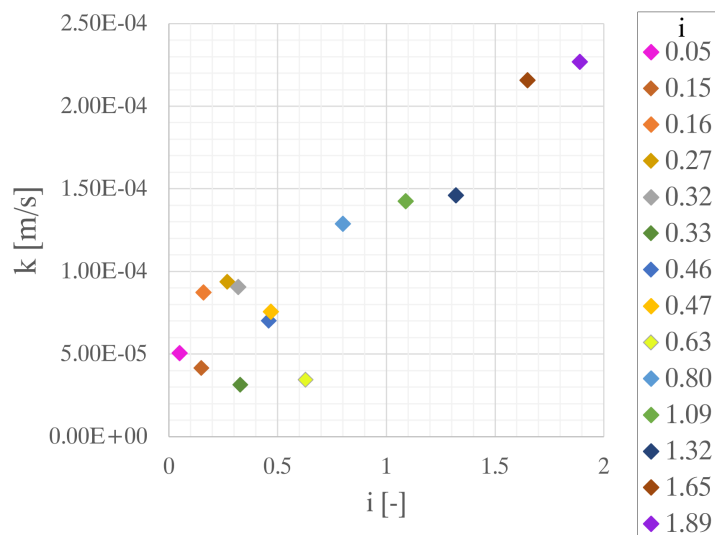


Figure 5.8. Comparison of the mean values of the last three measurements of k both set of tests

The graph (Figure 5.9) shows the amount of material eroded each step compared to the amount left in the sample belonging to that class. With regard to the medium particles, there is no significant erosion at the end of the step for each gradient, while

with regard to the class C material, a completely different behaviour is observed. In fact, once the critical gradient has been exceeded, the amount of removed material increases considerably, reaching a total of 114.83 g of fine material from the initial total of 334.80 g.

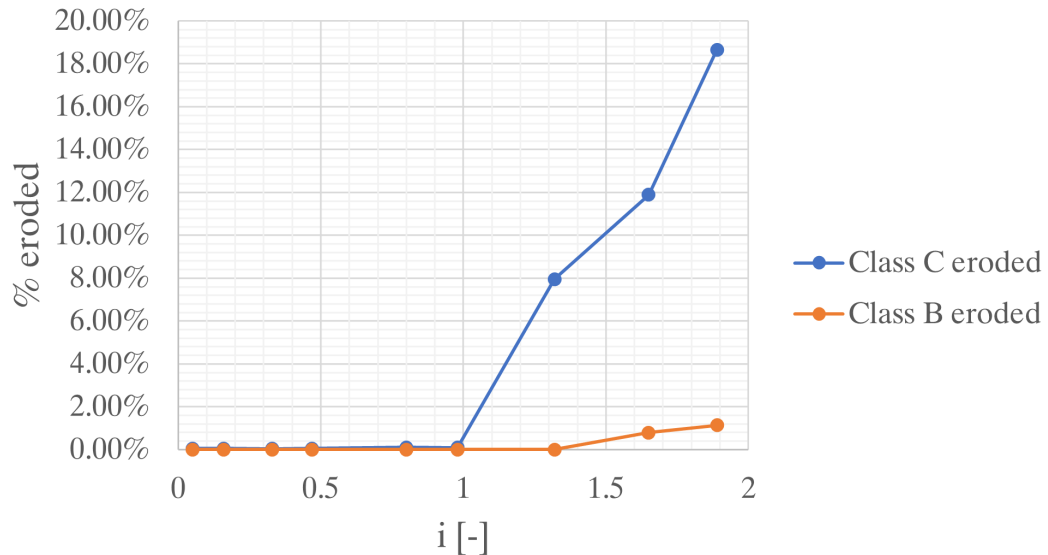


Figure 5.9. Eroded mass measured in the second set of tests

From the particle size distribution (Figure 5.10) it appears that the fine particles were eroded more from the lower part of the sample, but there was no accumulation in the upper area, differently from the previous case, because much of the material was carried away by the water flow. On the other hand, the medium diameter particles were dragged to the surface and into the middle to upper layer but failed to be lifted and collected in the downstream storage container.

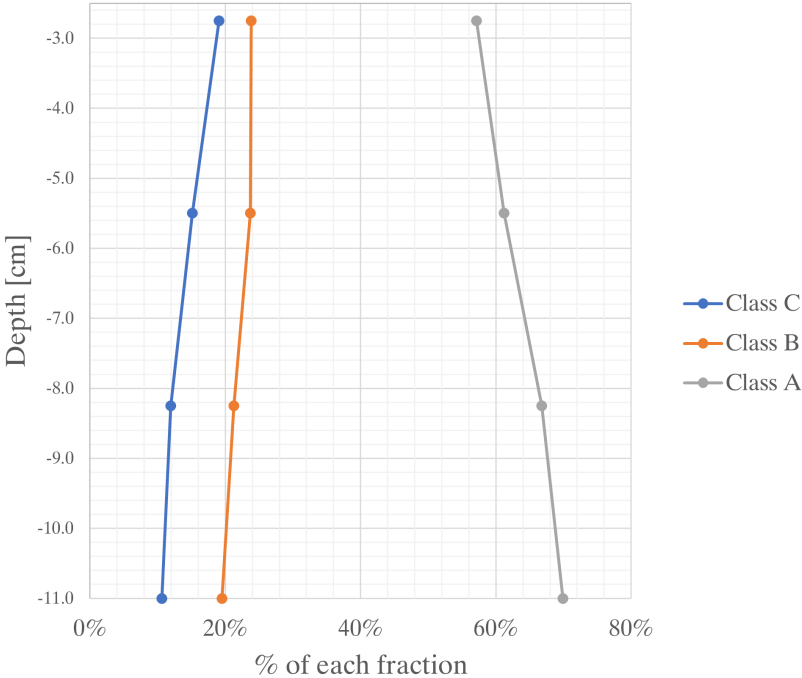


Figure 5.10. Particle size distribution along depth in the second set of tests

Chapter 6

Horizontal seepage in EPBox

The EPBox allows horizontal seepage tests to be carried out under fully (Figure 6.1) or partially saturated (Figure 6.2) sample conditions. The tests can be performed with or without applying additional pressure. In each case the measurements that can be made concern the hydraulic conductivity of the material and the amount of eroded material over time. If the length of the sample is sufficient to locate a piezometer, pressure measurements can also be taken at any time during the test.

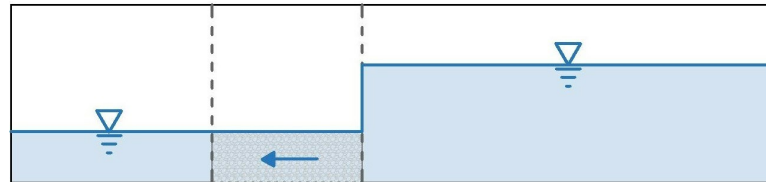


Figure 6.1. Schematic representation of a fully horizontal seepage test

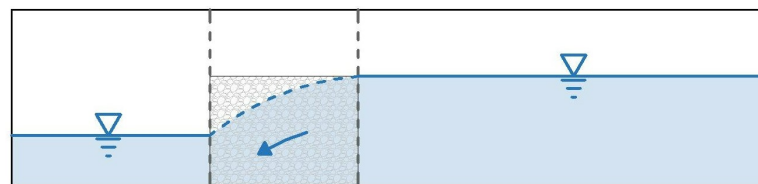


Figure 6.2. Schematic representation of a seepage test on a partially saturated sample

It was decided to carry out tests with completely saturated material, so as to obtain horizontal hydraulic conductivity values under conditions similar to those described in the previous chapter. Moreover, horizontal seepage with a fully saturated material makes it easier the interpretation of the phenomenon with respect to the case of seepage with a partially saturated medium. Comparing a horizontal seepage process with a vertical one, the differences due to the direction of the force of gravity with

Table 6.1. Summary of tests carried out in the EPBox

Test id	Sample	i [-]	Erosion measures	Granulometric distribution
#1	S1	0.84	At the end	No
#2	S1	0.16	At the end	Yes
#3	S2	0.64	During test	No
#4	S3	0.18	During test	No

respect to the movement of the particles must be taken into account. In fact, when considering horizontal seepage, the weight vector acts perpendicular to the direction of movement of an eroded particle, whereas in the case of vertical seepage the force of gravity has a direction opposite to the movement, making the uplift of the particle more difficult.

In addition to preliminary operations of filling and emptying of the box as overall check of the apparatus, the capacity of discharge and re-injection of water into the two reservoirs, to maintain constant upstream and downstream levels, was verified. Following this, tests were carried out with four different gradients and with durations from 5 to 26 hours. The tests were carried out to gain confidence with the equipment and verify and solve possible problems. A summary of the tests and the results obtained in Table 6.1.

6.1 Comparing horizontal and vertical seepage tests

Different values of vertical and horizontal hydraulic conductivities are available in the literature, often indicated respectively as k_V and k_H , with H being the direction of layering, usually horizontal, and V being the direction perpendicular to H. The disposition of layers of stratified rocks and soils depends on how sediments macroscopically settle and, at microscopic level, how particles tend to deposit in the condition of lowest possible energy. Depending on the shape of the particles this effect will be more or less marked, meaning that for spherical beads this effect does not occur.

The anisotropy of the hydraulic conductivity has very significant effects on both the flow and the transport of contaminants. For this reason, a knowledge of the characteristics of the hydraulic conductivity tensor can be useful in different problems

such as seepage beneath dams and dykes, internal erosion phenomena, but also for different applications such as the dimensioning of hydrocarbon extraction wells.

The anisotropy of k for unsaturated soils reaches much higher values than for saturated ones. The relationship between horizontal and vertical hydraulic conductivity in non-cohesive soils is much less studied than in rocks or cohesive soils. The reason for this difference is that permeameters are generally designed to perform vertical seepage tests, so there is a lack of data on horizontal seepage. There is also a dependence on the soil density. For sandy soils, for example, it may be stated that in a loose state the hydraulic conductivity is isotropic, but once thickened statically and vertically, a considerable increase in the difference between vertical and horizontal k is observed (Chapuis and Gill 1989).

Earth structures for water containment are subject to internal erosion and the water follows a path where the direction of flow differs from that of gravity in different areas of the embankment. In fact, as shown in Figure 6.3, in the section below the upstream reservoir the seepage path is directed as the force of gravity, becoming then parallel to the ground passing below the structure. Lastly, coming out of the downstream part of the ground, the direction is again the same as the vertical one, but the direction is opposite, opposite to the gravity. On the other hand, considering the embankment body the flow direction has both horizontal and vertical components. For this reason it is important to have the possibility to perform tests able to apply different directions to the flow. In particular, in the case of the EPBox, the same equipment allows to conduct both horizontal seepage tests if used in the standard way, and vertical tests or with any inclination.

The influence of the angle between flow direction and layer deposition on internal erosion is of considerable importance and has also been examined with special physical models (Pachideh and Hosseini 2019). In particular, the gradient required to observe erosion in the case of vertical upward flow is much greater than in the case of a horizontal or downward flow, due to the action of gravity, opposite to the direction of movement of the eroded particles. In addition, it was observed that in the case of seepage with the flow direction perpendicular to the soil layers pattern, the amount of eroded particles was lower than in tests with a parallel seepage. From the point of view of pipe development, in the case of flow perpendicular to the layers the pipes extend with sharp changes in direction, whereas in case of a parallel flow the pipes are straight.

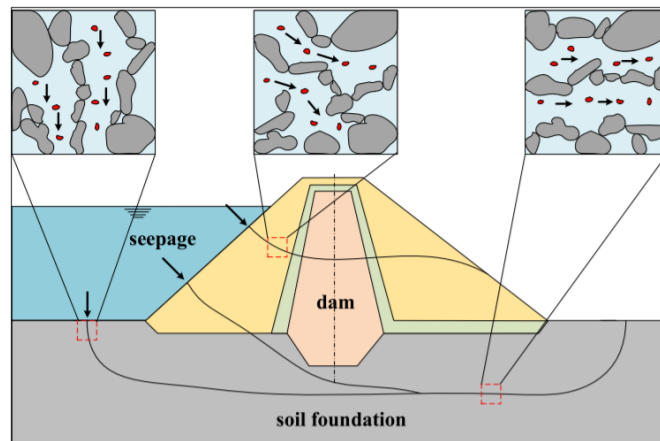


Figure 6.3. Seepage direction in different areas of an embankment dam (Xiong et al. 2021)

6.2 The EPBox tests

6.2.1 Setup and testing of the device

Once all the hydraulic connections required for the inlet and outlet of water were in place, a filling and emptying test was carried out on the device to check the possible presence of leaks both due to screws and gaskets and to taps and junctions. At this stage no problems were found and therefore the first test was carried out.

Since the device had to be employed for horizontal seepage, reaching a level of water in the upstream reservoir greater than the height of the sample placed in the EPBox, it was necessary to close the part of the upstream filter higher than the sample covering them with a transparent plastic film which worked very effectively, as shown in Figure 6.1. In addition, there is an evident problem of water pressure acting on the upper plate that confines the sample, linearly distributed between the maximum value on the upstream side to the minimum on the downstream. To counteract this pressure and prevent water from leaking above the sample, various solutions were tried, applying a uniform pressure on the upper plate and sealing the gap between the plate and the internal sides of the box, as well as every other opening corresponding to the corners of the filters. Since it was not possible to opt for a definitive and permanent solution such as silicone (in fact, one of the basic principles for which the box was created and sized was the possibility of reusing and varying the applications of the device, so a permanent solution could not be considered), various other methods of sealing were tried, such as vaseline grease applied along all the edges to create a water-resistant barrier. Each of the solutions proved to be completely ineffective.

Finally the effective solution was to use a plastic bag filled with water, so that it could adhere well to the walls of the box, adapting itself to the shape of the space to be covered, and also providing the necessary weight to compensate for underthrust. To test the effectiveness of the solution, the upstream tank was filled up to an height H_m , the filters and the bag were placed inside without the glass beads and the downstream tank was left empty (Figure 6.4). Indeed, no passage of water occurred from the upstream to the downstream tank, so the solution was considered effective.

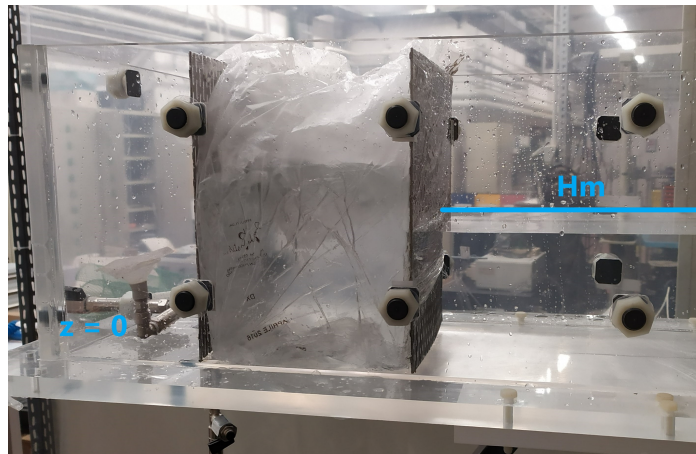


Figure 6.4. Effectiveness of confinement of the upstream reservoir by means of a bag filled with water

Once the effectiveness of the separation system between the upstream and downstream reservoirs had been verified, the sample required for the seepage tests was prepared. With the aim of achieving high gradients, the minimum possible sample length was imposed, meaning that the filters were positioned in locations corresponding to two adjacent screws, thus leading to 20.6 cm in length. The sample was placed with a height of 7 cm. Having width of 29.6 cm, the total volume is 4268.32 cm^3 and the mass 8260.19 g, with an initial void ratio e of 0.29. As a result of the saturation phase, a settlement of the sample equal to 0.5 cm was observed, resulting in a void ratio of 0.20. As noted by other authors (Pachideh and Hosseini 2019), for a proper representativeness of the sample the ratio between the maximum diameter of the grains and the minimum size of the specimen should be smaller than 0.2. In this case, the ratio gives a value of 0.031, which is acceptable.

The first test was to impose the maximum applicable gradient in order to verify the functioning of the equipment and the capacity to collect the eroded material through the trap box. In addition, the functionality of the filters was to be evaluated.

In particular, it was necessary to observe possible imperfections on the edges with the potential risk of allowing coarse material to pass through, which could cause problems when measuring the eroded mass. In fact, it would provide incorrect measurements due to a class of material that should not be counted as eroded considering that the openings of the filters should not allow particles of 2 mm diameters to be eroded. Moreover, particles with a larger diameter are more likely to obstruct the pipes connecting the trap box to the device, although all the hydraulic connections used to collect the eroded material have been designed to have an opening wider than the others, to avoid clogging problems.

6.2.2 First test

Since the purpose of the first test was to verify the overall functioning of the equipment, the focus was put on the hydraulic conductivity assessment only. The test lasted approximately 5 and a half hours, with nine measurements taken regularly throughout the test. As can be seen from the Figure 6.5, the hydraulic conductivity values obtained were all close to $8 \cdot 10^{-4}$, with a minimum of $6.92 \cdot 10^{-4}$ m/s and a maximum of $9.42 \cdot 10^{-4}$ m/s, with a final value of $6.99 \cdot 10^{-4}$ m/s after more than 5 hours. The results obtained in terms of eroded mass are reported in Table 6.2.

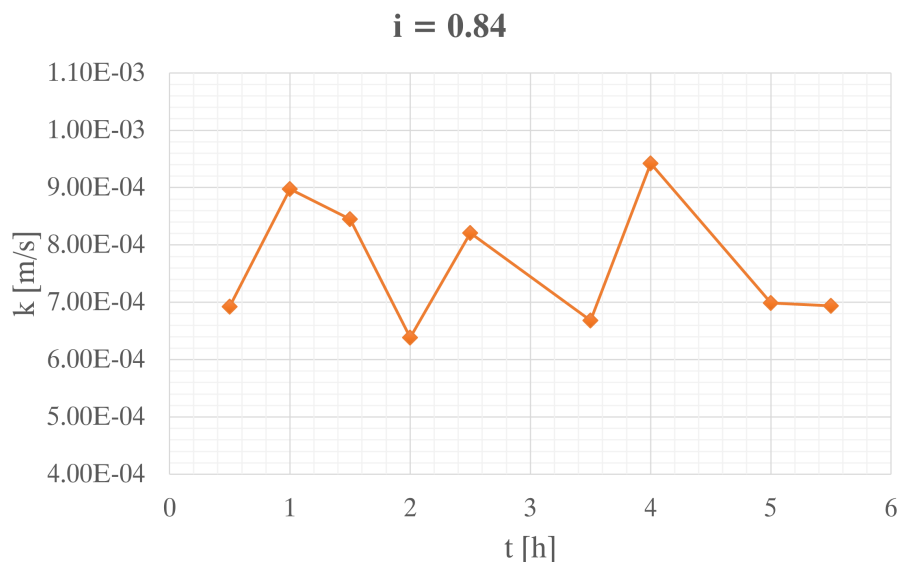


Figure 6.5. Hydraulic conductivity test in EPBox with $i = 0.84$

At the end of the test the amount of eroded material accumulated in the downstream reservoir during the test was measured, trying to avoid collecting also that

Table 6.2. Total eroded mass and percentage over the initial mass of each class in first test

	Class B		Class C	
i [-]	m [g]	% of m	m [g]	% of m
0.84	2.81	0.17%	30.73	1.86%

which had been removed from the sample due to imperfections in the operation of the filters. The results obtained are reported in Table 6.2.

6.2.3 Second test

The second test was carried out on the same sample employed in the previous test and therefore part of the material had already been subjected to erosion. A gradient of 0.16 was applied to measure a hydraulic conductivity value corresponding to a seepage process without erosion.

The upstream and downstream reservoirs were emptied after the conclusion of the 0.84 gradient test and the sample remained in the EPBox for a few hours before being saturated again. As a result of this process, the material further settled due to saturation. The voids created in the first test due to the removal of the material were compensated by this phenomenon, resulting in a density that was probably even higher than in the initial test.

In addition, during the first test, the displacement of the fine particles from the upstream to the downstream part of the sample may have resulted in the formation of a low-hydraulic conductivity zone that acted as a "cap". In fact, as shown in Figure 6.6, the test lasted about 7 hours and resulted in lower hydraulic conductivity values than in the previous case, equal to $9.30 \cdot 10^{-5}$ m/s.

At the end of the test the grain size distribution at 6 different locations of the sample (near the upstream filter, in the middle and near the downstream filter for both the surface and the deep part) was measured in order to understand where erosion acted the most. The sample may not have had a uniform distribution of the three classes throughout its volume from beginning of the test, because saturation may lead to a deposition of the finest particles at the base of the box, so this aspect must also be taken into account in the analysis of these results.

Observing the fraction of the sample collected near the surface (Figure 6.7) in the

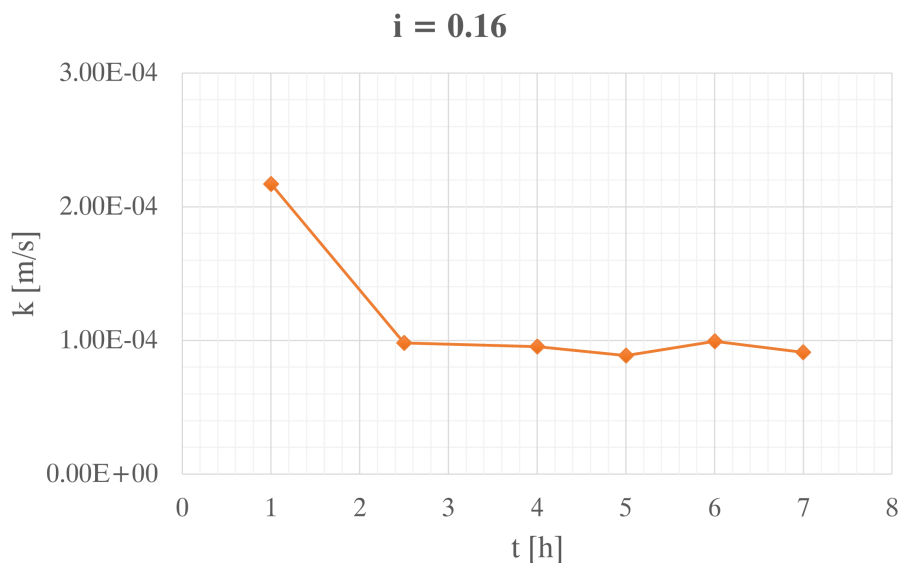


Figure 6.6. Hydraulic conductivity test in EPBox with $i = 0.16$

three positions, it can be seen that there is a percentage increase in the amount of eroded material belonging to class C and displacement of the finer particles downstream, both phenomena not acting on the 2 mm diameter material. In addition, the amount of fines increases along the seepage path (but remains below the initial composition of 20% with respect to the total mass) because some of the material is initially eroded and then redeposited further downstream.

The same phenomenon was also observed on the deep samples, but with less evidence (Figure 6.8). Probably as a result of the saturation phase some of the fine material was deposited in that area of the sample, so the composition of the material at the beginning of the seepage test was not the reference composition of 60% fraction A, 20% B and 20% C, but the fine was in a higher quantity, thus leading to an uncertain interpretation of these data.

The quantity of eroded material was negligible. It can be concluded that with such a low gradient the material is at most dragged towards the downstream part of the sample but the water does not have sufficient force to erode particles.

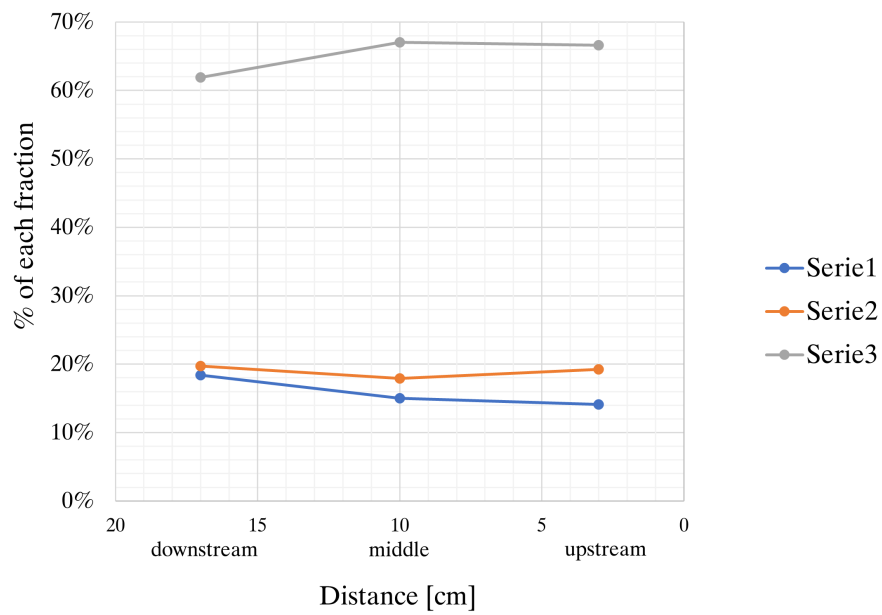


Figure 6.7. Grain size distribution of the superficial part of the sample

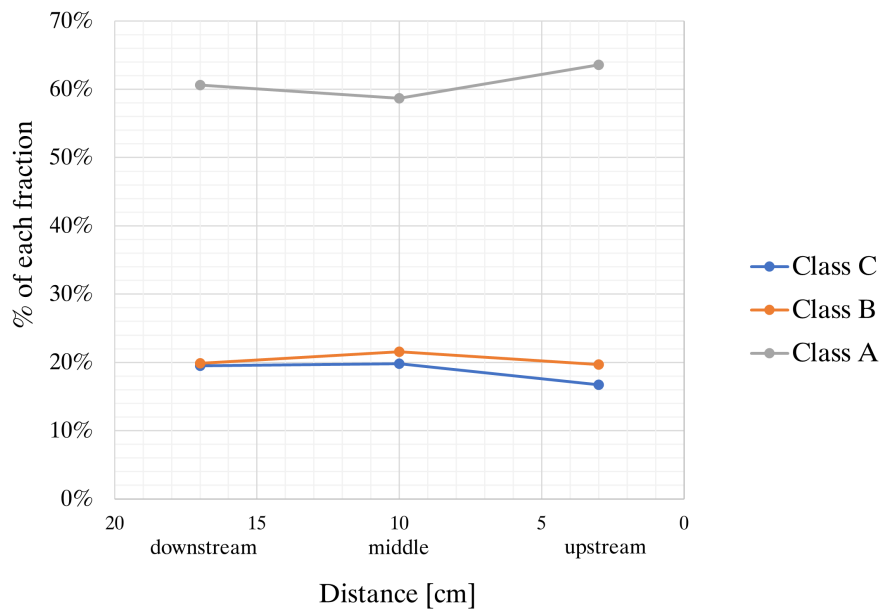


Figure 6.8. Grain size distribution of the deep part of the sample

6.2.4 Third test

Once the particle size analysis of the first sample employed was completed, the material was completely removed from the box and a new one was introduced for the second test with the same volume and characteristics. After the saturation phase, the upstream tank was filled until a hydraulic gradient of 0.64 was reached, with the intention of examining the effect of an intermediate value of gradients.

After an initial calibration phase to set up the bag, drains and material collection system, the test was extended to a total duration of 26 hours, taking five measurements of the amount of eroded grains and of the hydraulic conductivity. The duration of the test was not established in advance, the test was stopped when the amount of eroded material was negligible.

A few hours after the beginning of the test, it was observed that two pipes had been created, along the interface between the sample and the right and left sides of the EPBox, starting from the base of the sample at the upstream reservoir (Figure 6.9). The water finds no resistance in these pipes and therefore a preferential seepage path. The pipe assumes this typical direction because at the base the pressures are higher so the water is favoured to move into the sample, then it rises up to the opposite side because the pressure is lower.

The filter was not able to adhere completely to the walls thus leaving openings larger than 2 mm. This problem required intervention to be solved, affecting the amount of eroded material measured in the first hours of the test. Therefore more material was measured downstream than the quantity that was actually eroded, also class A material that should not be eroded according to how the filters were designed. In fact, observing Figure 6.10, the a large part of the erosion process occurred apparently in the first hour of the test, an anomalous result with respect to what was expected.

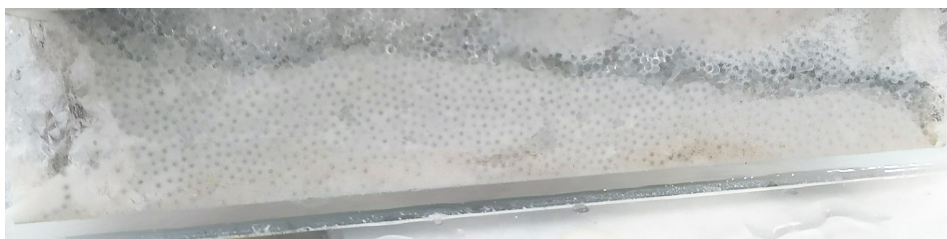


Figure 6.9. Picture showing the pipe formed during the test

Moreover, a reduction in the amount of eroded material can be associated with the formation of the two pipes, that have created a preferential path where water can flow without eroding particles.

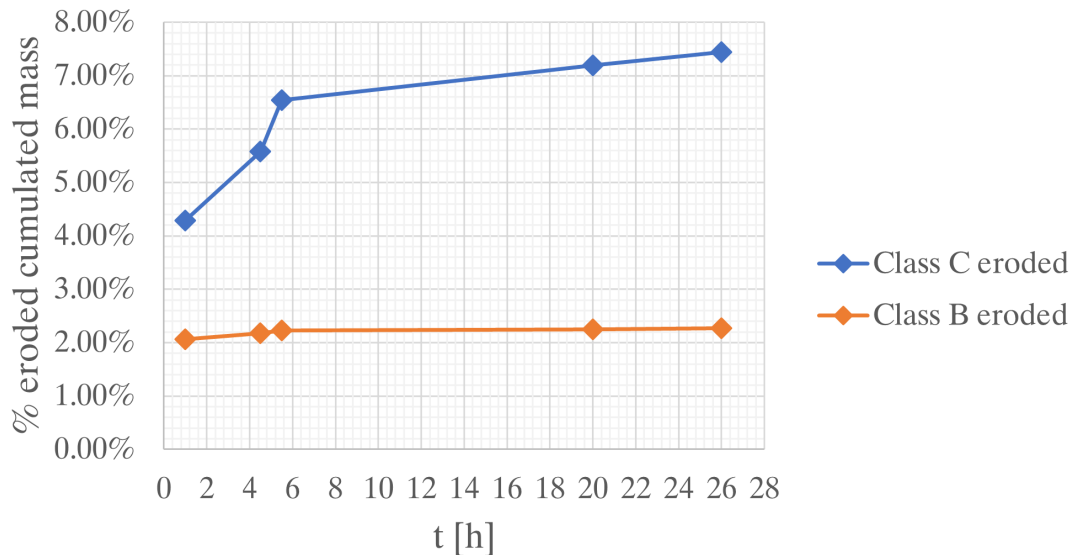


Figure 6.10. Cumulated eroded mass in percentage of class B and C ($i = 0.64$)

At the beginning of the test, the measured hydraulic conductivity exceeded values of $2 \cdot 10^{-4}$ m/s also due to the fact that the separation between the upstream and downstream reservoirs was not perfectly effective. The water managed to find a preferential flow channel without passing through the sample and therefore the assessment of k at this stage may be not accurate. Once 20 hours of seepage have passed, k decreased by almost an order of magnitude, reaching a final constant value slightly higher than $6 \cdot 10^{-4}$ m/s (Figure 6.11).

In order to better observe the relationship between the amount of material eroded and the variation in terms of hydraulic conductivity, these two quantities were combined. Observing the graph in Figure 6.12 it can be observed that a progressive removal of material of medium and fine size from the sample corresponds to a decrease in hydraulic conductivity. This relationship can be associated with the movement of the material downstream that leads to the creation of low hydraulic conductivity zones that induce a decrease in k , or with an increase in density due to the compaction of the material. Although a macroscopic compaction of the sample was not observed, a local collapse of large voids originated during erosion and the closure of the pore network may have occurred.

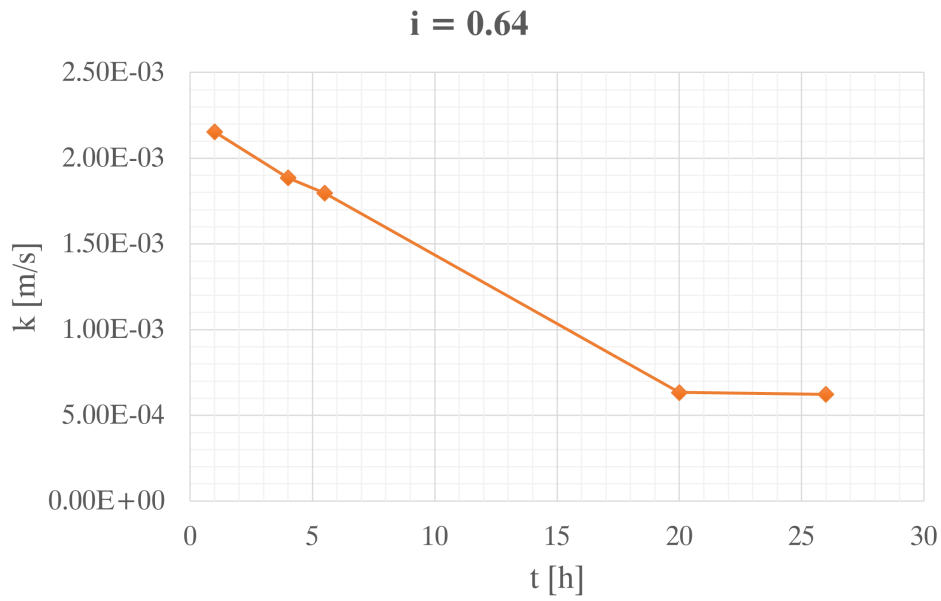


Figure 6.11. Hydraulic conductivity test in EPBox with $i = 0.64$

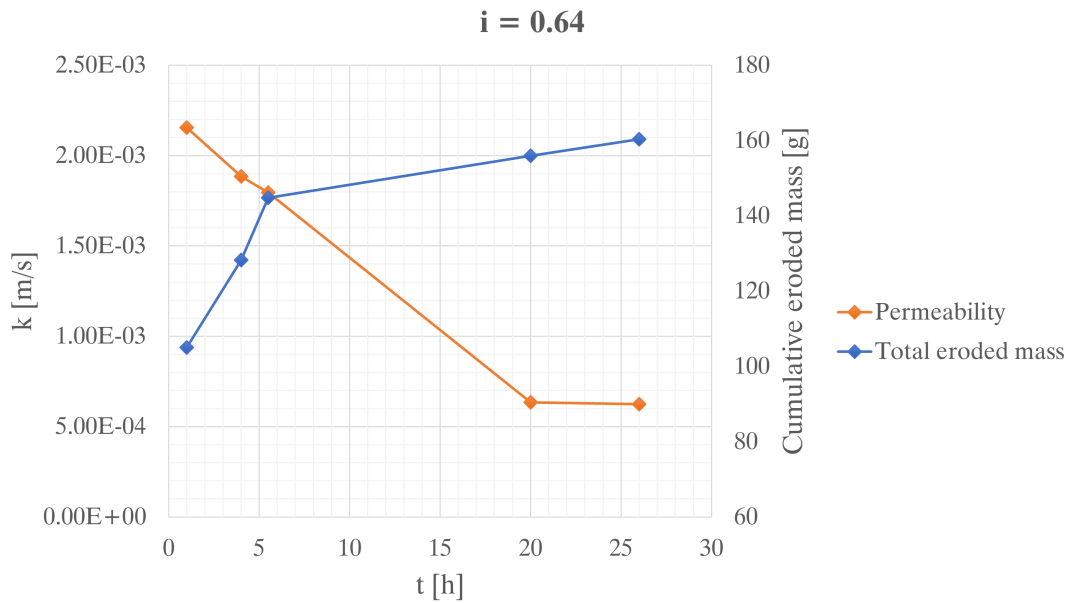


Figure 6.12. Joint representation of cumulated eroded mass and k

6.2.5 Fourth test

To complete the series of tests, a third sample with the same characteristics as the previous ones, with the same degree of saturation and density, was prepared. The objective of this last test is to obtain a hydraulic conductivity value without significant erosion by applying a low gradient equals to 0.18.

From the hydraulic conductivity variation over time, it can be observed that the decrease of k is faster than in the previous case, with the reduction from about $7 \cdot 10^{-4}$ m/s to about $2 \cdot 10^{-4}$ m/s in 6 hours (Figure 6.13).

As regards the mass eroded over time, the values observed compared to the previous case are lower, confirming the correlation between the quantity of eroded material and the hydraulic gradient. The largest amount of mass also in this case is observed in the first hours of the test, mainly for class C material rather than B, but not overcoming the 1.20% of the mass of the same class present in the sample (Figure 6.14).

A relation between the variation of k with the total mass eroded is obtained as in the previous test (Figure 6.15). Even with a low gradient that involves the removal of small amounts of material, the migration of fine material and the compaction of the entire sample lead to a sharp decrease in hydraulic conductivity.

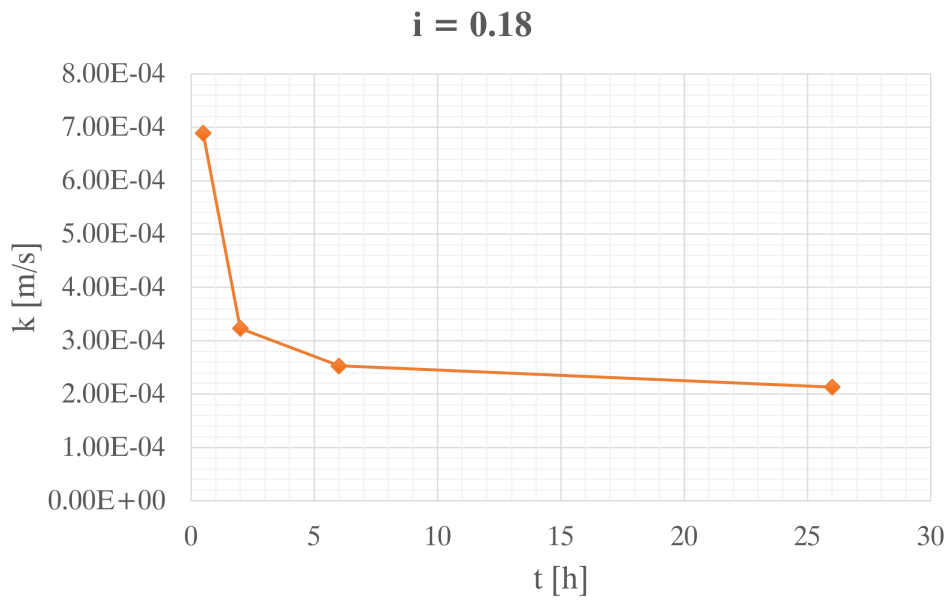


Figure 6.13. Hydraulic conductivity test in EPBox with $i = 0.18$

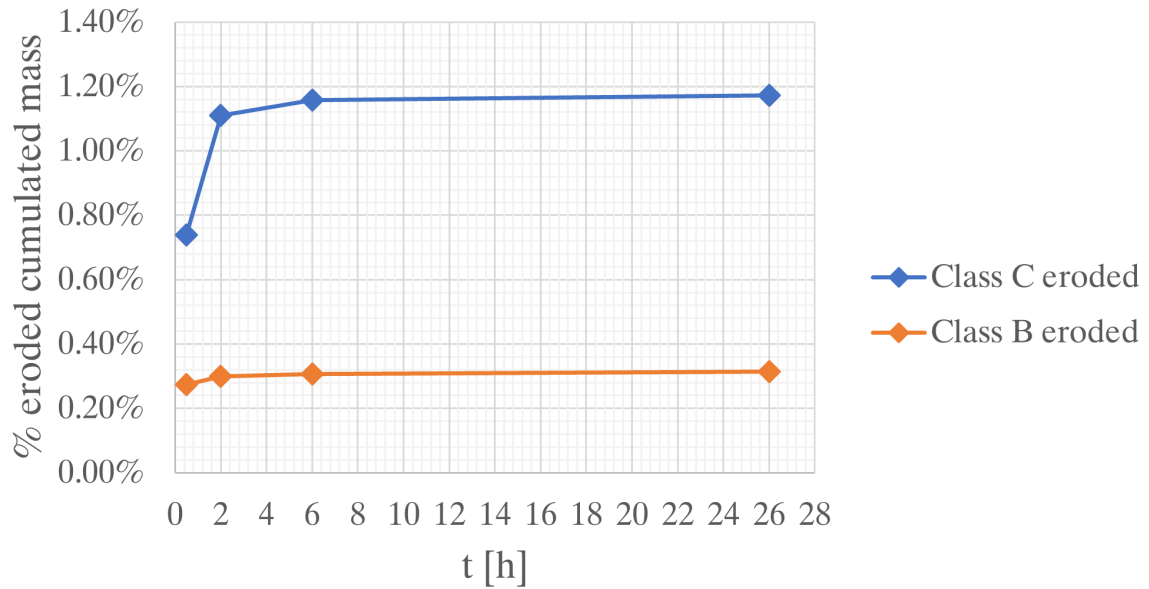


Figure 6.14. Cumulated eroded mass in percentage of class B and C ($i = 0.18$)

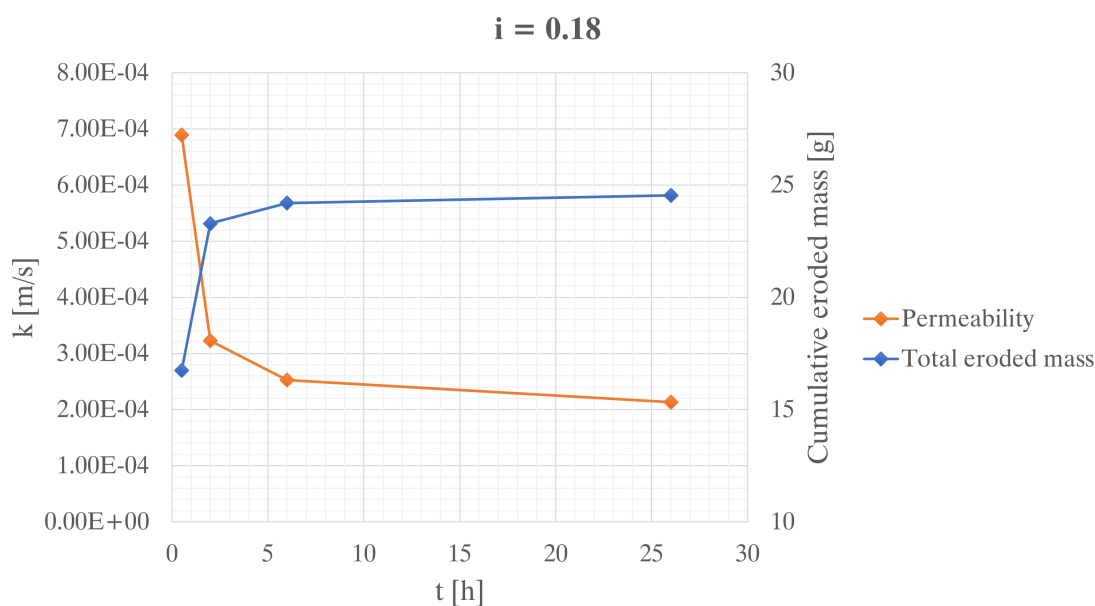


Figure 6.15. Joint representation of cumulated eroded mass and k

6.2.6 Comparison between the tests

It is now examined whether the results obtained are consistent and how they relate to the vertical seepage data, also on the basis of the considerations presented in 6.1.

Figure 6.16 shows that the average value of hydraulic conductivity depends linearly on the gradient. Since this consideration is based on only three values from the EPBox tests, additional data from future tests are required to validate this hypothesis. It is worth remarking that the second test, carried out on the same sample used in the first test, provided a hydraulic conductivity value that should not be compared with the others as it was assessed on a disturbed sample.

A comparison between the results of the vertical tests carried out in the permeameter and the horizontal tests in the EPBox shows a clear distinction between them (Figure 6.17). In fact, the horizontal seepage tests provided significantly higher hydraulic conductivity values than the vertical ones. The phenomenon of seepage acts in completely different ways: the particles that are subjected to an upward directed flow, if they do not receive a sufficient thrust to be dragged away from the sample, redeposit on the top of the sample creating a zone of low hydraulic conductivity and hindering the formation of pipes, that are quickly closed by the material redeposited inside. These effects result in experimental values of k lower than those from horizontal seepage. Moreover, in the horizontal seepage tests, local gradients higher or lower

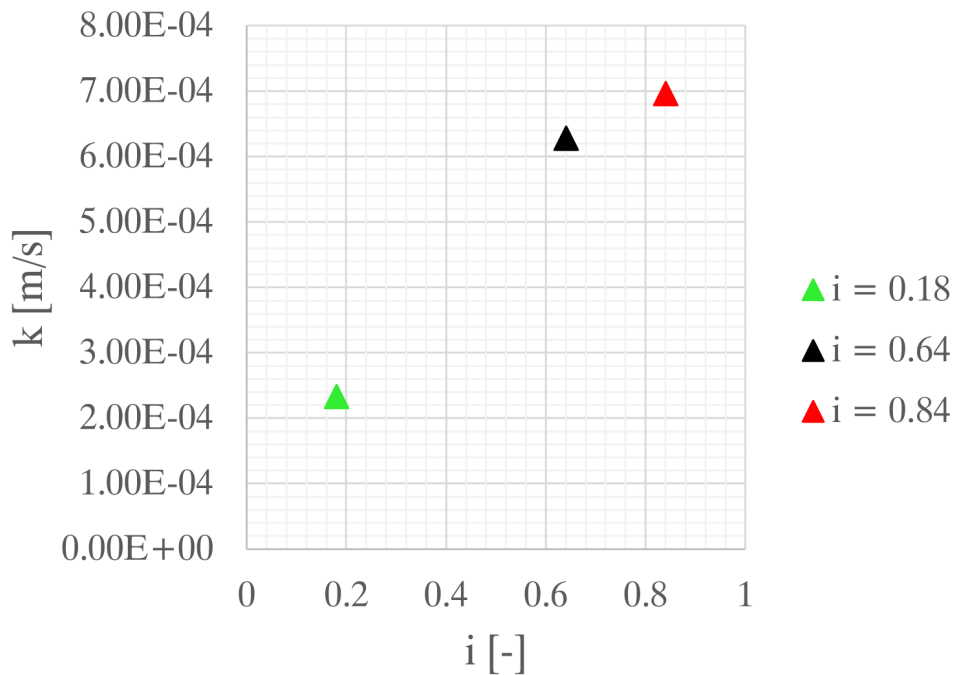


Figure 6.16. Graphical representation of the three horizontal seepage tests performed on new samples in the EPBox

than the average value are more likely to occur, in the nearby of the upstream and downstream sides of the sample. The water flow is therefore able to start erosion and induce development of channels, resulting in a higher hydraulic conductivity value than in the previous case and an amount of eroded material that decreases significantly over time.

Through the sedimentation of the fine material in the lower area of the sample during the saturation phase, a zone is obtained in which the fine material accumulates, while the larger particles remain in the superficial part of the sample. In the case of horizontal seepage, the water can flow through the upper part and coarser part of the sample, the areas with the greatest hydraulic conductivity. In vertical seepage, on the other hand, even if the fine particles are concentrated in the lower portion of the sample, the flow must necessarily cross it and therefore the hydraulic conductivity remains low (Figure 6.18).

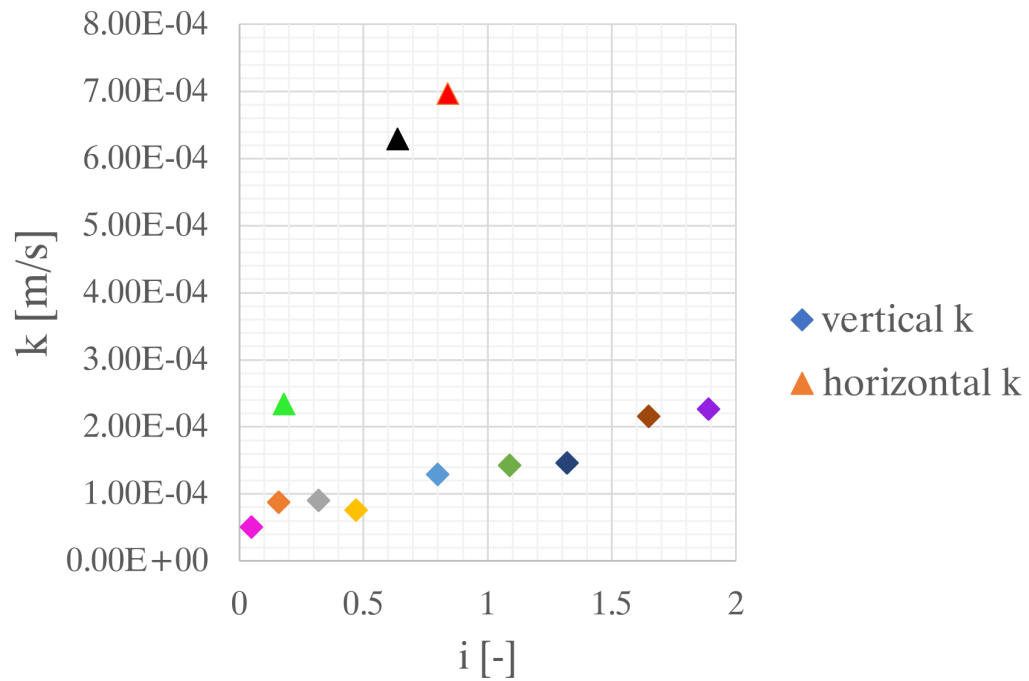


Figure 6.17. Comparison of vertical and horizontal seepage test results

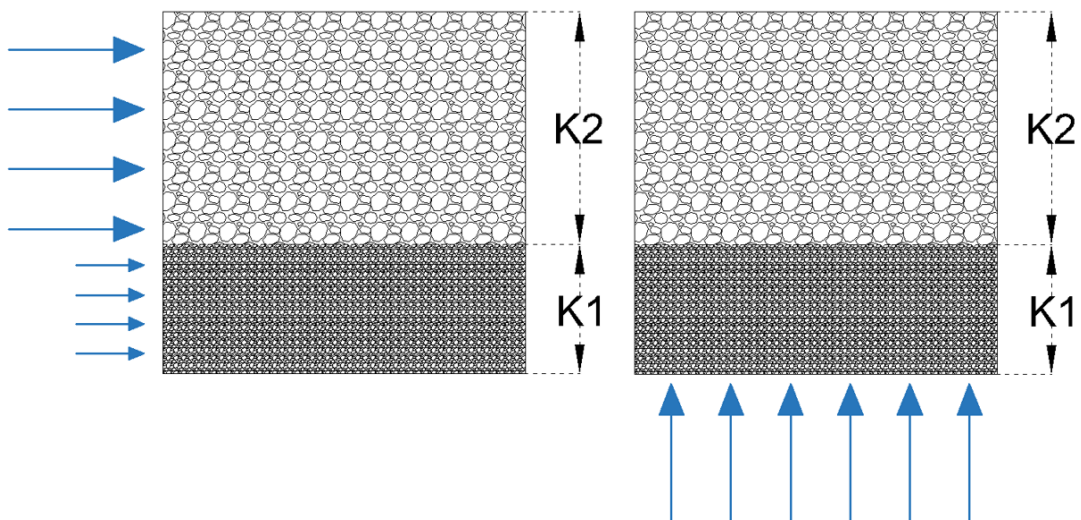


Figure 6.18. Schematic layout of direction of flow in relation with the disposition of fine material

Conclusions

In the context of land protection, the integrity and safety of earth structures is a major engineering concern.

The development of a device for analysing the internal erosion of embankments is of fundamental importance for the investigation of a natural process that may compromise their overall stability. Numerous systems for assessing diffuse and localised erosion are available in the literature, both at small and real scales, but the usefulness of a laboratory instrumentation that can be modified and adapted to a variety of conditions and application is evident. Reviewing the literature in this context was essential to understand what has already been developed and to take inspiration from it in terms of positive aspects, but even more important was to identify the limitations in order to develop a more complete and reliable system.

The EPBox here presented was designed with the objective of analysing internal erosion phenomena such as *suffusion* and *pipinq*. The material chosen had characteristics capable of making these phenomena evident, with a coarse part of 2 mm in diameter, and two other classes of material, finer in size and with a smaller proportion with respect to the first one (minimum diameter of 0.07 mm). The filters were created consequently, with the aim of being easily replicable in the future if a material with a different grain size is chosen or if other types of phenomena have to be investigated. In this sense, economic considerations were also taken into account, evaluating among the different options the one that was advantageous from an economic point of view as well as in terms of effectiveness.

The main objective of this thesis was the design, manufacturing and assembly of the device and of the hydraulic system, including the selection of suitable materials and tools required to perform the tests. The design process often had the necessity of modifications to be made by hand, or in the case of the non-existence of the most suited objects on the market, they were created using alternative materials or equivalent solutions. The difficulties of this phase were innumerable and required a

great deal of time both in terms of search for materials and actual realisation of the instruments.

In order to characterise the material, a number of tests were carried out to determine the minimum and maximum void ratio under dry and wet conditions. Along with quantitative analyses, qualitative considerations were also made regarding the arrangement of the material and the initial compaction conditions. Following careful visual analysis, it was decided to use the sample at loose state and at 8% moisture conditions because in the dry case excessive segregation of the fine material was observed.

In parallel with the realisation of the EPBox, seepage tests were carried out on a properly modified permeameter to obtain vertical seepage values to be compared with the results acquired from horizontal seepage in the EPBox. The permeameter tests also helped to familiarise with the use of the material and with seepage tests in general, being smaller and simpler. The use of glass beads led to a number of problems that it was useful to start identifying from the first standard tests, to have a starting point for improving the EPBox instrumentation. The tests in the permeameter were carried out with different hydraulic gradients, obtaining hydraulic conductivity values over time and measurements of eroded material over time. A piezometer was installed to verify the actual hydraulic gradient in the sample.

Once the EPBox was fully assembled, all the hydraulic connections necessary for filling and emptying the upstream and downstream tanks were made, modifying the inlet and outlet flow rate after a series of tests with the aim of checking the ability to keep the levels in the two tanks constant during the course of the test. In addition to the hydraulic connections, the greatest demands were placed on the filters, both in terms of maintenance to prevent corrosion, and in terms of dimensions, to prevent the material from passing along the side gaps.

The innovations introduced by EPBox in the context of seepage tests in soils are related to:

- the possibility of modifying the length of the sample by choosing the distance between the filters;
- the possibility of arranging the material in layers that are not parallel to the direction of seepage, thanks to a system that can rotate the body of the box with any inclination;

-
- the ability to simulate and induce different seepage paths either by changing the type of material used or by making holes inside the sample (for instance Hole Erosion and Slot Erosion tests could be performed);
 - the easy modification of the filters to adapt to the material used;
 - the possibility of measuring the amount of erosion over time during the course of the test without interrupting it;
 - the imposition of variable gradients by setting the level of the upstream and downstream reservoir or by performing a test under pressure;
 - the possibility of carrying out a test with perfectly horizontal seepage and a fully saturated sample, or with a partially saturated one and free surface seepage.

Four tests were carried out on three different samples, applying gradients from 0.16 to 0.84. The tests were conducted with the primary aim of testing and verifying the effective functionality of the equipment. In addition, hydraulic conductivity values and eroded mass measurements were obtained which can be compared with the results of the previous tests, even if with the necessary distinctions. The tests were carried out with a completely saturated sample. The tests showed that the eroded material decreases during the course of the test also due to the formation of pipes that allow water to pass inside the sample easily.

In particular, the first test had a limited duration and was carried out with the highest gradient of 0.84, followed by a second test with a gradient of 0.16 during which no eroded material was observed. Subsequently, a new sample was tested with a gradient of 0.64 and a duration of more than one day until the eroded material reached negligible quantities over time. As a final test, a gradient of 0.18 was imposed and a reduced amount of eroded material and a hydraulic conductivity value considered unaffected by the seepage process were observed.

In both vertical and horizontal seepage tests, fine and medium materials were considered as possible erodible fractions, also on the basis of considerations made on the same material in previous theses. It was observed that the amount of eroded material, with the limitations due to imperfections in the material collection procedure and the edges of the filters, increases with the hydraulic gradient, such as the hydraulic conductivity.

This work of thesis was not mainly focused on carrying out tests on the EPBox, but instead on the set-up of the entire system. The preliminary analyses could be a starting point for future improvements. In particular, many functions of the device have not been exploited yet, including the possibility of using an inclination of the layers not parallel to the flow direction, using the cover and the membrane to apply even higher gradients, employing longer samples to exploit the possibility to measure pressure variations along the flowpath, performing tests with a partially saturated sample. Furthermore, it is possible to combine the experimental tests with finite element models in order to provide a mechanical interpretation of the seepage and erosion processes.

Bibliography

- Canocher, A., & Dalrymple, J. B. (1977). The nine unit landsurface model: an approach to pedogeomorphic research. *Geoderma*, *18*(1/2), 1–154.
- Celada, C., & Magno, M. P. (2013). Progettazione e realizzazione di un modello a scala di laboratorio per lo studio dell' erosione in rilevati in terra.
- Chapuis, R. P., & Gill, D. E. (1989). Hydraulic anisotropy of homogeneous soils and rocks: influence of the densification process. *Bulletin of the International Association of Engineering Geology*, *39*(1), 75–86. <https://doi.org/10.1007/BF02592538>
- Das, B. M. (2006). *Principles of Geotechnical Engineering* (C. Learning, Ed.).
- Fell, R., & Fry, J.-J. (2007). The state of the art of assessing the likelihood of internal erosion of embankment dams, water retaining structures and their foundations. *Internal Erosion of Dams and their Foundations*, 1–23.
- Germaine, J. T. (2009). *Geotechnical Laboratory Measurement for Engineers*. John Wiley & Sons.
- Green, R. A., & Cubrinovski, M. (2010). GEER Association Report No. GEER-024: Geotechnical Reconnaissance of the 2010 Darfield (New Zealand) Earthquake, 6–5.
- Jansen, R. B. (1983). *Dams and Public Safety: A Water Resources Technical Publication*.
- Jones, A. (1981). The nature of soil piping: a review of research. (Norwich, Ed.).
- Jones, A. (2004). Pipe and piping. *Encyclopedia of Geomorphology*, *1*.
- Koltuk, S., Song, J., Iyisan, R., & Azzam, R. (2019). Seepage failure by heave in sheeted excavation pits constructed in stratified cohesionless soils. *Springer Nature*, *13*(6), 1415–1431. <https://doi.org/https://doi.org/10.1007/s11709-019-0565-zRESEARCH>
- Ladd, R. S. (1978). Preparing Test Specimens Using Undercompaction (E. T. Selig, Ed.). *Geotechnical Testing Journal*, *1*(1), 16–23. <https://doi.org/10.1520/GTJ10364J>

- Lane, E. W. (1934). Security from under-seepage masonry dams on earth foundations. *Trans ASCE* 60(4), 929–966.
- Lutz, F., Board, E., Curators, O. F., & Blanton, H. J. (1934). The Physico-Chemical Properties of Soils Affecting Soil Erosion. *Agricultural Experiment Station*.
- Pachideh, V., & Hosseini, M. (2019). A new physical model for studying flow direction and other influencing parameters on the internal erosion of soils. *Geotechnical Testing Journal*, 42(6), 1431–1456. <https://doi.org/10.1520/GTJ20170301>
- Richards, K., & Reddy, K. (2007). Critical appraisal of piping phenomena in earth dams. *Bulletin of Engineering Geology and the Environment*, 66(4), 381–402. <https://doi.org/10.1007/s10064-007-0095-0>
- Richards, K., & Reddy, K. (2012). Experimental investigation of initiation of backward erosion piping in soils. *Geotechnique*, 62(10), 933–942. <https://doi.org/10.1680/geot.11.P.058>
- Shields, A. (1936). Anwendung der Aehnlichkeitsmechanik und der Turbulenzforschung auf die Geschiebebewegung. *Versuchsanst. f. Wasserbau u. Schiffbau*, Heft 26, Berlin.
- Van Beek, V., Knoeff, H., & Schweckendiek, T. (2011). Piping: over 100 years of experience. *A Feeling for Soil and Water - A Tribute to Prof. Frans Barends*, 143–158.
- Van Beek, V., Van Essen, H. M., Vandenboer, K., & Bezuijen, A. (2015). Developments in modelling of backward erosion piping. *Geotechnique*, 65(9), 740–754. <https://doi.org/10.1680/geot.14.P.119>
- Wan, C. F., & Fell, R. (2004). Investigation of Rate of Erosion of Soils in Embankment Dams, 373–380.
- White, C. M. (1940). The equilibrium of grains on the bed of a stream. *Proceedings of the Royal Society of London. Series A. Mathematical and Physical Sciences*, 174, 322–338. <https://doi.org/10.1098/rspa.1940.0023>
- Xiao, M., & Shwiyhat, N. (2012). Experimental investigation of the effects of suffusion on physical and geomechanic characteristics of sandy soils. *Geotechnical Testing Journal*, 35(6), 1–11. <https://doi.org/10.1520/GTJ104594>
- Xiong, H., Yin, Z. Y., Zhao, J., & Yang, Y. (2021). Investigating the effect of flow direction on suffusion and its impacts on gap-graded granular soils. *Acta Geotechnica*, 16(2), 399–419. <https://doi.org/10.1007/s11440-020-01012-9>